

**The Development of Novel Window Systems
Towards Low Carbon Buildings**

HAOYANG LIU, BArch, MA

**Thesis submitted to the University of Nottingham
for the degree of Doctor of Philosophy**

September 2012

Table of Contents

Abstract	I
Acknowledgement	III
Nomenclature	IV
List of Figures	IX
List of Tables	XIII
Chapter 1 Introduction	1
1.1 Background	1
1.2 Aims and objectives	2
1.3 Research methodology and scope	4
1.4 Summary	5
Chapter 2 Zero/Low Energy Buildings	7
2.1 Introduction of Zero/Low energy buildings	7
2.1.1 Zero energy, net-zero, and life cycle zero energy buildings	8
2.2 Zero/Low energy building design strategies	9
2.3 Low energy building case	11
2.3.1 Tarmac Code 4 & Code 6 Homes (Creative Energy Homes Project, University of Nottingham)	11
2.3.2 The David Wilson Millennium Eco-House School of the Built Environment, University of Nottingham.....	13
2.3.3 Hockerton Housing Project (The Watershed, Gables Drive, Hockerton, Shouthwell, Nottinghamshire, England)	17
2.3.4 Hollies Barn (Eakring, Nottinghamshire, England)	20
2.3.5 Fosse Estate (Newark, Nottingham shire, England)	22
2.4 Findings	24
2.5 Summary.....	25
Chapter 3 Review of Previous Work on High Performance Glazing Types and Windows Technologies	26
3.1 Purpose of developing high performance window systems	26
3.1.1 Purpose of reviewing current state-of-the-art glazing types and window technologies.....	26
3.1.2 Applications for high performance window system	27

3.2 Advanced glazing types.....	27
3.2.1 Multilayer glazing	27
3.2.2 Suspended films	28
3.2.3 Vacuum glazing.....	29
3.2.4 Low-emissivity coating	32
3.2.5 Smart windows	34
3.2.6 Photovoltaic (PV) glazing	36
3.2.7 Aerogels	37
3.2.8 PCM filled glazing	38
3.2.9 Gas filled glazing	41
3.2.10 Self-cleaning glazing.....	41
3.3 Advanced window technologies	44
3.3.1 Window technologies for hot climate	44
3.3.2 Windows technologies for cold climate	47
3.4 Advanced glazing technology for low energy buildings in the UK	49
3.4.1 Solar window technology.....	50
3.4.2 Edge effects	52
3.5 Conclusion	56
Chapter 4 Novel Vacuum Tubes Window System	57
4.1 Introduction and objective	57
4.2 Vacuum tube window system.....	58
4.2.1 Prototype descriptions	58
4.2.2 Mathematical analyses of the energy transfer process and computer programme set up	59
4.2.3 Reference boundary conditions and calculation result.....	68
4.3 Calibrated hot-box method for vacuum tube windows tests	78
4.3.1 Test conditions and procedures	82
4.3.2 Window prototype test	83
4.3.3 Calculation and expression of results	85
4.4 Thermal image	89
4.4.1 Introduction of thermal imaging camera	89
4.4.2 Test procedure	90
4.4.3 Thermal image result.....	90
4.4.4 Result discussion	93

4.5 Economic and environmental analysis of the vacuum tube window system	94
4.5.1 Evaluation of the performance of the vacuum tube windows	94
4.5.2 Economic analysis	94
4.5.3 Environmental effect	99
4.5.4 Life cycle analyses	100
4.6 Summary	103
Chapter 5 Aerogel and Argon Window	105
5.1 Introduction	105
5.2 Translucent insulating material - Aerogel	105
5.3 Aerogel-argon window system description	107
5.4 Mathematical analyses of the energy transfer process	111
5.4.1 Energy flow chart and thermal transportation	111
5.4.2 Heat Transfer through vacuum tube glazing unit	113
5.4.3 Calculation result	113
5.5 Laboratory test for Aerogel and Argon window prototype	116
5.5.1 Test method and procedure	116
5.5.2 Test results and analysis	116
5.5.3 U-value calculation	119
5.6 Thermal imaging results	122
5.7 Summary	125
Chapter 6 Thermoelectric (TEC) Window System	126
6.1 Introduction	126
6.2 Thermoelectrics (TE) application	127
6.2.1 Thermoelectric devices as cooler	127
6.2.2 Thermoelectric devices for power generation	128
6.2.3 Thermoelectric devices as thermal energy sensors	130
6.3 Thermoelectric (TEC) window prototype description	131
6.4 Computational models for the thermoelectric window system	132
6.4.1 Theory of thermoelectric (TE) effect	132
6.4.2 Thermoelectric module performance of cooling mode	133
6.4.3 Thermoelectric module performance of heating mode	135
6.5 Laboratory test procedure	136
6.6 Results and discussion	139

6.6.1 Indoor test results	139
6.6.2 Outdoor test results.....	142
6.7 Summary.....	148
Chapter 7 Thermoelectric Generator (TEG) Window System.....	150
7.1 Introduction	150
7.2 Thermoelectric (TE) device.....	151
7.2.1 Introduction of thermoelectric materials	151
7.2.2 Introduction of thermoelectric device	151
7.2.3 Thermoelectric power generation device	152
7.3 System description.....	153
7.4 Computational analysis for the thermoelectric generator system and theoretic results.....	155
7.4.1 Computational analysis for the thermoelectric generator system	155
7.4.2 Theoretic data of 50Watt TEG power strip.....	161
7.5 Instrumentation and test procedure.....	163
7.6 Test results and discussion	165
7.6.1 Electricity power output for single TEG module	165
7.6.2 Electric power output for thermoelectric generator device tests.....	167
7.6.3 System experimental test results and discussion.....	171
7.7 Summary.....	174
Chapter 8 Conclusions and Future Works.....	175
8.1 Conclusions	175
8.1.1 Performance of vacuum tube window system.....	176
8.1.2 Performance of Aerogel window and Aerogel-Argon window system	176
8.1.3 Performance of Thermoelectric window system heating effect.....	177
8.1.4 Performance of Thermoelectric generator window system.....	177
8.1.5 Economic analysis of the novel window system.....	177
8.2 Future works	178
References.....	181
Appendix A: Thermoelectric Material Basic Data	191
Appendix B: Publication	196

Abstract

Buildings are responsible for over 70% of the average city's greenhouse gas emissions. As the key component of buildings, window serves very important role in architecture. In current energy efficient building practice, windows are considerably less well insulating component than other parts of the building envelope. Therefore improving windows thermal performance is an important issue to develop energy efficiency building design.

This research is carried out from the case studies of zero/low carbon buildings, in which windows were found the weakest part of building envelope. Within this work state-of-the-art window glazing types, latest best performing fenestration products in the market and advanced window technologies are reviewed. Vacuum window technology using evacuated tube panels will be presented in this research work, as well as Thermoelectric (TEC) window system and Thermoelectric power generation window system.

The objectives of the development of novel window systems are: (1) to develop the first-of-its-kind window technology using evacuated tube panels, its thermal transmittance (U-value) will be studied; (2) In order to compare U-values data with high performance windows, thermal performance of novel designed Aerogel and argon window system will be investigated; (3) to develop novel window system by combining evacuated tube panels and thermoelectric modules, which is functioned as a heat pump device; (4) to develop window system as a power generation device by interating thermoelectric generator. Novel windows technologies would meet the requirements of the Code for Sustainable Homes and those of commercial buildings.

The study on development of novel window systems is carried on from the current window technologies and includes:

(1) Computer modelling results show U-values about $0.59 \text{ W/m}^2\text{K}$ for double wall vacuum tube window, $0.61 \text{ W/m}^2\text{K}$ for single wall vacuum tube window. Laboratory measurements are carried out to validate theoretical results. The test results show that $1.0 \text{ W/m}^2\text{K}$ and $1.1 \text{ W/m}^2\text{K}$ for double and single wall vacuum tube window respectively. Economic and environmental assessments are also analysed.

(2) Numerical model and laboratory tests have illustrated the U-values of different thickness of aerogel, argon and combination of both filled window. Comparing to standard double glazed window unit with 20mm air gap (U-value of $2.8 \text{ W/m}^2\text{K}$), the U-value result of 6mm Aerogel-Argon window can be improved by 45% in theory and 30% according to the laboratory measurement results.

(3) Advanced glazing will become “Energy Suppliers” as well as “Energy Managers”. Novel design of thermoelectric window system may function as “a heat pump” contributing buildings’ heating load in winter. Laboratory and outdoor tests investigate the amount of heat supply under various voltage regimes and weather conditions.

(4) The electric power output of thermoelectric generator device combined with vacuum tube is examined under different experimental thermal conditions. The use of TEM has advantages of its maintainance free and can operate from any heat source. Window unit (sized $1\text{m} \times 1\text{m}$) installed such device can generate electricity approximately 70~180W.

Acknowledgement

I would like to thank my supervisor Professor Saffa B. Riffat who was abundantly helpful and offered invaluable assistance, support and guidance. Genuine gratitude are also due to Dr Francis, technicians Mr David Olive and Mr David Taylor. This research project would not have been possible without whose support, knowledge and assistance.

I would also like to convey thanks to the Department of Built Environment, Faculty of Engineering, the University of Nottingham for providing the research and laboratory facilities.

I would like to express my love and gratitude to my beloved families for their understanding and endless love through the duration of my studies.

Nomenclature

Symbol	Term	Unit
a	Width	m
A	Area	m^2
b	Height	m
C	Cost	£
COP	Overall coefficient of performance of the TE module	
COP_c	Coefficient of performance of the TE module cold side	
COP_h	Coefficient of performance of the TE module hot side	
e	Radiative coefficient	$W/m^2.K$
E	Radiation	W/m^2
$E_{Seebeck}$	Electromotive force induced by Seebeck effect	Volt
Em	Emission	kg
$f_{c,c}$	Carbon dioxide factor of gas	$0.2kgCO_2/kWh$
G	Geometric factors, area and length of TE element	
h	Heat transfer coefficient	$W/m^2.K$
α	Heat exchange coefficient	W/K
Λ	Heat conductance	$W/m^2.K$
β	Heat exchange coefficient	W/K
γ	Flanking heat loss coefficient	W/K
δ	Thickness	m
ε	Emissivity	-

σ	Stefan-Boltzmann constant	-
λ	Thermal conductivity	W/m.K
τ	Transmittance	-
ϕ	Heat flux through the metering area	W
ϕ_F	Flanking loss	W
σ	Material property for the specific type of TE element	
A	Effective Seebeck Coefficient	W/AK
α	Seebeck Coefficient of TE leg	W/AK
α_n	Seebeck Coefficient of N-type TE leg	W/AK
α_p	Seebeck Coefficient of P-type TE leg	W/AK
η	Thermodynamic efficiency	
I	External current in the circuit	Ampere
K	Thermal conductance of thermoelectric module	W/mK
K_n	Thermal conductivity of N- type TE leg	W/mK
K_p	Thermal conductivity of P- type TE leg	W/mK
N	Number of thermoelectric pairs in thermoelectric module	
P	Electric power generated by the modules	Watt
P_{TE}	Power output of the thermoelectric module	Watt
pp	Payback period	year
q	Heat supplied by the heat source	Joule
Q_c	The rate of removal heat	Watt
Q_h	The rate of supply heat	Watt

Q_{TEM}	The heat input into thermoelectric modules	Watt
q	Energy transportation per square meter	W/m^2
Q	Energy flow	W
R	Thermal resistance	$m^2.K/W$
R_0	Electrical resistance of a thermoelectric module	Ω
R_{load}	Electrical load electrical resistance	Ω
S	Seebeck coefficient of the thermoelectric material	
SF	Solar factor	
t	Temperature	$^{\circ}C$
T_a	Temperature of laboratory ambient	$^{\circ}C$
TE	Thermoelectric module	
T	Average temperature of the hot side and cold side of the thermoelectric Module	$^{\circ}C$
ΔT	Temperature difference between hot and cold end of TE module	$^{\circ}C$
T_c	TE module cold junction temperature	$^{\circ}C$
T_h	TE module hot junction temperature	$^{\circ}C$
T_{sol}	Solar energy transmittance	
T_{vis}	Visible transmittance	
U (U-value)	Heat transfer transmittance	$W/m^2.K$
V	Velocity	m/s
V	Open circuit voltage	Volt
V_s	Speed factor of velocity	m/s

<i>W</i>	Electrical power generated by TEG	Watt
<i>Z</i>	Figure of merit of thermoelectric material	K^{-1}

Subscript

Term

<i>dg</i>	double glazing window
<i>e</i>	environmental temperature
<i>ec</i>	evacuated cavity
<i>f</i>	frame
<i>g</i>	glazing
<i>i</i>	serial number
<i>in</i>	inside environment
<i>ng</i>	net area of glazing
<i>o</i>	overall amount
<i>out</i>	outside environment
<i>s</i>	static air space
<i>s1</i>	surface of the test element in the metering box
<i>s2</i>	surface of the test element in the cold box
<i>sol</i>	solar
<i>ss</i>	silicone sealant
<i>tac</i>	tube air cavity
<i>th</i>	thermal effect
<i>tr</i>	triple glazing window
<i>T</i>	vacuum tube

T_{in}	inside of tube
T_o	outside of tube
vis	visible
vt	vacuum tubes window
W	metering box wall
1	first object
2	second object

List of Figures

Chapter 2

Figure 2. 1: Outside image of David Wilson Millennium Eco-House (a. the vertical-axis wind turbine; b. PV tile arrays on the southern face of the roof)	15
Figure 2. 2: Inside view of solar chimney.....	16
Figure 2. 3: Image for Hockerton Housing Project (Web 2.3)	18
Figure 2. 4: Internal layout of six bay dwelling (Web 2.3).....	20
Figure 2. 5: Image for Fosse Estate (Web 2.3)	22
Figure 2. 6: The layout of terrace rows on either side of the glazed covered sheet (Web 2.3)	23

Chapter 3

Figure 3. 1: Before and after Empire State Building windows retrofit (Web 3.1, Web 3.2)	29
Figure 3. 2: Schematic diagram of a vacuum glazing (Web 3.3)	31
Figure 3. 3: The AIW appeared in the water-clear state without haze and color. The size was a square meter (H. Watanabe, 1998)	40
Figure 3. 4: The AIW changed to the paper-white state with enough shadow by solar energy. The size was a square meter (H. Watanabe, 1998)	40
Figure 3. 5: Schematic diagram of the decontamination process occurring on the superhydrophilic self-cleaning surface (Fujishima and zhang, 2006). ©2006, Elsevier Science Ltd.....	42
Figure 3. 6: Photo of the a-Si thin film PV module from Trony, Shenzhen, China (Web 3.4).	46
Figure 3. 7: Edge effects: Double glazing, 3-12-3, 1m ²	53
Figure 3. 8: Edge effects: Double, low-e (0.08), argon, 3-12-E3, 1m ²	54
Figure 3. 9: Edge Effects: Triple, 2 low-e, Krypton; 3-10-E3-10-E3, 1m ²	55

Chapter 4

Figure 4. 1: Vacuum tubes window prototype	59
Figure 4. 2: Single-wall Vacuum Tubes Window Construction Details and Solar/Heat Flow Process	60
Figure 4. 3: Double-wall Vacuum Tubes Window Construction Details and Solar/Heat Flow Process	61
Figure 4. 4: Schematic of Heat Transfer Through Single-wall Vacuum Tubes Window Unit in Winter	62
Figure 4. 5: Schematic of Heat Transfer Through Double-wall Vacuum Tubes Window Unit in Winter	62
Figure 4. 6: Thermal Network Model of Single-wall Vacuum Tubes Window Unit	63

Figure 4. 7: Thermal Network Model of Double-wall Vacuum Tubes Window Unit	64
Figure 4. 8: Heat transfer coefficient of outside air for various wind speeds	65
Figure 4. 9: Flow chart of calculation process	69
Figure 4. 10: Diagram of temperature changes through vacuum tube.....	71
Figure 4. 11: Overall thermal transmittance of various wind speeds of outside air	74
Figure 4. 12: Overall thermal transmittance of different frame types	75
Figure 4. 13: Overall thermal transmittance of different frame area to total window area	76
Figure 4. 14: Overall U-values of Single Wall Vacuum Tube Window in Various Conditions	77
Figure 4. 15: Overall U-values of Double Wall Vacuum Tube Window in Various Conditions	78
Figure 4. 16: Calibrated hot-box apparatus.....	80
Figure 4. 17: Prototype vacuum tube window test rig	81
Figure 4. 18: Measurement equipment	84
Figure 4. 19: Single-wall vacuum tube window U-values in specified test condition	87
Figure 4. 20: U-values in specified test condition	88
Figure 4. 21: Fluke TiS Thermal Imaging Scanner	90
Figure 4. 22: Test room for double wall vacuum tube window prototype	90
Figure 4. 23: Thermal imaging results	93
Figure 4. 24: Net cost benefits of replacing double and triple glazing windows with vacuum tube window for new-buildings with different house types.	100
Figure 4. 25: Net cost benefits of replacing double and triple glazing windows with vacuum pipe window for retrofit buildings with different house types.....	101

Chapter 5

Figure 5. 1: Manufacture Process for Super Spacer [®] Standard Insulation.....	108
Figure 5. 2: Image of Hot Melt Butyl Edge Sealant	109
Figure 5. 3: Schematic Drawing and Prototype of 6mm Thickness 300mm×300mm Aerogel-Argon Window	110
Figure 5. 4: Aerogel and Argon window construction details and heat Flow Process	111
Figure 5. 5: Thermal network model of Areogel & Argon window unit.....	112
Figure 5. 6: U-values of various thicknesses, cavity filled with Aerogel, Argon and Aerogel-argon window	115
Figure 5. 7: Aerogel Window Test Rig.....	116
Figure 5. 8: Time against Inside and Outside Glazing Surface Temperature Differences of Window Samples	117
Figure 5. 9: Time against Heat Flux of Window Samples.....	118
Figure 5. 10: U-Value of Aerogel Window sample.....	120
Figure 5. 11: U-Value of Window samples	121
Figure 5. 12: 4mm Aerogel glazing	123

Figure 5. 13: 5mm Aerogel glazing	123
Figure 5. 14: 6mm Aerogel-argon glazing.....	124
Figure 5. 15: 20mm Argon filled glazing	124

Chapter 6

Figure 6. 1: Conventional arrangement for thermoelectric power generation (Riffat and Ma, 2003).	129
Figure 6. 2: An example of a thermoelectric generator as a fluid preheating/parasite generation device (Riffat and Ma, 2003).	130
Figure 6. 3: The schematic of TEC window	132
Figure 6. 4: TEC window prototype	137
Figure 6. 5: TEC window lab test	137
Figure 6. 6: TEC window outdoor test set-up.....	138
Figure 6. 7: Hot and cold side temperatures for TEC window system in heating mode	141
Figure 6. 8: Light intensity of solar simulation lamp.....	141
Figure 6. 9: Hot and cold side temperatures for TEC window system in heating mode (20/04/11).....	143
Figure 6. 10: Light intensity measured by pyranometer (20/04/11)	143
Figure 6. 11: Hot and cold side temperatures for TEC window system in heating mode (25/04/11).....	144
Figure 6. 12: Light intensity measured by pyranometer (25/04/11)	144
Figure 6. 13: Hot and cold side temperatures for TEC window system in heating mode (19/04/11).....	145
Figure 6. 14: Light intensity measured by pyranometer (19/04/11)	145
Figure 6. 15: Hot and cold side temperatures for TEC window system in heating mode (22/04/11).....	146
Figure 6. 16: Light intensity measured by pyranometer (22/04/11)	147

Chapter 7

Figure 7. 1: Schematic diagram of the test section	154
Figure 7. 2: High temperature thermoelectric module used for proposed thermoelectric power generator system	154
Figure 7. 3: Proposed TEG power generation system (a) hot side; (b) cool side	155
Figure 7. 4: Illustrates the formation of induced electrical current inside the TEG model (C.T. Hsu et al., 2011).....	157
Figure 7. 5: Conventional arrangement for thermoelectric power generation (Riffat and Ma, 2003).	159
Figure 7. 6: Effect of ΔT on 50 Watt TEG power strip voltage generation (theoretic analysis)	161

Figure 7. 7: Effect of ΔT on 50 Watt TEG power strip direct current generation (theoretic analysis).....	162
Figure 7. 8: Effect of ΔT on 50 Watt TEG power strip power generation (theoretic analysis)	162
Figure 7. 9: Measurement equipments.....	164
Figure 7. 10: Experimental test set-up	166
Figure 7. 11: Effect of ΔT on P characteristic for single TEG module	166
Figure 7. 12: Light intensity of solar simulation lamp.....	168
Figure 7. 13: TEG modules hot side and cool side temperature	169
Figure 7. 14: System hot plate test setup	170
Figure 7. 15: Effect of ΔT on power output characteristic for thermoelectric generator device	170
Figure 7. 16: Effect of ΔT on Voltages generation.....	172
Figure 7. 17: Effect of ΔT on direct Current generation.....	172
Figure 7. 18: Effect of ΔT on power generation	172

List of Tables

Chapter 2

Table 2. 1: Tarmac Code 4 Home Construction Details	12
Table 2. 2: Tarmac Code 6 Home Construction Details	13
Table 2. 3: David Wilson Millennium Eco-House Constriction Details (Web 2.3)	16
Table 2. 4: Hockerton Housing Constrution Details (Web 2.3)	19
Table 2. 5: Hollies Barn Construction Details (Web 2.3).....	21
Table 2. 6: Fosse Estate Construction Details (Web 2.3)	23

Chapter 3

Table 3. 1 Literature data for some of the best low-e triple glazing products (B.P. Jelle, et al., 2011)	28
Table 3. 2 Literature data for suspended film glazing products (B.P. Jelle, et al., 2011)	29
Table 3. 3 Literature data for SPACIA-21 vacuum glazing (B.P. Jelle, et al., 2011)..	30
Table 3. 4 Examples of hard and soft low-e coatings currently available	34
Table 3. 5 Data for electrochromic windows, where the cycles column refer to the guaranteed number of colouring/bleaching cycles	36
Table 3. 6 Literature data for aerogel glazing products (Jelle, et al., 2011)	38
Table 3. 7 Literature data for self-cleaning glazing products (Jelle, 2011)	43
Table 3.8: The effects of edge component heat flow on window U-value, U_w (W/m ² K): Double glazed, 1m ² window, 3-12-3 (Robinson and Hutchins, 1994)	53
Table 3. 9: The effects of edge component heat flow on window U-value, U_w (W/m ² K): Double low-e, argon, 1m ² window, 3-12-E3 (Robinson and Hutchins, 1994)	54
Table 3. 10: The effects of edge component heat flow on window U-value, U_w (W/m ² K): Triple, 2 low-e, krypton, 1m ² window, 3-10-E3-10-E3 (Robinson and Hutchins, 1994).....	54

Chapter 4

Table 4. 1: Technical data of a double-wall vacuum tube provided by the vender	66
Table 4. 2: Frame U-values in W/ (m ² .k).....	68
Table 4. 3 Input parameters of vinyl frame single wall vacuum tube window unit for calculation	72
Table 4. 4: Output of vinyl frame single wall vacuum tube window unit under standard winter condition (Indoor temperature at 20°C, outdoor temperature at 5°C)	72
Table 4. 5: Capital cost calculation	95
Table 4. 6: Window areas of four typical types of houses in the UK	97
Table 4. 7: Annual energy savings of four typical types of houses in the UK	97

Table 4. 8: Costs for new buildings	98
Table 4. 9: Payback period for new buildings	98
Table 4. 10: Costs for retrofit buildings.....	98
Table 4. 11: Payback period for retrofit buildings.....	99
Table 4. 12: Environmental benefits of the vacuum tubes windows relative to the conventional double and triple glazing windows.....	99
Table 4. 13: Life cycle analyses of vacuum tubes windows.....	100

Chapter 5

Table 5. 1: Specifications of Window samples.....	110
Table 5. 2: Input parameters of vinyl frame 6mm Aerogel window unit for calculation	113
Table 5. 3: Output of vinyl frame 6mm Aerogel window unit under standard winter condition (Indoor temperature at 18°C, outdoor temperature at 10°C).....	114
Table 5. 4: U-values of various thicknesses, cavity filled with Aerogel, Argon and Aerogel-argon windows.....	114
Table 5. 5: U-value of different thickness Aerogel, Argon and Aerogel-Argon windows	121

Chapter 6

Table 6. 1: Thermal heat flux and <i>COP</i> for TEC window system laboratory test results	142
Table 6. 2: Thermal heat flux and <i>COP</i> for TEC window system outdoor tests	147

Chapter 7

Table 7. 1: Effect of ΔT on power output characteristics for single thermoelectric module.....	166
Table 7. 2: Effect of ΔT on power output characteristics for system setup with eight TEG modules	171

Chapter 1 Introduction

1.1 Background

The sign of climate change does affect earth living environment significantly, reducing environmental impact has become a worldwide awareness. Buildings are the single most damaging polluters on the planet, consuming over half of all the energy used in developed countries and producing over half of all greenhouse gases. The main greenhouse gas is CO₂ and the main source of CO₂ is from buildings. Houses consume around half of all the energy used in buildings. Therefore the concept of zero-energy homes/buildings that do not consume any nonrenewable or net energy from the utility grid has become the world wide interest.

As the key component of building envelope, window serves very important role in architecture. Window glass is prestigious for its positive functions such as transparency, natural brightness, modernity, freshness and indoor-outdoor interaction. However window is also a significant source of transmission heat loss or heat gain at different climate zones. In hot climates, the excessive solar radiation entering the internal space through the windows leads to increasing the cooling load of the refrigeration system. In cold climates, windows are responsible for 10-25% of the heat loss from the heated space to the external ambient (Ismail, 2007). As heat lost through windows represents about 20% of the total heat loss from an average home in UK. Therefore highly efficient window technologies are crucial issue to address in terms of designing low carbon buildings and reducing carbon foot print.

Reviewing current fenestration glazing products and advanced window technologies, on the market there are many kinds of thermally optically high performance glazing

available for different climate conditions. In the literature, advanced window technologies with thermal strategy design, such as integration with noble gas, aerogels, phase change materials (PCM), water, shading, ventilated panel, etc, such window systems were studied and examined by other researchers.

According to previous research, super insulating windows with U-values below $1 \text{ W/m}^2\text{K}$ can be constructed in several ways. Most common is triple glazed systems using coatings with low emissivity and noble gas filling the gap between window panes. U-values can be reduced even further by increasing the number of glass panes in the window. The drawbacks for multilayer glazing are lower solar energy transmittance. In addition, windows' edge seal can also help to increase the overall U-value. However it is a challenge to construct a glazing that at the same time has very high thermal resistance and high transmittance of solar energy and daylight (Duer and Svendsen, 1998).

1.2 Aims and objectives

The development of novel window systems study carried out upon high performance window technologies.

The work includes: (1) Numerical and experimental study on novel vacuum tube windows thermal conductivities and its economic and environmental analysis (2) Numerical and experimental study on thermal conductivities of various thickness of aerogels window, argon filled window, aerogels and argon filled window, comparing the U-values data with high performance windows (3) Study thermal performance of novel thermoelectric (TEC) window system under different conditions of solar radiation and applied voltage regimes (4) Examine electric power output of

thermoelectric generator device combined with vacuum tube under different experimental thermal conditions.

To achieve the above aims, the following objectives will be set:

- Window U-factor (U-value) - measuring the rate of window's heat loss

The U-value is the measurement of heat transmission through a material or assembly of materials. The U-value of a material is a gauge on how well heat passes through the material and the lower the U-value, the greater the resistance to heat and therefore has a better insulating value. The U-value is generally used in the building and construction industry to specify assemblies of components which provide a suitable insulation and energy efficiency value. U-Value is expressed in units of W/m^2 and relates to the amount of heat lost in watts (W) per square metre of material (Web 1.1). Computer modelling of window U-values takes into account parameters such as thermal, solar, visible transmittance etc. The results are used to validate by experimental tests. The measurement of novel window systems' U-values is the key part of this study, test apparatus is designed based on British standard methods for determining thermal insulating properties BS 874-Part3.

- TEC Window's thermal performance - measuring window's performance operated in the heating mode under different conditions of solar radiation and applied voltage regimes; cooling mode performance by switching electrical current direction

Both indoor and outdoor tests are carried out to investigate window's thermal performance operated in heating and cooling mode. System operating in heating mode

coefficient of performance (*COP*) is calculated under different test conditions to compare energy efficiency.

- Power generation – measuring electric power output of proposed power generation device integrated with vacuum tube

In previous research, drawbacks for photovoltaic (PV) glazing have been investigated in terms of investment cost, output efficiency and life expectancy. Comparing to PV system, thermoelectric module has the advantages of its maintenance free and longer life expectancy. This study develops thermoelectric power generation device integrated with vacuum tube window system. The electric power output will be investigated.

1.3 Research methodology and scope

The research started with case study of low carbon houses, explore latest sustainable energy technologies applied to energy efficient buildings, with the successful examples of low carbon buildings in practice, to seek research possibilities in related to improvement of buildings envelope thermal performance. The U-values results from existing buildings components show windows are the weakest link between indoor and outdoor environment. Advanced fenestration glazing type and high performance window technologies are thereby reviewed. In previous studies low thermal conductivities can be achieved by all means, such as multilayer vacuum glazing window, noble gas filled glazing, aerogels window, etc., from literature data the best window thermal performance can be achieved by aerogels window, U-value about $0.1\text{W/m}^2\text{K}$. Manufacturing of windows using vacuum tubes has not been previously reported. Numerical models were set up and calculated in various boundary conditions to evaluate the U-values of novel vacuum tubes windows. The

computer modelling results show that U-value below $0.6\text{W/m}^2\text{K}$ can be achieved. The process of manufacture of vacuum tubes windows is less complex than manufacturing vacuum glazing. However the application of this type of window is limited on daylight but not clear view dominated fenestration of the building, which is similar to aerogel windows application. The investigation involved the examination of thermal conductivities of vacuum tubes windows using experimental work. The project is also concerned with the use of vacuum tubes windows for energy supplier and power generation.

1.4 Summary

U-values of novel vacuum tube window and aerogel-argon window system have improved significantly comparing to standard double glazed window unit with 20mm air gap (U-value of $2.8\text{ W/m}^2\text{K}$). Laboratory tests are focused on windows thermal character, optical properties of windows are not covered in this study.

There are six chapters to illustrate this research work in the thesis.

Chapter 2 is the case study of low carbon buildings/houses. In this chapter, windows have been identified as an important area for energy efficiency improvements since the transmission losses through a window are ten times higher than through the wall. Furthermore, windows are easier to be renovated or replaced than most other parts of the building envelope.

Chapter 3 is literature review of state-of-the-art fenestration glazing products and high performance windows technologies. The advantages and drawbacks of current advanced glazing types and window technologies are discussed, such as multilayer glazing, suspended films, vacuum glazing, low-emissivity coating, smart windows,

etc. Studies on evacuated tubes window system and thermoelectric generator window system are introduced.

Chapter 4 is novel vacuum tube window system. For evacuated glass tubes, heat transfer by conduction and convection can be significantly reduced, therefore to achieve high thermal performance. Windows using evacuated tube panels to achieve low U-value are developed and studied by both computer modelling and experimental measurements.

Chapter 5 is Aerogel and argon window system. In order to compare the U-value data for high performance window, different thickness of aerogel-argon filled double glazing window systems are examined by both computer modelling and experimental tests.

Chapter 6 is thermoelectric window system. Vacuum tubes window system integrated with thermoelectric modules turn window into a heat pump device. The use of thermoelectric modules' Peltier effect can contribute the heating demands in winter or cold climate.

Chapter 7 is Thermoelectric generator window system. The design of power generation device used vacuum tube and thermoelectric generator. By establishing temperature differential between the hot and cold ends of the semiconductor material, a voltage is generated. The novel thermoelectric generator window system makes window as an "Energy Suppliers".

Chapter 2 Zero/Low Energy Buildings

2.1 Introduction of Zero/Low energy buildings

In order to investigate window component thermal performance within the buildings, this chapter will focus on several case studies of zero/low energy buildings. The design and technology strategies applying on to achieve zero/low energy buildings will be investigated, the U-values of each building component are also illustrated.

The concept of zero energy buildings (ZEB) has been paid much attention worldwide during last few years and now is becoming as the future target for designing buildings (Marszal et al., 2011). Torcellini et al. (2006) indicate that the unit applied in the ZEB definition can be influenced by the project goal, the intentions of the investor, the concerns about the climate and green-house gas emission and the energy cost. Thereby four different ZEB are defined as site ZEB, source ZEB, emission ZEB and cost ZEB, respectively. The advantages and disadvantages of each definition were pointed out, which are easy implementation of ‘zero site energy’ and ‘zero energy cost’ definition, more international and not regional feature of ‘zero source energy’ definition and calculation complexity of ‘zero energy emission’ definition (Marszal et al., 2011). Kilkis (2007) states that to assess the complete building’s impact on the environment the metric of the balance in the ZEB definition should address both the quantity as well as the quality of energy. He proposes a new ZEB definition as ‘a building which has a total annual sum of zero energy transfer across the building district boundary in district energy system, during all electric and any other transfer that is taking place in a certain period of time’ (Kilkis, 2007).

Early definition of low carbon (low energy) buildings emphasized balance between the need of living organisms, buildings and climate (Li, 2011). Low energy building

concept is based on improving the building envelope to reduce heating and cooling demand, and using high efficiency equipments as well as renewable energy sources. The improvements of the building envelope and HVAC systems depend on the climatic conditions. Heating demand is reduced by improving the envelope thermal insulation and air tightness, using heat recovery ventilation systems as well as recovering solar and internal heat gains. Cooling demand is decreased by using solar protection, smart building orientation, good thermal inertia couples with night ventilation among others (Thmosen et al., 2005 and Wolfgang et al, 2005)

The design of a low energy building should comply to many issues related to the environmental impact, indoor thermal comfort and air quality (Chlela et al., 2009).

2.1.1 Zero energy, net-zero, and life cycle zero energy buildings

“Zero energy” or “net zero” energy building are defined variously in the literature. In most of cases, the definitions refer only to the energy that is used in operating the building, such as heating, cooling, ventilation, lighting, etc, ignoring the aspects of energy use for the construction and delivery of the building and its components (Hernandez and Kenny, 2010). The term net-zero is frequently used to present the annual energy balance of a grid connected building but it does not consider the energy inputs to deliver the building and its components. Life cycle zero energy buildings (LC-ZEB) are defined as where the primary energy used in the building in operation plus the energy embodied within its constituent materials and systems, including energy generating ones, over the life of the building is equal to or less than the energy produced by its renewable energy systems within the building over their lifetime (Hernandez and Kenny, 2010). The following contents of zero energy buildings refer

to energy use in the building in operation, life cycle zero energy analysis is not covered.

2.2 Zero/Low energy building design strategies

Buildings as big energy-consumption systems are responsible for approximately 40% of total world annual energy consumption, in the forms of lighting, heating, cooling and air conditioning (Omer, 2008). Sustainable design and construction can contribute energy saving and reduce the impact on the environment.

There are many ways to develop the use of renewable energy, which comes from natural resources such as solar, wind, rain, tides and geothermal heat, which are naturally replenished, termed renewable. By employing renewable energy technologies, zero/low energy building is achievable of the balance between energy use by the buildings' occupants and systems and energy produced by its renewable energy systems. Passive House is the world well-known leading low-energy building concept and was developed in Germany (Web 2.1). Today various techniques of passive, active and hybrid energy efficiency technologies have been developed worldwide, in which, high insulation, good air tightness and heat recovery ventilation systems become increasing popular principles for low energy buildings (Hernandez and Kenny, 2010).

Solar house practices were first documented attempts to deliver zero energy into realities. Vagn Korsgaard zero energy home and Saskatchewan conservation house are the early example in 1970s. Vagn Korsgaard zero energy house was constructed at the Technical University of Denmark (Esbensen and Korsgaard, 1977). The house can be heated all winter without artificial energy supply only by the use of solar energy. For energy conservation strategies, high-insulated constructions (30–40 cm mineral

wool insulation), movable insulation of the windows and heat recovery in the ventilating system, the total heat requirement for space heating is calculated to 2300 kWh per year. For a typical, well insulated, one-storied, one-family house built in Denmark, the corresponding heat requirement is 20,000 kWh. The solar heating system is dimensioned to cover the heat requirements and the hot water supply for the Zero Energy House during the whole year on the basis of the weather data. The solar heating system consists of a 42 m² flat-plate solar collector, a 30 m³ water storage tank (insulated with 60 cm of mineral wool), and a heat distribution system. A total heat balance is set up for the system and solved for each day of the “Reference Year”. Collected and accumulated solar energy in the system is about 7300 kWh per yr; 30 per cent of the collected energy is used for space heating, 30 per cent for hot water supply, and 40 per cent is heat loss from the accumulator tank. For the operation of the solar heating system, the pumps and valves need a conventional electric energy supply of 230 kWh per year (corresponding to 5 per cent of the useful solar energy) (Esbensen and Korsgaard, 1977).

The applications of renewable energy technologies can significantly reduce conventional resource consumption in buildings. Currently solar-based energy systems, ground source-based systems and day-lighting systems have been widely concerned as they could cover most or all of the energy usage in buildings (Ma and Wang, 2009).

2.3 Low energy building case

2.3.1 Tarmac Code 4 & Code 6 Homes (Creative Energy Homes Project, University of Nottingham)

In order to promote sustainable design ideas in terms of new ways of providing affordable, environmentally sustainable housing, six homes as a showcase of innovative state-of-the-art energy-efficient homes of the future are designed and constructed to various degrees of innovation and flexibility to allow the testing of different aspects of modern methods of construction (mmc) including layout and form, cladding materials, roof structures, foundations, glazing materials, thermal performance, building services systems, sustainable/renewable energy technologies, lighting systems, acoustics and water supply.

The site is situated within the grounds of Nottingham University and comprises an undeveloped plot of land at the end of Wortley Hall Close. Tarmac is to build a pair of two-storey, three-bedroom semi-detached homes that meet the minimum requirements of the Code for Sustainable Homes Level 4 and 6.

The Code for Sustainable Homes (CSH) is a national standard for the sustainable design and construction of new homes. The Code uses a sustainability rating system - indicated by 'stars', to communicate the overall sustainability performance of a home. A home can achieve a sustainable rating from one to six stars depending on the extent to which it has achieved Code standards. One star is entry level - above the level of the Building Regulation; and six stars is the highest level - reflecting exemplar development in sustainability terms (Web 2.1). The Code star rating system measures the sustainability of a new home against categories of sustainable design, which includes energy/CO₂ pollution, water, health and well-being, materials, management,

surface water run-off, ecology, waste. Since April 2007, the developer of any new home in England has been able to choose to be assessed against the Code, from 1st May 2008, rating against the Code has become mandatory for new homes.

➤ Project Objectives

Tarmac home project aims to build an energy efficient masonry home that can be mass produced, is visually appealing to the majority of potential home owners and that is affordable to buy and maintain.

➤ Construction and thermal design

Tarmac project has demonstrated that traditional masonry construction can also meet code level requirements. Building constructions materials used and U-values of building envelope components are illustrated in the flowing Table 2.1 and 2.2.

Table 2. 1: Tarmac Code 4 Home Construction Details

Construction Details	Construction/Materials	U-value (W/m²K)
Walls	103mm facing brick, 50mm clear cavity & 100mm Kingspan TW50, 100Hemelite, Plasterboard on dabs	0.19
Roof	Timber trussed roof designed with an asymmetric pitch with the long south facing elevation at a 22 degree angle to the horizontal to accommodate and maximise the potential for solar thermal hot water and micro generation of electricity. Traditional timber I joists 220mm deep finished with 22mm tongue and groove chipboard. Underside finished with 12.5mm plasterboard. Acoustic barrier provided by 100mm of quilted mineral wool laid between joists. Traditional roof coverings – felt, battens and concrete tiles.	0.11
Floors	Tarmac Heat save Plus suspended ground floor	0.14
Windows	PVC-U double argon filled glazed units	1.50 Green Guide Rating “A+”.
Doors	Composite insulated front door IG, all doors compliant with Part L and M. External doors conform to Secure by Design Standards	

Table 2. 2: Tarmac Code 6 Home Construction Details

Construction Details	Construction/Materials	U-value (W/m ² K)
Walls	150mm EPS insulation & render finish, 215mm Durox Supabloc, 13mm lightweight plaster	0.15
Roof	Timber trussed roof designed with an asymmetric pitch with the long south facing elevation at a 22 degree angle to the horizontal to accommodate and maximise the potential for solar thermal hot water and micro generation of electricity. Traditional timber I joists 220mm deep finished with 22mm tongue and groove chipboard. Underside finished with 12.5mm plasterboard. Acoustic barrier provided by 100mm of quilted mineral wool laid between joists. Traditional roof coverings – felt, battens and concrete tiles	0.11
Floors	Tarmac Heat save Plus suspended ground floor	0.14
Windows	Softwood casement frames with argon filled double glazing	1.50 Green Guide Rating “A+”.
Doors	Composite insulated front door IG, all doors compliant with Part L and M. External doors conform to Secure by Design Standards	

2.3.2 The David Wilson Millennium Eco-House School of the Built Environment, University of Nottingham

David Wilson Millennium Eco-House is to provide a fully instrumented, occupied test house, to demonstrate and evaluate energy efficiency and sustainable energy systems, and to provide a test bed for new domestic scale systems. This four bedroom detached property situated on the University Park campus of Nottingham University. It is occupied continuously by a group of researchers working at the School of the Built Environment who monitor and appraise the environmentally friendly energy features that are built into the property. The house is constructed by traditional building materials. The design of the property is such that new technologies, techniques and building systems can be easily assimilated into the structure. They are connected to the existing systems and services, monitored and appraised by the researchers, and

then removed or replaced if necessary. The house also provides an educational resource to university students, to industry and to local schools and colleges. The university sees this as an essential role in inspiring future generations of engineers, architects and builders in the possibilities of sustainable technology.

➤ Construction details

The Eco-House is built using traditional brick and block construction techniques. It was designed deliberately to meet the 2000 Building Regulation requirements, which permits research to be carried out on novel techniques for upgrading the thermal performance of standard new build homes. The house is orientated to maximise solar gains in the winter. It has a prominent location on the University Park campus. Flexibility of the structure was an important design criterion for the project. The steel frame in the southern half of the house, supporting two solar thermal collectors either side of the central solar chimney. The integration of a steel frame (see Figure 2.1) into the structure of the house means the fabric that makes up the rear of the property can be individually removed and replaced with other test materials. The frame also provides a convenient mounting for the rapid testing of new sustainable energy systems such as solar thermal tubes and wind generators.

As Figures 2.1 & 2.2 show, a solar chimney – referred to as a thermal chimney using convection of air heated by passive solar energy (Web 2.2), is integrated into the south facing facade. Air within the chimney is warmed by the sun and circulated into the property. The summer operation of the chimney is modified to vent warm air from inside the house and replace it with cooler air from a void beneath the concrete ground floor slab. Taken from the first floor landing, the internal upper vent of the solar chimney can be seen central. During the winter, air preheated by solar gain passes

from the chimney onto the landing. During the summer, warm air from the landing is passively extracted and vented to the outside. Uppermost in the photograph is the landing light pipe.

Monitoring sensors and data logging equipment are located throughout the property. Access for installing the required sensors and pipe and cable runs has been provided by a half basement below the ground floor slab, integrated conduit runs throughout the building and a clear span attic space.



Figure 2. 1: Outside image of David Wilson Millennium Eco-House (a. the vertical-axis wind turbine; b. PV tile arrays on the southern face of the roof)



Figure 2. 2: Inside view of solar chimney

Table 2. 3: David Wilson Millennium Eco-House Constriction Details (Web 2.3)

Construction Details	Construction/Materials	U-value (W/m ² K)
Walls	The 280mm thick external walls comprise of an outer leaf of either 103mm facing brickwork or a two coat sand cement render on 100mm thick 7N blocks. The inner leaf is 100mm thick 7N blocks and the 77mm cavity is fully filled with blown mineral fibre. The walls are lined internally with 9.5mm plasterboard.	0.45
Roof	Photovoltaic tile arrays designed to produce approximately 1250 kWh of electricity per year are fitted in place of conventional concrete roof tiles on the southern facing side.	0.35
Floors	The ground floor above the half basement consists of 150mm deep beam and block flooring finished with 16mm levelling screed, 40mm expanded polystyrene insulation and 19mm of moisture resistant grade chipboard.	0.45
Windows	The double glazed units are set in wood grain finished uPVC frames.	3.30
Doors	Treated softwood doors on treated softwood rebated frames.	

2.3.3 Hockerton Housing Project (The Watershed, Gables Drive, Hockerton, Shouthwell, Nottinghamshire, England)

Hockerton Housing Project (HHP) consists of a row of five terrace dwellings designed to incorporate the principles of passive solar design with the techniques of earth sheltering. The dwellings were built, to a large degree, by the residents themselves. The construction is super-insulated, with a high thermal mass, and covered on three facades with a layer of soil at least 400mm thick. This lessens the visual impact of the construction and reduces heat loss. The south facade is heavily glazed using high specification windows and is buffered from the outside by a timber conservatory. The conservatory acts as a solar collector, providing heating to the homes by natural convection, and heating the domestic hot water supply via an air-to-water heat pump. To provide good daylighting, all the main living rooms have windows that open onto the conservatory, which offsets the need for artificial lighting. The project aims to develop working opportunities onsite. All residents contribute an agreed number of hour's work each year towards community purposes, such as land management, food growing and onsite cooperative business. A communal office facility has recently been built, which will serve also as a resource centre for visitors. A number of research and networking projects are underway, through which the group hopes to stimulate more projects of this type around the country.

The following awards have been won by the project:

- A 'Major Commendation' was awarded in the Business Commitment to the Environment (BCE) Awards for 1999, in recognition of exemplary achievement in environmental activities.

· Winners of the 'Not For Profit' category of the Eurosolar UK Awards (2000), for outstanding service to the promotion of renewable energy

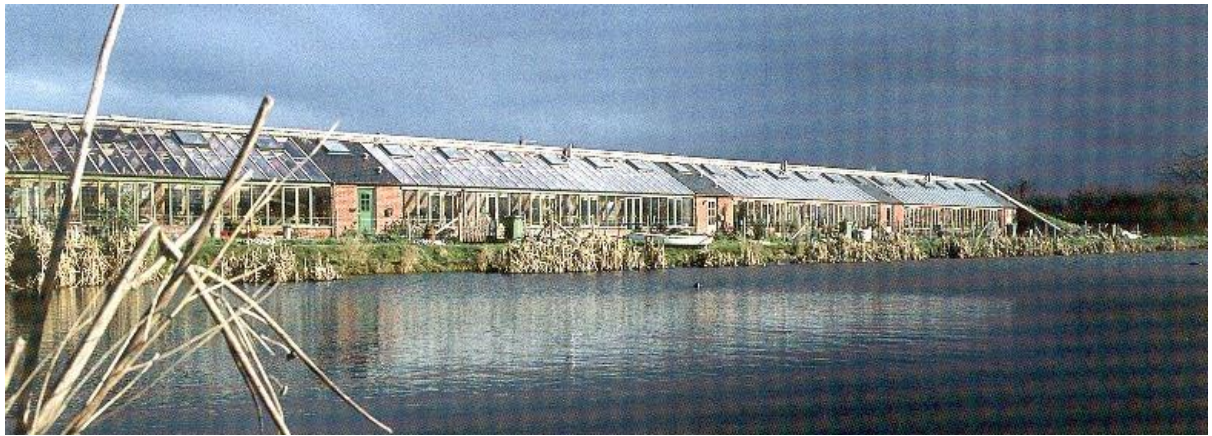


Figure 2. 3: Image for Hockerton Housing Project (Web 2.3)

➤ Project Objectives

The project aims to create one of the most energy efficient, purpose-built developments in Europe that demonstrates a zero-energy design by reducing life cycle energy to a minimum. The houses are earth covered and have passive solar heating without a space heating system. The project aims to be as autonomous as possible in terms of energy and water, and provides homes that offer financial savings in the medium to long term, with no loss of comfort or modern amenities.

➤ Construction Details

The initial development consists of a terrace of five earth-sheltered dwellings. Two further dwellings have been constructed on an adjacent field, as well as a Sustainable Resource Centre. The site is white field and planning permission was only approved subject to a S. 106 Agreement. The dwellings are designed to be heated purely from passive solar gains and incidental internal gains. The structure's high thermal mass moderates the internal temperature against external variations, as heat gains are stored and released over long periods of time. The entire building envelope is highly

insulated with 300mm of Jablite expanded polystyrene surrounding the external sidewalls, roof and slab floor of the structure. Within this insulating envelope lie a 200mm thick reinforced concrete roof, a 300mm floor slab and a 450mm thick rear wall. On top of the insulating envelope is an impermeable double-layer waterproof membrane and 400mm of grassed earth.

Table 2. 4: Hockerton Housing Construction Details (Web 2.3)

Construction Details	Construction/Materials	U-Value (W/m²K)
Walls	The front wall (conservatory rear wall) has a 150mm Drytherm filled cavity. The conservatory and entrance porch act as thermal buffer zones on the exposed south facade. The design allows the conservatory to be completely isolated from the main house during winter.	0.11
Roof	The soil on the roof acts as a thermal flywheel, as the temperature of the soillags weeks behind seasonal changes in air temperature. During the summer, the winter/spring temperature soil draws heat from the structure and provides cooling. Conversely, during the winter, the summer/autumn temperature soil lessens the temperature difference between inside and out, therefore reducing heat loss.	0.11
Floors	The internal structure is kept as exposed as possible, which maximises its ability to absorb and emit heat. Carpets have an insulating effect on the floor's heat transfer capability, therefore clay tiles have been used for most of the floor coverings. The floor slab extends three metres in front of the main living space to accommodate the conservatory floor. This is thermally broken from the house floor slab to reduce heat loss to the conservatory space during cold weather.	0.11
Windows	Two layers of high specification glazing are used across the south facade. Between the bays and the conservatory, triple glazed windows with two layers of low-emissivity coating, insulated spacers and argon gas filling are used. The outer conservatory glazing is double glazed with a low-e coating. All window frames and doors are imported by Swedhouse Ltd. and are made of timber from a sustainable Swedish redwood source. There are no glazed elements on any other facade.	1.15 (triple glazed) 1.90 (double glazed)

➤ Construction Impact

The onsite environmental impact of the construction process was limited through the careful choice of materials and the reduction of construction waste, including packaging. The self-build nature of the construction meant that waste produced from a particular operation was often incorporated into another aspect of the project. The concrete used was quarried locally to reduce transport energy use, and the project has planted over 4000 trees on the land to offset the CO₂ generated by the energy embodied in the construction materials. The facing bricks used on the south-facing facade were supplied by a local company that uses landfill gas (methane) to fire them. The earth covering significantly lessens the visual impact of the houses from the surrounding roads.

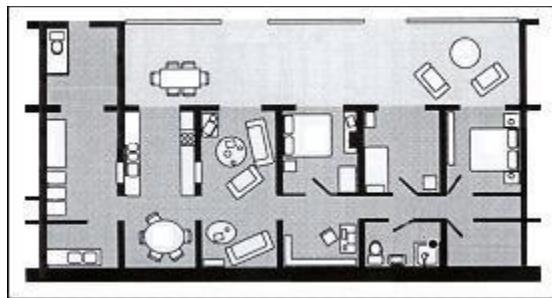


Figure 2. 4: Internal layout of six bay dwelling (Web 2.3)

2.3.4 Hollies Barn (Eakring, Nottinghamshire, England)

Hollies Barn is a private development that sees the refurbishment of a former Victorian barn into a large, four-bedroom dwelling. It is a detached, U-shaped, barn conversion. The original solid brick walls have been upgraded internally to provide a highly insulated and airtight envelope, which incorporates a high level of internally exposed thermal mass. The methodology is very similar to that employed by the Hockerton Housing Project, which to a large extent inspired the current owner to take

this route. Other technologies and methods used in the development have also been chosen as a result of the influence and availability of local expertise and systems that now exist within this area of Nottinghamshire. Hockerton’s earth sheltered scheme, the Vale’s Autonomous House and Gusto Construction Ltd are all within easy reach and appear to be having a positive influence on other developments within the region. The project also includes high specification glazing, rainwater harvesting and reed-bed grey water treatment, space for home-working and good accessibility features. Passive Solar Design (PSD) has been considered in the internal layout of the dwelling and the finished design will provide a high quality and contemporary home for the residents.

➤ Project Objectives

The project aims to create a comfortable home that is CO₂ neutral in its day-to-day energy consumption and that can be used to inspire other people to do the same.

➤ Construction Details

Table 2.5 illustrates the building construction details and materials used of walls, roof, floors windows and doors.

Table 2. 5: Hollies Barn Construction Details (Web 2.3)

Construction Details	Construction/Materials	U-value (W/m²K)
Walls	300–350mm original solid brick wall, lined internally with 150mm polystyrene sheet, and enclosed by 100mm dense concrete block to provide a large amount of thermal mass. This is then faced with wet plaster, to increase the air-tightness of the structure.	0.20
Roof	Clay-pantiles fixed to wooden battens upon 40mm Kingspan insulated sarking board. The space between the rafters is filled with either 100mm of rigid polystyrene, or 100mm of fibreglass. A further 40mm of insulated Kingspan plasterboard is attached to the underside of the rafters to reduce thermal bridging.	0.14

Floors	A 100mm concrete slab is used to tie the walls together at ground level. On top of this is laid a 300mm EPS slab, upon which a 200–300mm concrete raft is laid, giving the internal room area a very large amount of exposed thermal mass.	0.16
Windows	Bespoke double glazed units with oak timber frames, low-emissivity coated glass and a 28mm gap filled with argon gas.	1.80
Doors	Bespoke units made from English oak.	1.80

2.3.5 Fosse Estate (Newark, Nottingham shire, England)



Figure 2. 5: Image for Fosse Estate (Web 2.3)

This project was built in 1999 on a brownfield site and incorporates high levels of thermal insulation, a covered street, level access to all properties and four units built for residents with higher needs as a result of physical disabilities. The construction incorporates the Masonite ‘I’-beam system, which is sourced from sustainable Scandinavian wood, reduces waste onsite and incorporates element recycled wood waste. This system also allows for the easy construction of wide cavities, providing for high levels of insulation, and reduces the amount of heat lost through thermal bridging via the studs when compared to traditional timber frame systems. The dwellings are orientated to maximise solar gains and are arranged internally so that the main living areas face south. Communal space is provided internally by the covered street, and externally by communal gardens.

➤ Project Objectives

The project aims to create a group of energy efficient bungalows for older persons.

➤ Construction Details

This was a brownfield site, formerly occupied by three 5-storey blocks of flats that were demolished. The development consists of 33 terrace dwellings arranged in five groups around the site. The largest group consists of 20 units while others contain three or four units each. The units are orientated to maximise passive solar thermal gain, thereby reducing heating costs and greenhouse gas emissions.

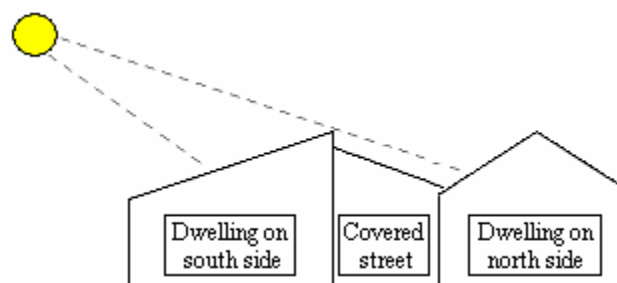


Figure 2. 6: The layout of terrace rows on either side of the glazed covered sheet

(Web 2.3)

The use of a mono-pitched roof on the southern dwellings provides shading to the covered street shown in Figure 2.6, prevents it from overheating during the summer. The covered street encloses a peripheral wall of the dwellings, thereby reducing heat loss by buffering this element from external weather conditions. In the case of the largest group of dwellings, the covered street is nearly 50 metres long and provides a valuable circulation space for the residents.

Table 2. 6: Fosse Estate Construction Details (Web 2.3)

Construction Details	Construction/Materials	U-value (W/m ² K)

Walls	Timber frame breathing wall construction Masonite 'I'-beam studs to provide a 150mm cavity that is filled with recycled cellulose (paper) slabs	0.21
Roof	Concrete tiles upon prefabricated timber trusses. The loft floor is insulated with 200mm of mineral wool insulation.	0.18
Floors	Timber raft floor above insulated concrete base.	0.35
Windows	U-PVC double-glazed units	2.50

2.4 Findings

As interest increases in the concept of zero-carbon homes-buildings that do not consume any non-renewable energy, there are many ways to improve buildings energy efficiency, such as optimizing building's form, orientation, construction and materials used. Above low energy buildings cases have illustrated each building's function, form, construction details and materials used. This case of Tarmac Code 6 home shows zero carbon buildings are achievable. However, windows within the building are still the weakest part in terms of heat loss.

The results show in above Tables that the heat losses (U-Values) through the thermal envelope have been reduced to a significant low level. The best thermal performance window in the case has U-Value of 1.5 W/m²K, which are PVC-U framed double glazing with one low-e coating and argon-gas filled in the gap. Comparing to other building envelope components, it can be seen that windows are the significant heat loss part within the buildings. Therefore to achieve further reduction of energy consumption and to reach "zero carbon level", development of windows with lower thermal properties is an essential issue to carry out. Literature data of some energy-efficient buildings in Denmark has also explored the same problems of windows (Tommerup, 2007).

2.5 Summary

The UK's 21 million homes are responsible for 27% of CO₂ emissions. Space heating is a crucial area to address in order to reduce energy demand. Windows have thus been identified as an important area for energy efficiency improvements since the heat transmission losses through a window may be ten times higher than through the wall. Furthermore, it is easier to renovate or replace windows than most other parts of the building envelope. Base on this fact, currently available window products and technologies will be reviewed and study on the development of novel window system will be carried out.

Chapter 3 Review of Previous Work on High Performance Glazing Types and Windows Technologies

3.1 Purpose of developing high performance window systems

3.1.1 Purpose of reviewing current state-of-the-art glazing types and window technologies

In the context of energy conservation, glazing has been regarded as the weak point in the building envelope. No matter how low window U-values become, they will hardly approach those of the walls that can always be made more insulating by being thicker. Windows with poor U-values can cause significant heat loss and gain in summer and winter, which increase buildings' heating and cooling loads through the year. In modern architecture, highly glazed buildings have become a worldwide design trend for whatever climate. This has given more concern on the global environmental issue of energy wastage. To cope with the sustainability and conservation needs, window glazing has been given revised identities and a wide range of design options (Clarke and Janak, 1998, Corgnati and Perino, 2007). The current advanced fenestration systems may have changeable physical configurations as well as optical and thermal properties in response to weather condition, occupant preferences and building system requirements (Gardiner and Morris, 2009).

The state-of-the-art windows technologies development are not only limited on glazing type study but also keen on integrating with other materials or devices to create termed window system, such as integration with inert gases, water, phase change material (PCM), photovoltaic (PV), etc. The literature review will explore the currently available high performance window products and technologies.

3.1.2 Applications for high performance window system

The new built buildings tend to use low thermal conductive windows in order to reach energy rating system. Better thermal performance windows replacements for old buildings are also required by habitants who wish to cut their energy bills. The development of high performance glazing and window technologies can help in reducing buildings annual energy consumption.

3.2 Advanced glazing types

Glazing can be considered the most important part of fenestration products because it always has large area of the constitute part. U-value of glazing does affect overall window's U-value significantly. State-of-the-art glazing materials and technologies are aim to provide high performance insulation (HPI) or solar gain control (SC) or daylighting (DL) solutions or a combination (S.B. Sadineni, S. Madala and R.F. Boehm, 2011).

3.2.1 Multilayer glazing

Multilayer glazing is mostly for commercial use. Usually multilayer glazing can achieve low U-value, in which triple glazing is the most common glazing type. When the cavities between glass panes are filled with inert gases such as argon or krypton, the thickness, weight and U-value of the window will all reduce. Some samples of the best low U-value triple glazing are shown in Table 3.1 (B.P. Jelle, et al., 2011), glazing U-value (U_g), solar transmittance (T_{sol}), visible solar transmittance (T_{vis}) and the solar factor (SF). Table 3.1 shows that krypton is the most common gas fill for the high performance glazing. Argon is considerably lower cost than krypton, but the best U-value for argon filled triple glazing is $0.64W/m^2K$ and the uses of cavity thickness

of 18mm, which is 12mm wider than the glazing width compared to the glassed in Table 3.1.

Table 3. 1 Literature data for some of the best low-e triple glazing products (B.P. Jelle, et al., 2011)

Manufacturer	Product 4:/12/4/12/:4 Kr90%	U_g (W/m²K)	T_{vis}	T_{sol}	SF	Reference
AGC GlassUK	Top N ⁺	0.50	0.70		0.48	www.float-glass.co.uk/products/AGC_Glaverbel/Summary-tables.pdf (VII. PerformanceSummaryTables)
GUARDIAN Flachglas GmbH	ClimaGuard N ³	0.49	0.72	~0.37	0.54	www.passiv.de and www.eu.en.sunguardglass.com/SunguardProducts/GlassConfigurator/index.htm (calculation tool)
	ClimaGuard N	0.50	0.71	~0.45	0.53	www.guardian-europe.com and www.eu.en.sunguardglass.com/SunguardProducts/GlassConfigurator/index.htm (calculation tool)
INTERPANE Glas	iplus 3CE iplus 3CL	0.49 0.53	0.71 0.72		0.47 0.55	www.passiv.de
Industrie AG						

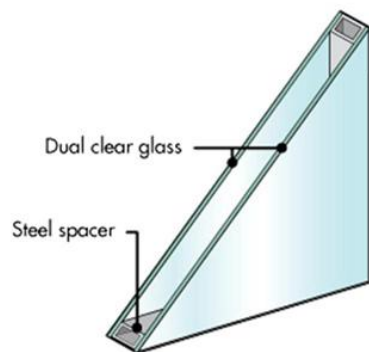
3.2.2 Suspended films

Suspended films are one of the products on the market for multilayer glass with gas fill. Substituting glass panes in between the outer and inner panes, suspended coated films (SCF) or only suspended films are employed for its advantage of lightness. Because they are thinner than ordinary glass panes, these films can reduce the weight of the window and also allow larger gas cavity thickness. Table 3.2 gives two examples of suspended film products on the current market. Comparing to the ordinary multilayer glazing products, suspended films products have competitive U-values as shown in Table 3.2, however drawbacks of these products are the relatively low solar factor (SF) and visible solar transmittance (T_{vis}). In Table 3.2, Serious material product can achieve a very low U-value of 0.28 W/m²K by using high cost xenon fill. SCF technology can work on retrofit of exiting windows as shown in Figure 3.1 without putting away of existing frame and glazing.

Table 3. 2 Literature data for suspended film glazing products (B.P. Jelle, et al., 2011)

Manufacturer	Product	Configuration	U_g (W/m^2K)	T_{vis}	SF	Reference
Serious Materials	1125 Picture Window (SeriousGlass™ 20)	Dual pane, 3low SHG films; Xenon fill	0.28	0.23	0.17	www.vereco.ca/green_document/SeriousWindows_1125_Dsheet1271084115.pdf "SeriousWindows 1125Savesmore energy than any other window. Period." www.SeriousWindows.com
Visionwall Solutions Inc.	Series 204 4-Element Glazing System	6:/26*/20*/26/6 Air 100%*film	0.62	0.50	0.303	VisionwallSolutionsInc.— Performance Values Values for Series 104 and 204 4-element Glazing Systems (from Goran Jakovljevic', jakovljevic@visionwall.com)

Existing window glass units in Empire State Building



New super-insulating glass units with SeriousGlass™ technology

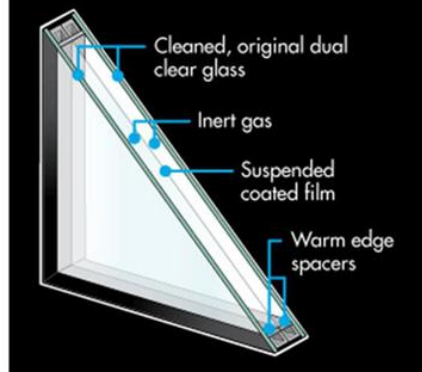


Figure 3. 1: Before and after Empire State Building windows retrofit (Web 3.1, Web 3.2)

3.2.3 Vacuum glazing

The concept of vacuum glazing was first described in a patent literature in 1913 (Zoller, 1924). Despite the idea of using vacuum glazing to increase window thermal resistance has been realized for many years, the first published report of the successful fabrication of a vacuum glazing with low gas conduction was from the University of Sydney until 1989 (Robinson and Collins, 1989). As shown in Figure 3.2, vacuum

glazing consists of two sheets of glass separated by a narrow vacuum space with an array of support pillars keeping the two sheets of glass apart. The tiny sizes of support pillars have no effect on the clear view through vacuum glazing (Garrison and Collins, 1995). The vacuum eliminates heat transport between the glass sheets due to gaseous conduction and convection. In addition, when incorporating a transparent low emittance coating on the internal surfaces of one or both of the glass sheets, radiative heat transport between the glass sheets can be reduced to a low level (Collins and Simko, 1997). Since vacuum glazing were first manufactured and withstand long term tests in University of Sydney, the results show that evacuated glazing with edges sealed using solder glass is suitable for window application as the materials used to seal conventional glazing are far too permeable (Garrison and Collins, 1995).

Jelle (2011) details the best vacuum glazing product on the current market as shown in Table 3.3. This study finds that the thickness of double vacuum window product is half of an ordinary multilayer glass with the same U-value $0.70\text{W/m}^2\text{K}$.

Table 3. 3 Literature data for SPACIA-21 vacuum glazing (B.P. Jelle, et al., 2011)

Manufacturer	Product	Configuration	U_g ($\text{W/m}^2\text{K}$)	T_{vis}	T_{sol}	R_{sol}	SF	Reference
Pilkington/NSG	SPACIA-21	3:/12/3/0.2*/:3 Ar 90% *vacuum	0.70	0.533	0.228	0.401	0.32	www.nsg-spacia.co.jp/spacia21/performance.html

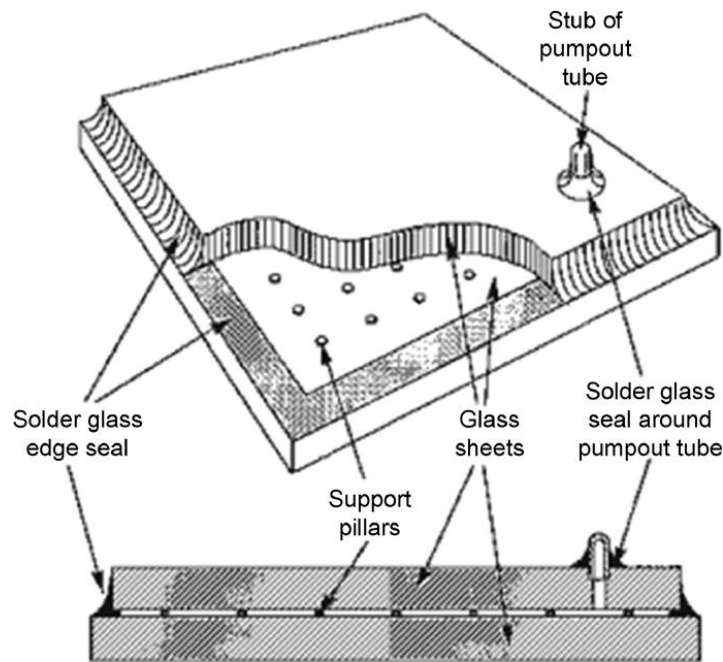


Figure 3. 2: Schematic diagram of a vacuum glazing (Web 3.3)

Other researchers suggested that use of triple vacuum glazing concept can significantly reduce the thermal transmittance compared to the current double vacuum glazing product. According to the research by Manz (2006), a center of glazing thermal transmittance of less than $0.2\text{W}/\text{m}^2\text{K}$ can be achieved by using stainless steel support pillars, 6mm/4mm/6mm sheets of untempered soda-lime glass and four low-emittance coatings ($\epsilon=0.03$). The previous study also explores that the second cavity of triple vacuum glazing can result the thermal resistance twice that of double vacuum glazing.

Electrochromic evacuated advanced glazing has been recently developed by Papaefthimiou (2006). Electrochromic evacuated glazing prototypes have been fabricated using vacuum techniques and chemical methods, combining optimum dynamic control of the solar radiation penetrating into buildings with a high degree of thermal insulation. This was achieved by the optimisation of the electrochromic device materials (electrochromic, ion storage, protective layers, transparent

conductors and polymer electrolytes) and by refinement of a sealing method for evacuated glazing. The prototypes demonstrate excellent optical and thermal performance, with a contrast ratio up to 1:32 (visible dynamic transmittance range in relation to real working environment conditions has been assessed through indoor and outdoor testing. Such a glazing can be used in building applications to improve occupant thermal comfort, contribute to a reduction in space heating and cooling loads and allow for increased areas of fenestration thereby reducing artificial lighting loads. (Papaefthimiou et al., 2006).

3.2.4 Low-emissivity coating

Low-emissivity (low-e) refers to a low emissivity over the long wavelength portion of the spectrum. Spectrally selective low-e coatings exist which allow a high proportion of the visible light in the solar spectrum to be transmitted but block much of the other wavelengths responsible for solar heat gains. The effect of these spectrally tuned soft low-e coated double glazed units, with the coating positioned on the inside surface of the outer panes, is to allow good day lighting without the penalties of overheating or increased cooling load. The positioning of the coating is important for reducing heat gain. With the coating on the outer pane, most of the absorbed energy will be dissipated to external ambient, rather than re-radiated inwards.

Low-e coatings in colors of gold, silver or copper offer a range of solar control characteristics. A typical coating (of thickness around $0.1\ \mu\text{m}$) has three layers, i.e. a thin metal layer sandwiched between two dielectric layers. Its application is able to change the original long wave ($\lambda > 3\ \mu\text{m}$) emissivity of around 0.9 to less than 0.1. There are two basic coating techniques: pyrolytic and sputtered, which can be categorized into hard and soft coatings. In pyrolytic coating, high temperature metallic

oxide is deposited directly onto the glass surface. This method results a hard surface layer with good durability. The low-temperature sputtered process produces soft coats that can be deposited both on flat glass sheets and thin plastic films. Soft coatings have higher infrared reflection and are more transparent than hard coatings. But they are less durable and should be protected against humidity and physical contact. The reductions in room heat gain through the addition of the low-e coating are around 48%. The SHGC and U-factor values are also reduced, but good values of visible solar transmittance can be maintained. The glass surface temperature is extensive ($>40^{\circ}\text{C}$). Reversing the glass plate (i.e. with low-e coating at surface) is able to reduce the glass temperature by $5\text{-}9^{\circ}\text{C}$, but the room heat gain will be increased by 14-21%.

Low-e-coated glazing is popular used in modern architecture over the world. Low-e window coated with a thin film layer that exhibits low thermal emittance and high solar transmittance. With low-e coating, large quantity of heat transfer by radiation could be reduced. Therefore low emittance windows are used to reduce the thermal losses. Low -e coating has significant influence on glazing U-value. Substantial amount of the long-wave radiation could be reflected by employing a low-e coating either on one glass surface or both surfaces bounding the air gap of window units. In previous study, generally the effective emissivity ranges from 0.05 to 0.12 for low-e coatings, and for uncoated float glass the emissivity ε is 0.88. In air cavity of a double-pane window with uncoated surfaces, the long-wave radiation exchange between glass surfaces is larger than the case with low-e coating, thus the glazing U-value could be substantially reduced (J. Han, L. LU and H. Yang, 2010).

Different products exist with different visible (T_{vis}) and total solar energy transmittances. A key characteristic is the ratio of visible to solar transmittance – the higher this ratio the cooler the daylighting provided. The current best performing

products is $T_{vis}=66\%$ and total solar transmission=34% (manufacturers figures). The physical theoretical limit is roughly $T_{vis}=60\%$ and total solar transmission=25% (Johnson, 1991). The problem with low-e coated windows is slight decrease in the light transmittance that makes darker inside building and higher reflectance when viewed from the outside. If several low-e panes are used, the room might be perceived as darker and more enclosed (Bülow-Hübe, 1995). Also the cost of low-e windows production is higher.

Jelle (2011) gives the examples of available hard and soft low-e coatings in the current market as shown in Table 3.4.

Table 3. 4 Examples of hard and soft low-e coatings currently available

Manufacturer	Product	Coating	ϵ	Reference
Pilkington	K Glass™	Hard	0.17	www.pilkington.com/Europe/Norway/Norwegian/products/bp/bybenefit/thermalinsulation/optitherms3/default.htm
	Opitherm™ S3	Soft	0.037	
	Opitherm™ S1	Soft	0.013	
Saint-Gobain Glass UK Ltd	Planitherm	Soft	0.05	www.energy-efficient-glass.com/technical-support.asp
	Total+			
	Planitherm Ultra N	Soft	0.03	

3.2.5 Smart windows

“Smart windows” are able to vary solar factor (SF) and transmittance properties so that a desired level of lighting or heating by solar energy can be obtained. This technology is of much interest for energy efficient architecture, as well as in other fields of emerging technology. Smart windows are categorized into mainly three types: (thermo-, photo- and electro-) chromic materials, liquid crystals and suspended particle devices (Baetens, Jelle and Gustavsen 2010). The variable optical properties require chromogenic materials (LamSmart and Granquist 1990, Granqvist 1991), to make windows are essentially “variable tint” glazing. The use of chromogenic

technologies are to change optical properties in response to external stimulus, such as electrochromic (EC), which responds to electrical voltage or charge; thermochromic (TC), which responds to temperature; photochromic (responding to UV light); gasochromic (responding to reducing or oxidizing gases). An electrochromic (EC) coating, typically about 1 μm thick, consists of five layers on glass substrate. A thin metallic coating of nickel or tungsten oxide is sandwiched between two transparent electrical conductors, through which a distributed electrical field is set up when a voltage is applied. The glazing switches between the clear (bleached) and fully colored (transparent prussian blue tinted) states with little degradation in view, and can be modulated to any intermediate state as well. The switching action requires only low-voltage power (0-10V DC). The upper and lower limits of VT are within the ranges of 0.50-0.70 and 0.02-0.25, respectively. The switching speed is tied to the size and temperature of the window, typically longer for coloring than bleaching. The SHGC ranges from 0.10 to 0.50. At the fully colored state, its energy performance is similar to the tinted glazing (Chow and Li, 2010). The previous research suggested that EC windows cannot provide full control uncomfortable direct sunlight effects, such as disability glare and high-luminance spots (Piccolo and Pennisi, 2009; Piccolo and Simone, 2009). According to literature review by Jelle (2011), along with suspended films, smart windows have the potential to be widely applied to existing windows. Smart windows with light adjustment function are generally based on the electrochromic type or other types using a wired electric control system and the autonomously responsive type without wire. The latter is a thermally sensitive system that achieves light adjustment by relying on the temperature. The previous research on laminated glass using hydrogel (D. Chahroudi, 1974 and H.R. Wilson, 1995) or

polymer blend (H.R. Wilson, 1994) and on a glass coated with a thin film of vanadium oxide (G.V. Jorgenson, 1986 and S.M. Babulanam, 1987).

The best electrochromic windows today are shown in Table 3.5.

Table 3. 5 Data for electrochromic windows, where the cycles column refer to the guaranteed number of colouring/bleaching cycles

Manufacturer	Product	Size (mm×mm)	U_g (W/m ² K)	T _{vis}	T _{sol}	SF	Cycles	Reference
ChromoGenics AB		800×800						www.chromogenics.com
EControl-Glas GmbH & Co.KG	EControl	1200×2200	1.1	0.50-	0.36-	0.15	0.12	10-year gurantee
	Double Glass							
	EControl Triple Glass Kr		0.5	0.45-	0.30-	0.14	0.10	
GESIMAT GmbH		800×1200		0.75- 0.08	0.52- 0.06		10-year gurantee	www.gesimat.de
SAGE Electrochromics, Inc.	ClassicTM	1080×1500	1.59	0.62-	0.40-	0.48-	10 ⁵	www.sage-ec.com
	ClassicTM			0.035	0.015	0.09		
	Triple Glass Kr		0.62	0.52- 0.03	0.27- 0.012	0.38- 0.05		

3.2.6 Photovoltaic (PV) glazing

Increasingly use of solar energy on buildings can reduce carbon footprints. Photovoltaic PV glazing provides both sun shading and electricity generation. The majority come as mono-crystalline silicon wafer (c-Si) solar cells laminated in clear glass panes. The area of the solar cells has significant effect on the total heat gain (Fung and Yang, 2008). Other than using opaque c-Si solar cells, the technology of semi-transparent amorphous silicon (a-Si) solar cells on glass has been developed and commercial products are available (Chehab, 1994; Fath and Nussbaumer, 2002). During the production process, the a-Si cells are made thin by adding a regular pattern of tiny holes. The solar transmittance of the translucent glazing can be adjusted by changing the area of these holes. For this reason, the power output reduction is equivalent to its visual transmittance. The uniformity in visible light transmission

makes it desirable for working environment applications. Comparing the performance of PV glass with 4.3% a-Si cell and clear glass, a reduction of 54.2% of the room heat gain can be achieved in the room with PV glass and an electricity generation of 25.7W. The SHGC is lowered to 0.28, which is comparable to the reflective on tinted glass performance.

At present, investment cost, output efficiency and life expectancy are all drawbacks of PV products. Electricity saving through daylight scheme is considered not substantial for residential applications (Wong and Shimod, 2008).

3.2.7 Aerogels

Aerogels are regarded as one of the most promising high performance thermal insulation materials for buildings application today. The aerogel products reviewed are silica aerogel but they can be made from various materials (Jelle, et al., 2011). Silica aerogel is not a new invention as it was described by Kistler (1931). Monolithic silica aerogel is a highly porous material with pore diameters in the range of 10-100nm. The porosity is above 90%, which combined with the nanometre pore size makes the aerogel a highly insulating material with a thermal conductivity lower than of still air (Fricke, 1986). Optical and thermal properties make the materials possible as insulation layers in windows. Aerogel glazing have high solar energy transmittance (g-value) compared to other highly insulating glazing, which has large influence on annual energy consumption for space heating in cold climate (Schultz, Jensen and Kristiansen, 2005).

Schultz (2005) describes that aerogel has low tensile strength, which makes the material fragile. If aerogels are in contact with water, the surface tension in the pores would demolish the aerogel structure. Hence the application for aerogel window

glazing requires the aerogel to be protected against water and tensile stress. Aerogels need to be placed between two layers of glass with a gas and vapour tight rim seal (Schultz, Jensen and Kristiansen, 2005). In the previous study, Duer (1998) explained aerogel is very strong in compression, which makes it possible to use the material in a sandwich construction, e.g. between two sheets of glass.

Today Aerogel products are more suitable to roofing and facades in commercial buildings or sports halls because their translucent optical characters. Until a clear aerogel glazing is available, it can be applied to conventional residential windows.

Table 3.6 shows the properties of available aerogel products (Jelle, et al., 2011).

Table 3. 6 Literature data for aerogel glazing products (Jelle, et al., 2011)

Manufacturer	Product	Configuration (mm)	U_g ($W/m^2 K$)	T_{vis}	SF	Reference
Advanced Glazings Ltd.	Solera+Nanogel	76.2(just aerogel, glass to order)	0.31	0.07-0.32	0.31-0.07	http://www.advancedglazings.com/nanogel/
Cabot Corporation	Nanogels Aerogel	10	1.38	0.80		“Nanogel Aerogel Daylighting—The New Standard in Eco-Daylighting Solutions” www.nanogel.com
		20	0.78	0.62		
		40	0.42	0.39		
		70	0.25	0.19		
Okalux GmbH	Okagel	4/30/6 or 4/60/6 outer glass /aerogel/ inner glass	0.6 or 0.3	≤ 0.59 or ≤ 0.45	≤ 0.61 or ≤ 0.54	http://www.okalux.de/en/products/brands/okagel.html

3.2.8 PCM filled glazing

Ideally using a window system consisting of insulating glass is to provide comfort living, simultaneously achieve energy conservation in both winter and summer. Application of phase change material into the window is not new technology. The Affinity Intelligent Window (AIW) was used experimentally in a new environmentally compatible building in Tokyo in 1997. Japanese researcher presented research to develop on AIW in 1998. The window used the phase transition materials to achieve autonomously responsive and light adjustment functions. The materials are

used such as highly viscous polymer aqueous solution or hydrogel, which consists mainly of water, water-soluble polymer with hydrophobic groups, an amphipathic molecule and sodium chloride (H. Watanabe, 1998). The previous problems of the hydrogel were developed, such as lack of durability and toxicity. The special type of hydrogel developed in that time was an intelligent material that undergoes phase transition with homogeneous reversibility by utilizing solar energy and sensing environmental temperature changes. Such a window system would transmit direct sunlight in winter to alleviate the interior heating load but shield off direct sunlight to alleviate the cooling load in summer. Also peripheral technologies were established for sealing and lamination, the Affinity Intelligent Window (AIW) can be produced with a large area of 1m^2 for practical use (H. Watanabe, 1998). Figure show AIW demonstrated excellent phase transition from a water-clear state (Figure 3.3) to paper-white state (Figure 3.4) due to solar energy, and the reversible change occurred repeatedly. There was also no special problem with hydrogel downflow due to gravitation when left in a vertical position (H. Watanabe, 1998).

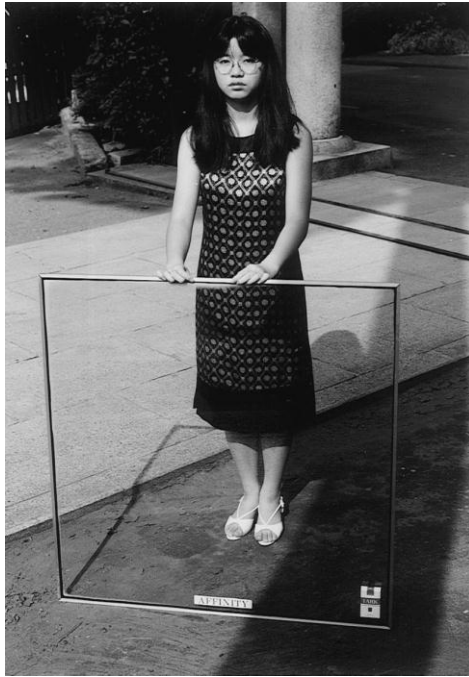


Figure 3. 3: The AIW appeared in the water-clear state without haze and color. The size was a square meter (H. Watanabe, 1998)

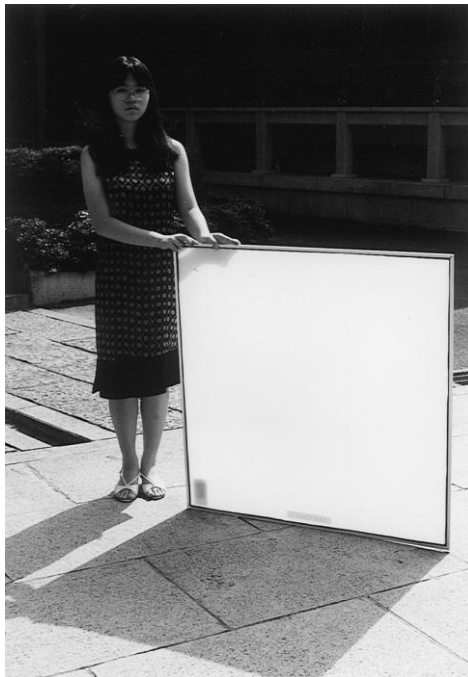


Figure 3. 4: The AIW changed to the paper-white state with enough shadow by solar energy. The size was a square meter (H. Watanabe, 1998)

3.2.9 Gas filled glazing

Apart from vacuum glass panels, aerogels and PCM filled glazing, noble gas filled glazing can also offer good thermal insulating effects. In general, gas has relative high thermal conductivity, i.e. thermal conductivity of air is about 26mW/mK at the room temperature and atmospheric pressure, argon (Ar) 18mW/mK, krypton (Kr) 9.5 mW/mK, xenon (Xe) 5.5 mW/mK. Argon is widespread used as a gas fill in today's fenestration products because of its lower cost compared to krypton and xenon.

3.2.10 Self-cleaning glazing

Watanabe, Hashimoto and Fujishima (1992) first demonstrated self-cleaning concept on a titania-coated ceramic tile in 1992. The TiO₂ surface can decompose organic contamination with the aid of ultraviolet light. One of the first commercialized products using this technique was the self-cleaning cover glass for highway tunnel lamps. This type of lamp, which is often a sodium lamp in Japan, emits UV light of about 3mW/cm² at the position of the cover glass. This UV light is of no use for lighting, but it is sufficient to decompose the contamination from exhaust compounds. As a result, the cover glass can maintain transparency for long-term use.

The efficacy of self-cleaning surfaces was found to be dependent on the relative rates of decontamination vs. contamination. The TiO₂ photocatalyst can maintain the surface clean only when the photocatalytic decontamination rate is greater than that of contamination. Wang observed that the self-cleaning effect of TiO₂ surface could be enhanced when water flow, such as natural rainfall (Wang and Hashimoto, 1998). They attributed this enhancing phenomenon of water flow to the superhydrophilic property of TiO₂ surface as shown in Figure 3.5. Water penetrated the molecular-level space between the stain and superhydrophilic TiO₂ surface. In other words, this

phenomenon has effectively removed the limitation of the self-cleaning function of TiO_2 photocatalysis set by the number of incident photons. Even though the number of photons maybe insufficient to decompose the adsorbed stain, the surface is maintained clean when water is supplied there. Thus, they suggested that the best use of self-cleaning TiO_2 surfaces should be exterior construction materials, since these materials could be exposed to abundant sunlight and natural rainfall (Fujishima and Hashimoto, 1999). Such materials, including tiles, glass, aluminium siding, plastic films, tent materials, cement, etc., have already been commercialized in Japan since the late 1990s and in other countries in recent years (Fujishima and zhang, 2006 and Cassar, 2004).

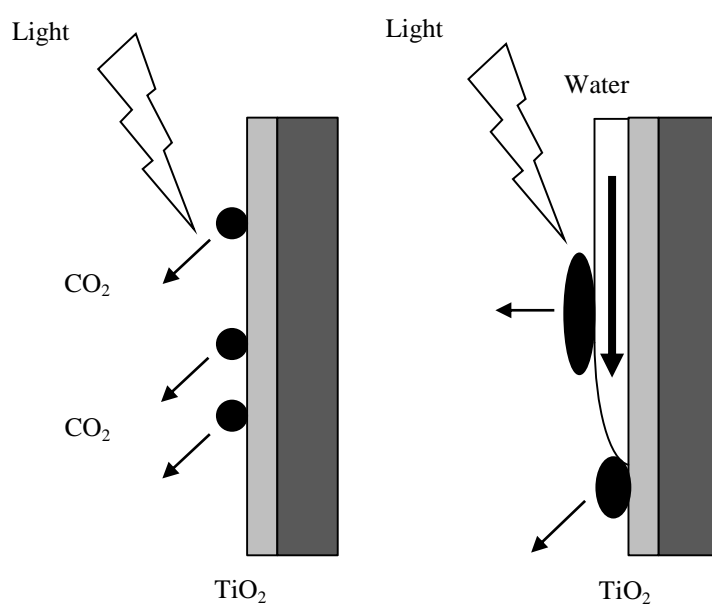


Figure 3. 5: Schematic diagram of the decontamination process occurring on the superhydrophilic self-cleaning surface (Fujishima and zhang, 2006). ©2006, Elsevier Science Ltd.

As estimated by TOTO, Ltd., the pioneer of self-cleaning technology, a building in a Japanese city covered with ordinary tiles should be cleaned at least every five years to maintain a good appearance, while that covered with self-cleaning tiles should remain

clean over a span of twenty years without any maintenance. Therefore, self-cleaning technology can lead to large decreases in maintenance costs. In Japan, several thousand tall buildings have been covered with TOTO's self-cleaning tiles. The Central Japan International Airport, which opened in February, 2005 near Nagoya, Japan, used over 20,000m² of self-cleaning glass manufactured by the Nippon Sheet Glass Co. Self-cleaning tent materials have been widely applied for storage structures, business facilities, bus and train stations, sports centres, sunshades in parks and at the seaside. The PanaHome Company, one of the major house manufacturers in Japan, has marketed “eco-life”-type houses since 2003; self-cleaning tiles and windows, in addition to a solar cell-covered roof-top, are utilized. New applications of self-cleaning technology are also under examination. Table 3.7 shows properties of some self-cleaning glazing products (Jelle, 2011).

Table 3. 7 Literature data for self-cleaning glazing products (Jelle, 2011)

Manufacturer	Product	Configuration	U_g (W/m ² K)	T_{vis}	SF	Reference
Pilkington Group Ltd	Pilkington Activ™ Neutral/Pilkington Optitherm™ S4	:4/16/:4 Ar 90%	1.2	0.44		http://www.pilkingtonselfcleaningglass.co.uk/pdf/literature/0819292%20Activ%20Neutral%20D%20Sheet.pdf
Saint Gobain Glass UK Ltd	SSG BIOCLEAN/SSG PLANITHERM TOTAL+	:4/16/:4 Ar 90%	1.2	0.77	0.67	http://www.selfcleaningglass.com/performance.asp

From Table, it can be seen that U-values of these self-cleaning glazing products are slightly higher than other products reviewed but are still compliant with the UK building codes value.

3.3 Advanced window technologies

Window thermal strategies such as the selection of glazing type and certain window technology are crucial to satisfy different climate needs worldwide. The review of advanced window technologies mainly contains dealing with hot and cold climates.

3.3.1 Window technologies for hot climate

In hot climate or summer season, to decrease heat gain through windows can reduce buildings' cooling load. There are many ways to achieve lower windows heat gain. Sustainable window design for warm climates should follow two basic principles (Chow, et al., 2010): (a) to minimize the solar transmission in particular the infrared portion; (b) to utilize the incident solar radiation as a renewable energy source and thereby to reduce the air-conditioning load.

- Solar absorbing window as water-heating device

Chow (2010) studies the thermal performance of water-flow absorbing window compared to conventional single and double pane absorptive glazing. The device was described as, by connecting the cavity of a double pane window to a water-flow circuit, absorbed solar heat at the glasses can be readily removed by water stream. The simulation result by Chow (2010) shows that the absorbed solar heat at the window glasses can be effectively removed by the feedwater stream that flows at the window cavity, thereby annual heat gain and cooling loads will be reduced.

- Reversible low solar heat gain windows

Windows with low solar heat gain coefficients (SHGC) are designed to reduce glare and solar heat gains during the hot season. Low (SHGC) double glazing windows, with the exterior pane tinted or selectively absorbing can reduce summer cooling loads. In winter windows facing the equator can accept more useful solar radiation

when they are reversed. However windows with SHGC based on reflective coatings are not suitable for reversing because they reflect solar radiation in both positions (D. Feuermann and A. Novoplansky, 1998). According to literature Reversible window frame can be suitable for places with distinct heating and cooling seasons (Chow et al., 2010).

➤ Electrochromic windows with overhangs

Switchable electrochromic (EC) windows rely on a nanometer-thick switchable coating on glass to reversibly change tint (clear to Prussian blue) without loss of view (E.S. Lee and A. Tavit, 2007).

➤ Double-pane window integrated with see-through a-Si PV cells with low-e coatings

Building-integrated photovoltaic (BIPV) systems have been developed rapidly over the past few years. The installations of PV systems could be any possible part of the buildings relying on incident solar radiation angle. There is increasing numbers of PV systems integrated into energy efficient buildings' façade, especially on the window panes. Comparing with conventional structures, less solar radiation is transmitted through the panels while PV is integrated on window panes as shown in Figure 3.6.

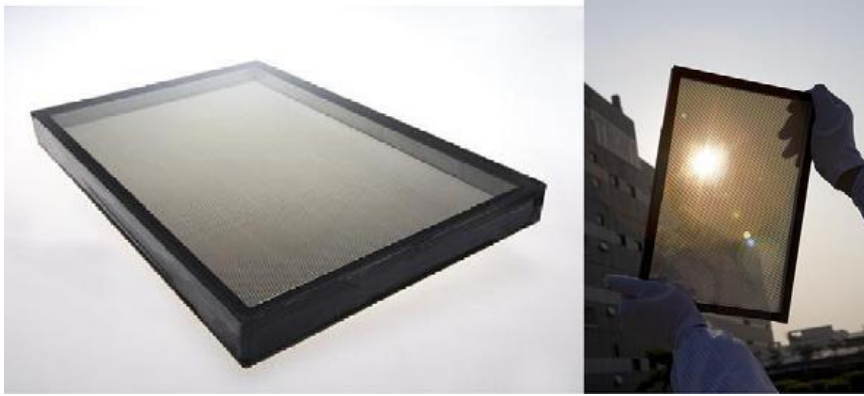


Figure 3. 6: Photo of the a-Si thin film PV module from Trony, Shenzhen, China (Web 3.4).

In order to reduce buildings' cooling loads in summer, shading and blinds are usually employed in the air cavities of the double glazed-window in order to decrease solar transmission through windows. Collins and Simoko (1998) found that a low-e coating on one or two glass surfaces within a vacuum gap of the vacuum glazing can reduce radiative heat transfer across the glazing significantly. Shahid and Naylor (2005) examined the effect of the presence of venetian blind on the thermal performance of a window. Results prove that the presence of a venetian blind improves the energy performance of a single and double-glazed window. Theoretical and experimental work of traditional double-skin façades related to heat transfer by natural convection or multi-mode heat transfer was illustrated by other researchers in their early works, in which, findings of double-skin façades are to reduce buildings' heating and cooling consumptions (J. Han, L. Lu and H. Yang, 2010).

Buildings' façade integrated with semi-transparent PV is a promising application in recent years. The benefits for these kinds of cells are not only to generate electricity but also to provide shade (J. Han, L. Lu and H. Yang, 2010). Li (2009) also finds integrating PV cell with window system could reduce both artificial lighting and cooling energy consumption.

A two-dimensional numerical analysis of the mixed convective heat transfer in double-pane window integrated with see-through a-Si PV cells with low-e coatings was studied by J. Han, L. Lu and H. Yang (2010). The study evaluated the effect of PV glass with low-e coating as thermal control strategy on the heat transmittance. Results indicate that a large quantity of heat transfer by radiation within the air cavity could be reduced by employing PV double-pane window with low-e coating. The finding also shows that in air cavity of a double-pane window with uncoated surfaces, the long-wave radiation exchange between glass surfaces is larger than the case with low-e coatings, thus the glazing U-value could be substantially reduced.

3.3.2 Windows technologies for cold climate

In cold climate or winter season, to increase heat gain through windows can reduce buildings' heating load.

➤ Highly insulating glazing systems

The previous study has summarized the performance of the various advanced glazing technologies for low U-value windows. For passive solar heating applications, materials with low U-value coupled with high total solar energy transmittance are most effective. There is always a trade-off between U-value and solar transmission. Measures to reduce U-value also usually reduce solar transmission, for example: extra panes of glass, low-e coatings or greater thicknesses of transparent insulation material and aerogel.

The study found monolithic aerogel (thickness of 20mm) between two panes of glass evacuated to 0.1 atmospheres performs extremely well with a U-value below $0.5\text{W/m}^2\text{K}$ yet retains a high total solar energy transmittance of nearly 70%. This technology has its problem though; it is expensive and awkward to manufacture and

product gives a hazy view and in appearance is slightly blue in reflection and yellow in transmission due to scattering.

Transparent insulation materials (TIMs) also exhibit good performance but can't be used for view windows.

Multi paned glazing systems, or super-windows, comprise several panes of glass or plastic films, one or more low emissivity coatings, gas cavity fillings and sometimes insulating frames and spacers. These have a poorer performance with regard to U-value and solar transmission but do provide a clear view out.

For triple glazing with two low-e coats of emissivity=0.1, the U-value is approximately 0.9-1.0 W/m²K. For triple glazing with two low-e coating, emissivity of zero (i.e. the ideal case), the U-value is about 0.8W/m²K, thus it can be seen that this technology is reaching its theoretical limit. However the durable and cheaper to manufacture hard low-e coats still have some catching up to do on the sputtered soft coats. Advancements are still to be made in lowering emissivity, though solar transmission properties are superior.

These improvements in hard coatings will also greatly enhance the U-value of evacuated glazing systems which use one or two hard low-e coats to reduce radiative heat flow. (Evacuated glazings comprise two panes of glass separated by an array of barely visible glass pillars of a fraction of a millimetre in depth. A glass welded edge forms the vacuum seal.)

By filling triple glazing cavities with gases of lower conductivity than air, the theoretical limit for triple glazing (e=0.1) is 0.2 W/m²K, but unless convection could be inhibited the practical lower limit is 0.5 W/m²K, with krypton.

➤ PCM filled glass windows and absorbing gas filled windows

The application of phase change material (PCM) into the window has been explained in section 3.2.8. The use of absorbing gases filling the gap between glass sheets appears to be an alternative solution or thermally insulated glass windows (K. A. R Ismail, C.T. Salinas and J.R. Henriquez, 2008).

➤ Ventilated double window

The ventilated double window is composed of two parallel windows forming a gap through which airflows. The gap that is formed between the windows is supplied with fresh air from outside through vents on the base of the outer window. The air that circulates through this gap is warmed by the heat loss transmitted from indoors and by solar gains. Pre-heated rising airflow, by stack effect and wind pressure enters the room through a vent on the top of the roller shutter's case, so the ventilated double window can provide the required ventilation air warmer than the air outside (J.S. Carlos, H. Corvacho and P.D. Silva, 2011).

Results were studied by both mathematical model and experimental measurements over a wide range of design and parameter. The result has shown useful energy of delivered air by ventilated double window system influenced temperature difference between indoors and outdoors, incident solar radiation and airflow rate.

3.4 Advanced glazing technology for low energy buildings in the UK

A study of potential energy and environmental benefits of advanced glazing in the UK was carried out by IEA Task 18 in 1992 (Robinson and Hutchins, 1994). Task 18 of the International Energy Agency Solar Heating and Cooling Programme is the World's largest collaborative research and development project on Advanced Glazing Technology. Fifteen OECD countries have committed more than 100 people years of

effort to this five year project. The national implications of the adoption of advanced glazing systems in the UK both domestic and office sectors are significant in terms of energy saving, such as annual auxiliary heating energy and overheating, annual lighting energy, annual cooling energy.

The purpose of energy rating is to stimulate the use and development of products with better energy performance. In order to rate the energy performance of glazing or windows it is necessary to include both U-value and g-value. To make it easy for private consumers to compare different products to be used in heating dominated house the net energy gain during the heating season can be used.

3.4.1 Solar window technology

Most buildings in the warm climate are single-glazed, with clear glass offered for residential developments and tinted/reflective/low-e glass for commercial applications. Double-glazing is increasingly in use in hot climate region (Chow and Li, 2010). A solar control window is a window coated with a thin film that exhibits low solar transmittance (C. G. Granqvist, 1991 and T. E. Johnson, 1991). Solar control windows are used to reduce the cooling load. In buildings, the net energy gain from glazing and windows both depends on the thermal transmittance (the U-value) and the total solar energy transmittance (the g-value) (T.R. Nielsen, K. Duer and S. Svendsen, 2000).

➤ Tinted glazing

Tinted glass is often called ‘absorptive’ glass because of its high extinction coefficient, low transmittance and high absorptance. Tinted glass is specially formulated to cater for maximum absorption at part of the solar spectrum. The low transmittance reduces the quantity of transmitted daylight. Therefore it’s mainly used to reduce the effects of

discomfort glare and solar transmission. All absorbed radiant energy is initially transformed into heat within the glass, thus raising the glass temperature. The test was done by Chow (2010), with the indoor and outdoor temperatures are 25 and 33°C respectively, the temperature of tinted glazing is 6.6°C higher than the clear glazing. Therefore, a room with tinted glass can reduce 22.4% thermal load.

Traditional tinted glazings are available in bronze and gray colour, which allow a greater reduction in visible transmittance (VT) than in SHGC. New development has discovered that light blue/green tint have higher visible performance and favourably lower solar heat gain in terms of practicality (Chow, 2010).

➤ Reflective glazing

The reflective coating, usually consisted of thin metallic or metal oxide layers, comes in various metallic colors such as bronze, silver, or gold. The SHGC varies with thickness and reflectivity of the coating as well as its location in the glazing system. Reflective coating glazing can achieve higher reduction of 44.9% in solar gain comparing to tinted glazing.

Reflective glazing can cause disturbance on traffic roads and nearby buildings because of its sun mirror effect, therefore the usage of it is limited. However architects are generally fond of reflective glazing because its glare control and appealing outside appearance.

➤ Anti-reflective coated window

Glass with low-e coatings based on SnO₂ (usually) referred to as hard coatings) provides a cost-effective replacement of one of the panes in ordinary double-pane windows. It considerably improves the energy efficiency of the window and at the same time preserves the appearance of old hand-crafted windows. Adding a low

refractive index anti-reflective (AR) coating on both sides of the low-e coated pane in such a double-glazed window makes it possible to achieve high light and solar transmittance, while the U-value remains unaffected (Rosencrätz and Bülow-Hübe, 2005). Previous studies show that the light transmittance (T_{vis}) and the direct solar transmittance that (T_{sol}) increase by up to 10% and 6% respectively by applying AR—coatings on a single low-e pane (Hammarberg and Roos, 2003).

For a double-glazed window with one low-e hard coating, light transmittance was found to increase by as much as 15%, from 74 to 89% transmittance, if both panes were AR-treated, while the emissivity of the low-e coated pane was virtually unaffected. Compared to clear double glazing, the visual transmittance was increased by 7%. The simulation was done by Rosencrätz and Bülow-Hübe (2005), a result shows that monthly average solar factor (g-value) increased by 7% compared to low-e double-glazed window without AR-coatings. The annual heating demand decreased by 4% due to the higher solar transmittance of the window. The AR-coating increased the daylight factor by 21% according to the simulation result. The study has shown that the main benefit of using AR coatings in a low-e window is the improvement of visual transmittance and the resulting increase in the daylight factor.

3.4.2 Edge effects

This study also indicated that U-values of glazing systems are degraded by the edge components: spacers and frames. Therefore new advanced glazing will require new types of frame and edge seal products. Table 3.8-3.10 below show how the centre of glazing U-value, U_{CG} is degraded by the presence of spaces (as represented by the insulating glass unit U-value, U_{IG}) and frames (as represented by the overall window U-value, U_w). Data is shown for traditional and improved materials. Three different

glazing systems, double glazing, double low-e with argon, and triple 2 low-e krypton, are used to illustrate the effect. U-values were calculated by WINDOW 4 program software.

Table 3.8: The effects of edge component heat flow on window U-value, U_w (W/m^2K):

Double glazed, $1m^2$ window, 3-12-3 (Robinson and Hutchins, 1994)

Spacer material	Frame material				Insulating glass only, U_{IG}	Centre of glass, U_{CG}
	aluminium	Aluminium with thermal break	Wood	PVC		
fibreglass	4.55	3.45	2.69	2.54	2.84	2.81
glass	4.63	3.53	2.77	2.62	2.94	2.81
butyl/metal	4.60	3.49	2.73	2.59	2.89	2.81
aluminium	4.65	3.55	2.79	2.64	2.96	2.81

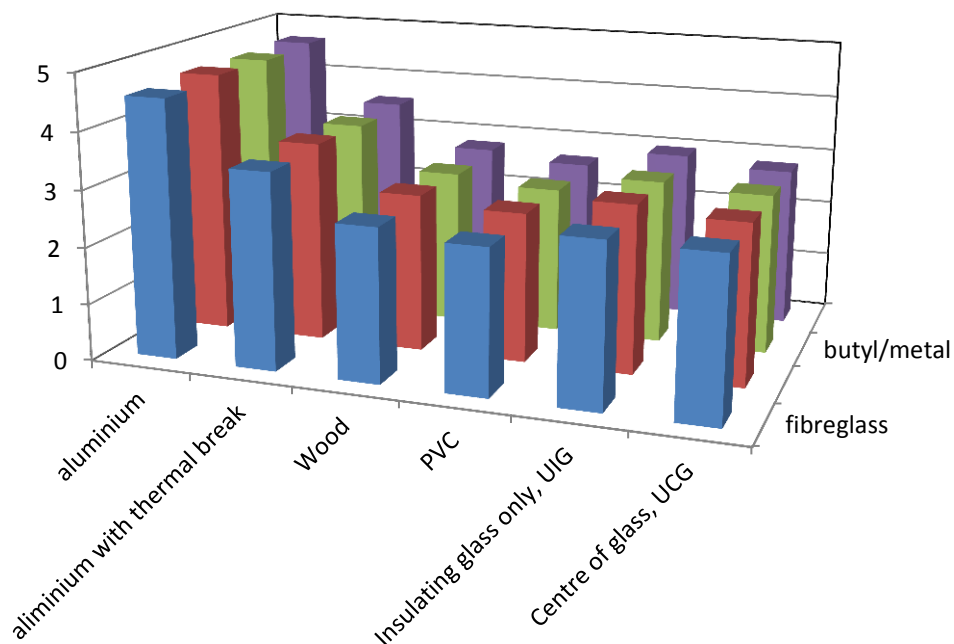


Figure 3. 7: Edge effects: Double glazing, 3-12-3, $1m^2$

Table 3. 9: The effects of edge component heat flow on window U-value, U_w (W/m²K): Double low-e, argon, 1m² window, 3-12-E3 (Robinson and Hutchins, 1994)

Spacer material	Frame material				Insulating glass only, U_{IG}	Centre of glass, U_{CG}
	aluminium	Aluminium with thermal break	Wood	PVC		
fibreglass	3.50	2.40	1.70	1.55	1.50	1.43
glass	3.57	2.47	1.77	1.62	1.59	1.43
butyl/metal	3.57	2.47	1.77	1.62	1.59	1.43
aluminium	3.69	2.59	1.89	1.74	1.75	1.43

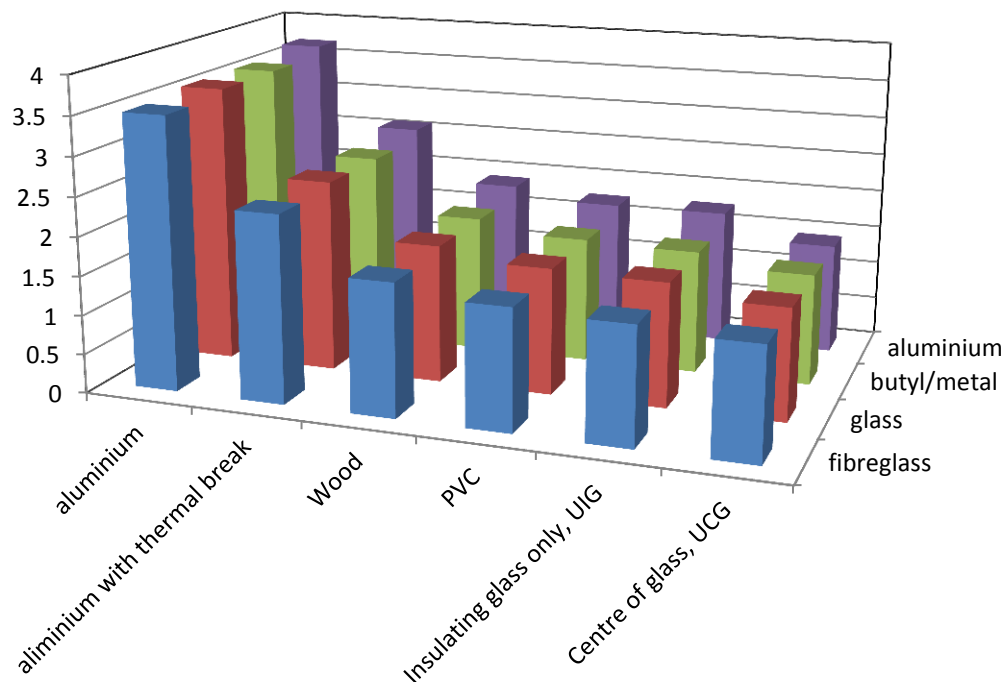


Figure 3. 8: Edge effects: Double, low-e (0.08), argon, 3-12-E3, 1m²

Table 3. 10: The effects of edge component heat flow on window U-value, U_w (W/m²K): Triple, 2 low-e, krypton, 1m² window, 3-10-E3-10-E3 (Robinson and Hutchins, 1994)

Spacer material	Frame material				Insulating glass only, U_{IG}	Centre of glass, U_{CG}
	aluminium	Aluminium with thermal break	Wood	PVC		
fibreglass	2.89	1.79	1.13	0.98	0.73	0.65
glass	2.91	1.81	1.14	0.99	0.75	0.65
butyl/metal	3.02	1.92	1.25	1.11	0.90	0.65
aluminium	3.20	2.09	1.42	1.27	1.12	0.65

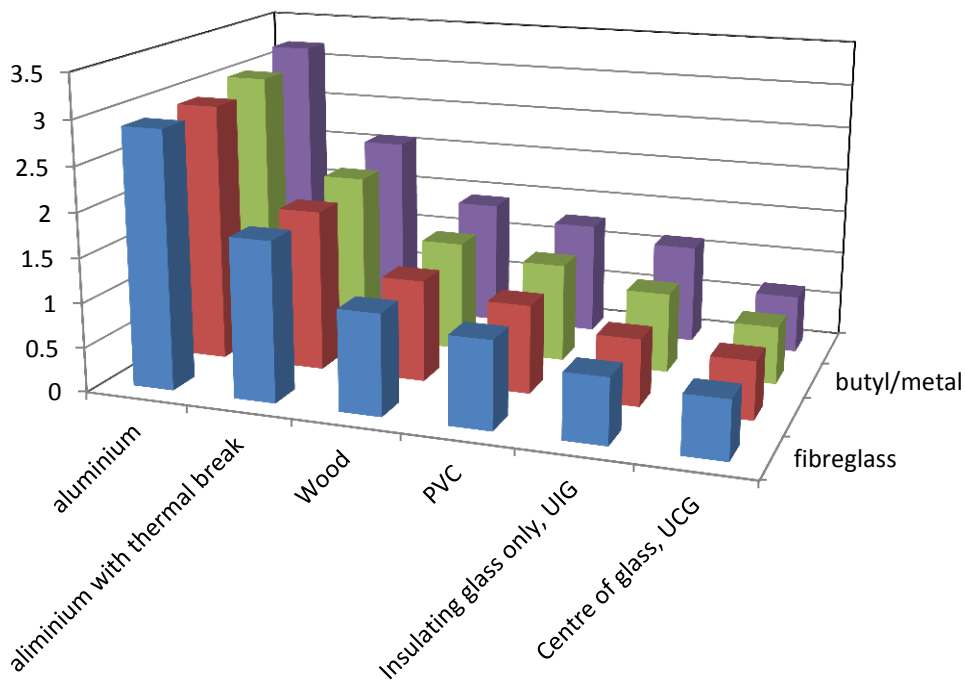


Figure 3. 9: Edge Effects: Triple, 2 low-e, Krypton; 3-10-E3-10-E3, 1m²

The data from Tables 3.8-3.10 is shown graphically in Figures 3.7 to 3.9. The results show that triple glazing technology becomes more advanced than double glazing, however, to achieve lower U-values need to pay more attention on edge heat loss effects. Edge effects are more pronounced the smaller the dimensions of the windows. For high performance windows low profile frames and large glazing area units give the lowest U-values, especially when combined with insulating spacers and frames.

3.5 Conclusion

State of the art glazing materials and technologies that are aimed at providing high performance insulation (HPI) or solar gain control (SC) or day lighting (DL) solutions or a combination. Several currently commercial available low U-values glazing products are reviewed from literature, which include multilayer glazing filled with insert gases, suspended films, vacuum glazing. However drawbacks of these products are heavy, relatively low solar factor (SF) and visible solar transmittance (T_{vis}), complicated manufacture process and high cost, respectively. Manufacturing of windows using vacuum tubes has not been previously reported. This PhD research focuses on energy efficiency issues in terms of reduction of window heat loss, is also concerned with the use of vacuum tubes windows for power generation.

Chapter 4 Novel Vacuum Tubes Window System

4.1 Introduction and objective

Windows are a significant source of transmission heat loss or heat gain at different climate zones. As heat lost through windows represents about 20% of the total heat loss from an average home in UK, energy efficient window technologies are crucial to energy efficiency, and reduction of fuel costs and CO₂ emission. Also increasing thermal resistance of window may help to reduce the condensation problem which is commonly complaint by customers.

A conventional vacuum glazed window consists of two plane sheet of glass separated by a vacuum and small support pillars. The vacuum provides a high insulating value as heat loss via conduction is virtually eliminated. The pillars are positioned between the glass panes with gap of 0.2mm. Vacuum glazed window can eliminate heat transport between the glass sheets due to gaseous conduction and convection. However the main problems with conventional vacuum glazing are: a) High manufacturing cost; b) Difficulty to assemble the glass module; c) Glass is not strong enough and so can easily break; and d) Difficulty to maintain the vacuum seal for a long period. The proposed vacuum tube window will address these issues and would provide a simple and cost effective solution for high performance window systems.

The main aim of this research is to develop the first-of-its-kind high performance window technology using evacuated tube panels. The novel vacuum tube window is expected to provide a simple and cost effective solution for high performance window systems theoretically by achieving a window technology with a U-value less than 0.6 W/m²·K. This new technology would be compatible with the higher levels of the Code for Sustainable Homes and the future requirements of commercial buildings.

4.2 Vacuum tube window system

4.2.1 Prototype descriptions

Termed thermally efficient windows are such as windows having selective solar radiation characteristics, evacuated glass panels, etc. The selective properties due to design of deposited films on the glass sheets, which can absorb or reflect certain wavelength of incident solar radiation and allow to change windows' transmittance, reflectance and absorptance (Lampert, 1981). For evacuated glass tubes, heat transfer by conduction and convection is significantly reduced, which achieves high thermal performance.

This novel window system is constructed by single/double wall vacuum tubes embedded in the frame as shown in Figure 4.1. A vacuum level of 0.001 Pa or lower can be maintained and the insulation cavity can be 5mm or more, which eliminates conductive and convective heat loss. The tubes are made of extremely strong transparent glass that is able to resist a large impact. A prototype window of 1m x 1m has been constructed by Vale Window Company Ltd. The window unit will incorporate vacuum tubes with 48 mm external diameter.



Figure 4. 1: Vacuum tubes window prototype

4.2.2 Mathematical analyses of the energy transfer process and computer programme set up

➤ Energy flow chart

Energy flow through windows normally via (1) conductive and convective heat transfer caused by the temperature difference between outdoor and indoor air, (2) net long-wave (above 2500 nm) radiation exchange between the window and its surroundings and between glazing layers, and (3) short-wave (below 2500 nm) solar radiation incident on the window, either directly from the sun or reflected from the ground or adjacent object (ASHRAE, 2009) (Figure 4.2 and Figure 4.3).

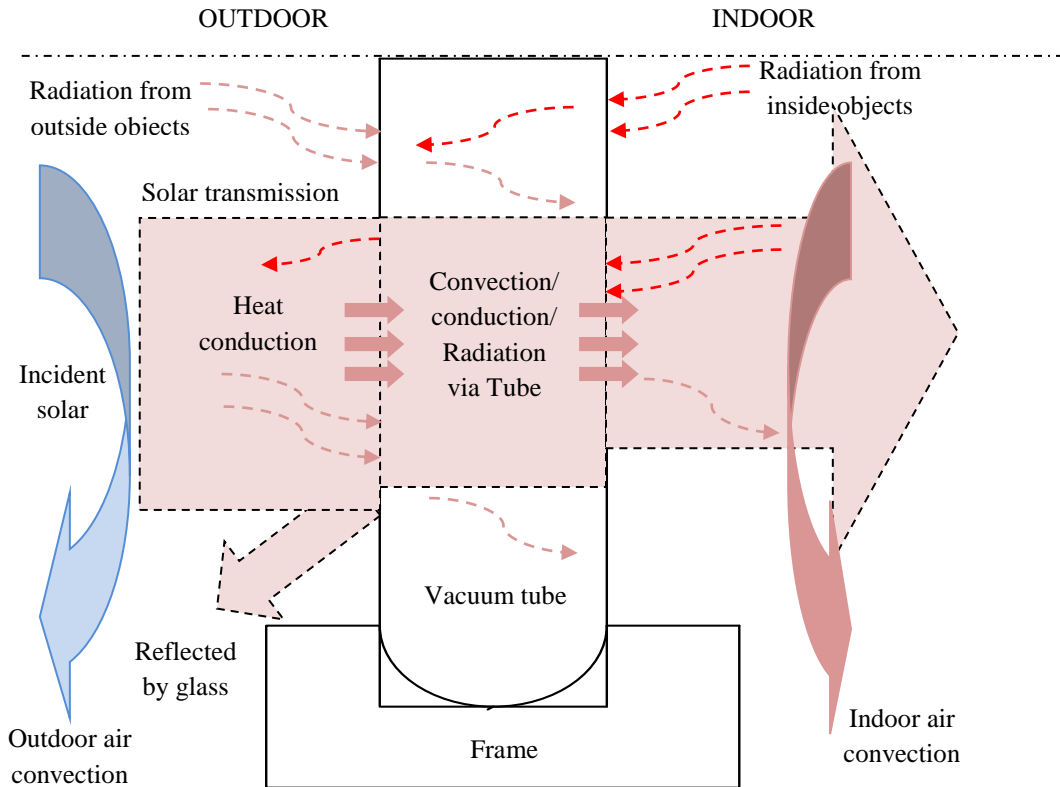


Figure 4. 2: Single-wall Vacuum Tubes Window Construction Details and Solar/Heat Flow Process

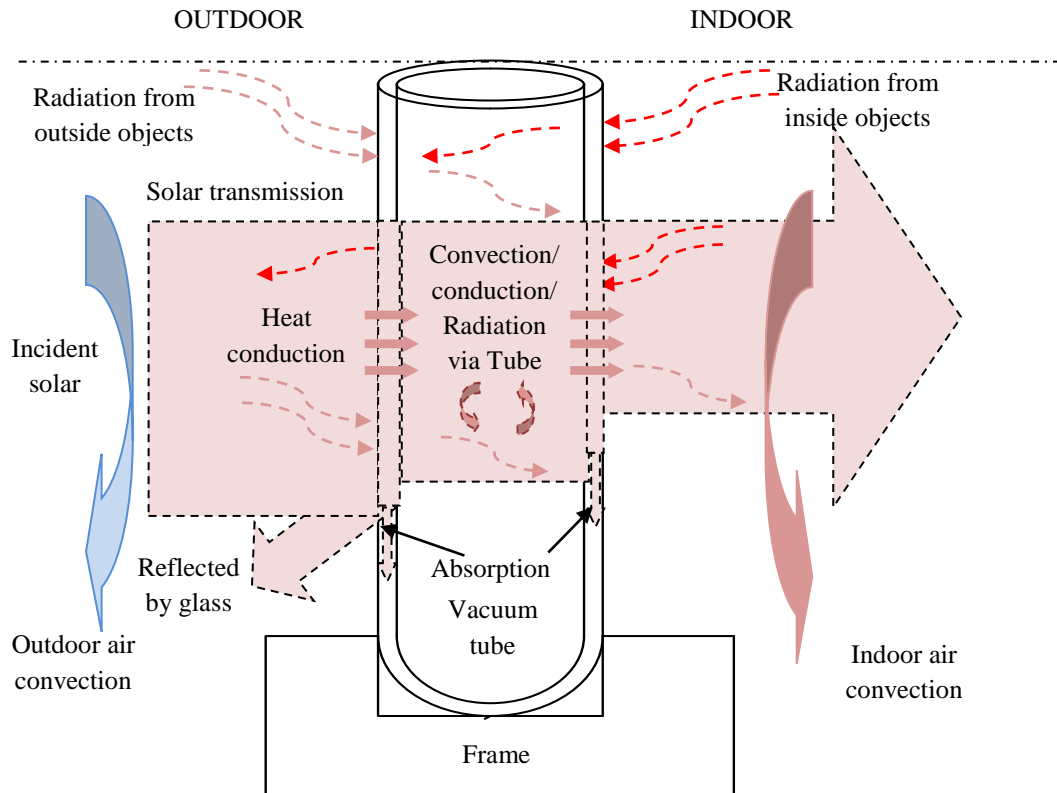


Figure 4. 3: Double-wall Vacuum Tubes Window Construction Details and Solar/Heat Flow Process

➤ Derivation of thermal transportation

For the simplified model, heat transfer in vacuum tube glazing contains (i) the heat transfer to and from the tube surfaces; (ii) heat transport in the evacuated cavity inside the tube; and (iii) heat transfer through connective silicone sealant. Heat transfer in the vacuum tube is composed of conduction and radiation shown as Figure 4.4 and 4.5.

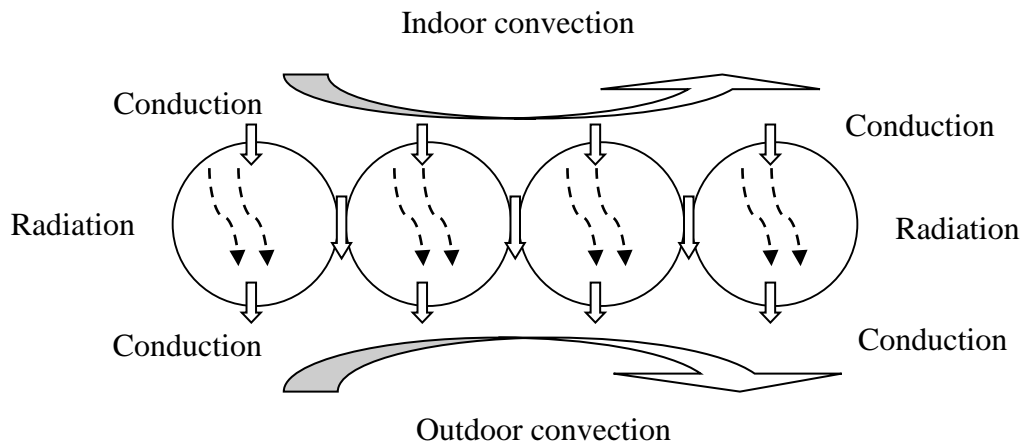


Figure 4. 4: Schematic of Heat Transfer Through Single-wall Vacuum Tubes Window Unit in Winter

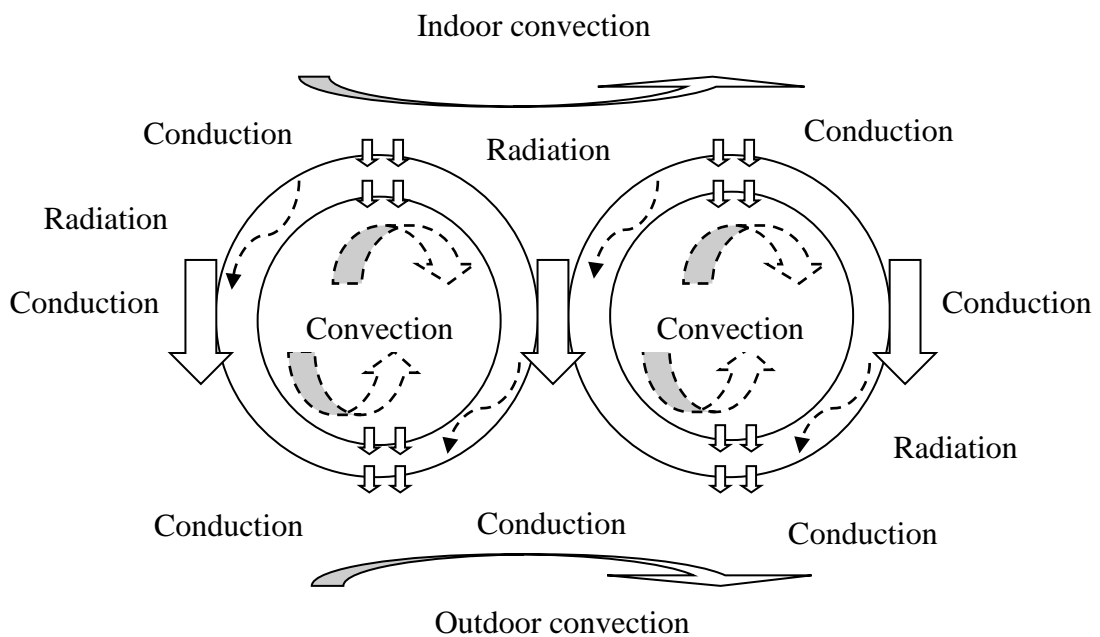


Figure 4. 5: Schematic of Heat Transfer Through Double-wall Vacuum Tubes Window Unit in Winter

The window consists of subdivisions like silicone sealant and frame. The overall heat flow Q_{th} is simply calculated as:

$$Q_{th} = A_g q_g = A_g U_o (t_{max} - t_{min}) = A_{ng} q_{ng} + A_{ss} q_{ss} + A_f q_f \quad (4-1)$$

where q is heat transmittance per square meter, W/m^2 ; A is the square meters, m^2 ; U_o is the overall heat transmittance; t is the temperature, $^{\circ}C$; the subscript ng , g , ss and f refer to the net glazing areas, glazing unit, silicone sealant and frame respectively.

Based on equation (4-1), the overall heat transmittance (U_o) is then estimated by using the area-weighted U-values for contribution (ASHREA, 2009):

$$U_o = \frac{A_{ng}U_{ng} + A_{ss}U_{ss} + A_fU_f}{A_g} \quad (4-2)$$

In principle, the thermal transmittance is the reciprocal of the total thermal resistance (Holman, 1981):

$$R = 1/U_o \quad (4-3)$$

Thus the overall thermal resistance of this novel vacuum tube window unit could be given as following Figure 4.6 and 4.7:

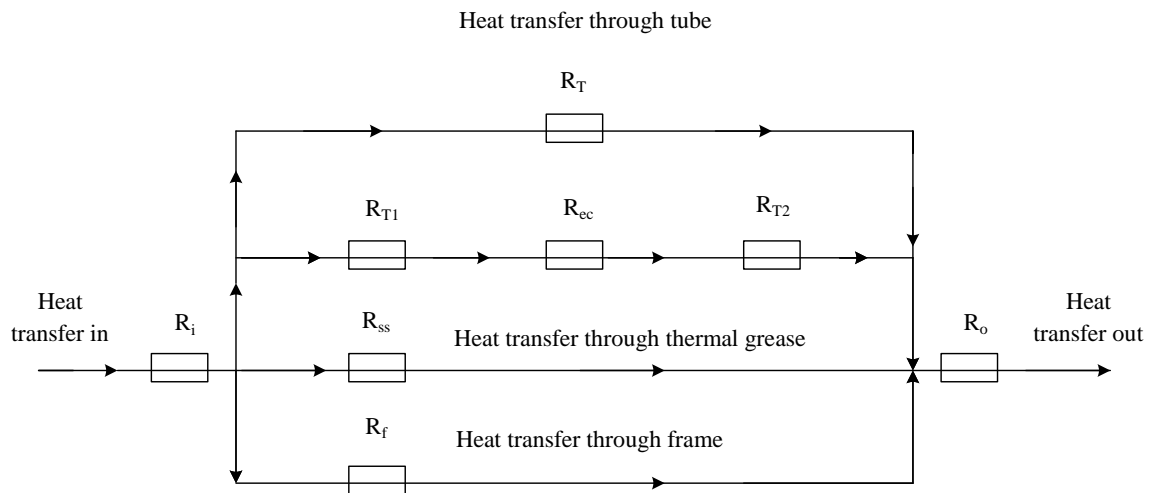


Figure 4. 6: Thermal Network Model of Single-wall Vacuum Tubes Window Unit

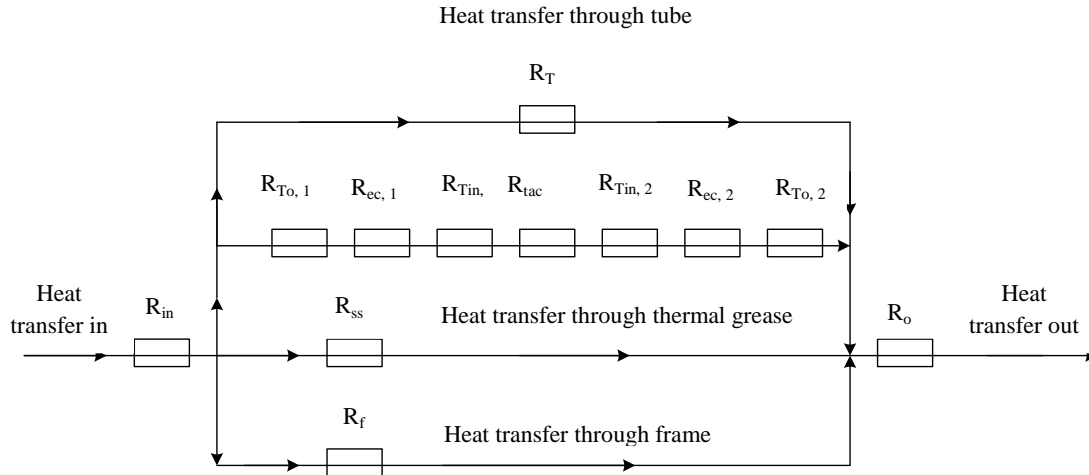


Figure 4. 7: Thermal Network Model of Double-wall Vacuum Tubes Window Unit

➤ Heat transfer through vacuum tube glazing unit

For the thermal transmittance of glazing unit, an analytical solution of heat transfer through the multiple glazing units can be derived from a double glazing unit. Figure 4.4 and 4.5 illustrate the heat transportation process in winter condition. The overall thermal transmittance of vacuum tube glazing unit is written by the following equation (4-4) for single wall vacuum tube window and (4-5) for double wall vacuum tube window.

$$R_{ng} = \frac{1}{h_o} + \sum_{i=1}^2 R_{T,i} + R_{ec} + \frac{1}{h_{in}} \quad (4-4)$$

$$R_{ng} = \frac{1}{h_o} + \sum_{i=1}^2 R_{T,i} + \sum_{i=1}^2 R_{ec,i} + \frac{1}{h_{tac}} + \frac{1}{h_{in}} \quad (4-5)$$

where h is the heat transfer coefficient, W/m^2k and subscription o , T , ec , tac and in respectively represent the outdoor environment, tube layer, evacuated cavity, tube air cavity and indoor thermal coefficient.

- Convective heat transfer on the external side of the building occurs between the surface of the building and the surrounding air at a rate that is determined by

several factors. Since those factors are highly variable, an exact mathematical analysis of the external surface convective heat transfer is not possible. The correlations are based on the building experimental work given in Reference (ISO 15099, 2003 and ITO, 1972).

$$h_o = 4.7 + 7.6V_s \quad (4-6)$$

where, V is the velocity of outdoor air.

-if the surface is windward: $V_s = 0.25 V$; $V > 2$ m/s; $V_s = 0.5$; $V \leq 2$ m/s

-if the surface is leeward: $V_s = 0.3 + 0.05 V$.

Heat transfer coefficient of outside air is given in Figure 4.8, the results show proportional increase when surface is windward (from the point $V > 2$ m/s) and Leeward.

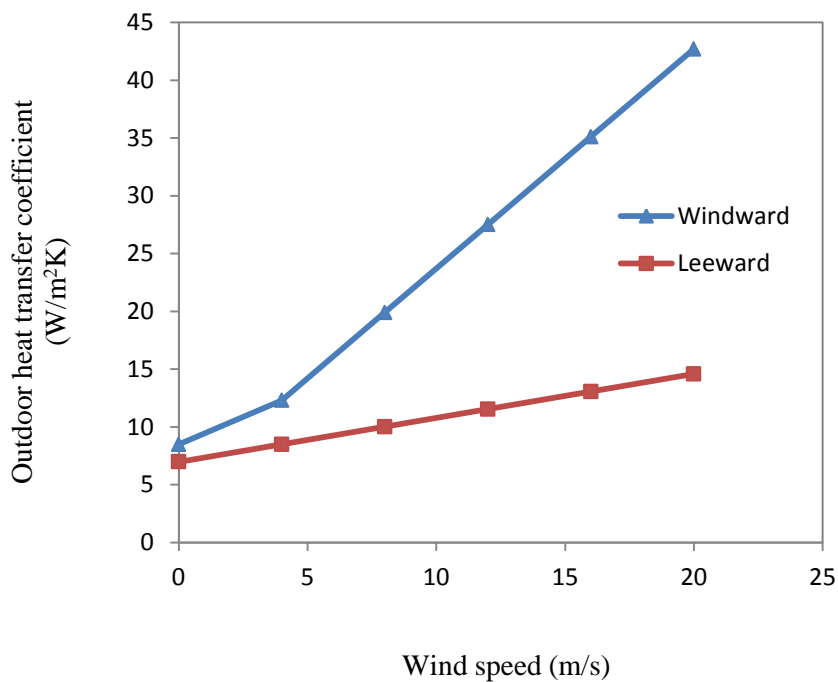


Figure 4. 8: Heat transfer coefficient of outside air for various wind speeds

- The air space in a window constructed using glass with no reflective coating on the air space surfaces has a coefficient nearly constant (ASHREA, 2009).

$$h_{s,i} = h_{tac} = 7.4 \text{ W}/(\text{m}^2 \cdot \text{k}) \quad (4-7)$$

When a reflective coating is applied to an air space surface, h_{tac} can be selected from Table 3 in 15 chapter of reference (ASHREA, 2009).

- Thermal resistance of simplified rectangularity tube layers could be derived from the basic Fourier's law with an unfolded length of πr , where $i \in (1, 2)$:

$$R_{T,i} = \delta_{T,i}/\lambda_{T,i} \quad (4-8)$$

where, δ and λ are the tube glass thickness and conductivity respectively.

Table 4. 1: Technical data of a double-wall vacuum tube provided by the vender

Varieties	Value	Unit
Outer tube diameter	48	mm
Inner tube diameter	38	mm
Glass thickness	1.5mm	mm
Thermal conductivity	1.2	W/(m ² ·k)
Material	Borosilicate Glass 3.3	
Transmittance coefficient	87	%
Emission coefficient	10	%
Vacuum	1x10 ⁻³	Pa

- Table 4.1 gives technical data of a double-wall vacuum tube provided by the vender, which will be used for overall vacuum tube window's U-value calculation. The high vacuum effectively eliminates heat transfer by gaseous conduction and convection, and radiative heat transfer is reduced to a low level by the incorporation of one or two transparent, low emittance coatings on the internal surfaces of the glass. Previous research has shown that a high vacuum pressure

normally less than 0.1 Pa will decrease both conduction and convection through the air on the total glazing heat transfer to the negligible level (Collins, 1995). Assuming an infinite extension of tube glass surfaces (outside-inside) opposite each other (Holman, 1981), thermal resistance due to radiative heat transfer in cavity i , where $i \in (1, 2)$, is given by:

$$R_{ec,i} = \left(\frac{1}{\varepsilon_{To,i}} + \frac{1}{\varepsilon_{Tin,i}} - 1 \right) (4\sigma t_{ec,i}^3)^{-1} \quad (4-9)$$

where, σ is Stefan-Boltzmann constant and ε is the emissivity of the two tube layers arrayed the evacuated cavity. Tube diameter has no influence on overall thermal transmittance according to above analysis.

- For natural convection and radiation at the indoor surface, designers often consider $h_{in} = 3.6 \text{ W}/(\text{m}^2 \cdot \text{k})$ and $h_{in} = 2.5 \text{ W}/(\text{m}^2 \cdot \text{k})$, which respectively correspond to winter and summer standard boundary conditions (Holman, 1981).

➤ Heat transfer through frame

Window frame usually consists of lots of structural elements like sash, jamb, head, still and so on. So to estimate its overall thermal transmittance becomes much complicated by (1) variety of window products and therefore frame configurations, (2) different combinations of materials used for frames, (3) different sizes available, (4) glazing unit width and spacer type. For early phases of design (ASHRAE, 2009), the thermal transmittance could be estimated from the frame library of window 6 of LBNL (Lawrence Berkeley National Laboratory) given by Table 4.2.

Table 4. 2: Frame U-values in W/ (m².k)

Name	U_f
Aluminium with thermal break	5.68
Al flush	3.97
Wood	2.27
Vinyl	1.70

The total solar and visible transmittances of the window are simplified based on original algorithm (ASHREA, 2009) and will be calculated by:

$$\tau_{sol} = \tau_{sol,g}^2 \tau_{sol,T}^4 \quad (4-10)$$

$$\tau_{vis} = \tau_{vis,g}^2 \tau_{vis,T}^4 \quad (4-11)$$

where, τ_{sol} and τ_{vis} are solar and visual transmittance respectively.

4.2.3 Reference boundary conditions and calculation result

➤ Standard boundary conditions

Unless a specific set of boundary conditions is of interest (e.g., to match test conditions, actual conditions or to satisfy a national standard), the following standard boundary conditions in winter shall be used to calculate the properties of a window unit (ISO 15099, 2003): $t_{in} = 20 \text{ }^\circ\text{C}$, $t_o = 0 \text{ }^\circ\text{C}$, $h_{in} = 3.6 \text{ W}/(\text{m}^2 \cdot \text{K})$, $h_o = 20 \text{ W}/(\text{m}^2 \cdot \text{K})$.

➤ Calculation procedure and results

The heat transfer processes will finally achieve a balance when the window unit operates at a steady state condition and each section of the unit remains at a certain

temperature. The algorithm used for the modelling set-up in Microsoft Excel 2010 is indicated as following Figure 4.9:

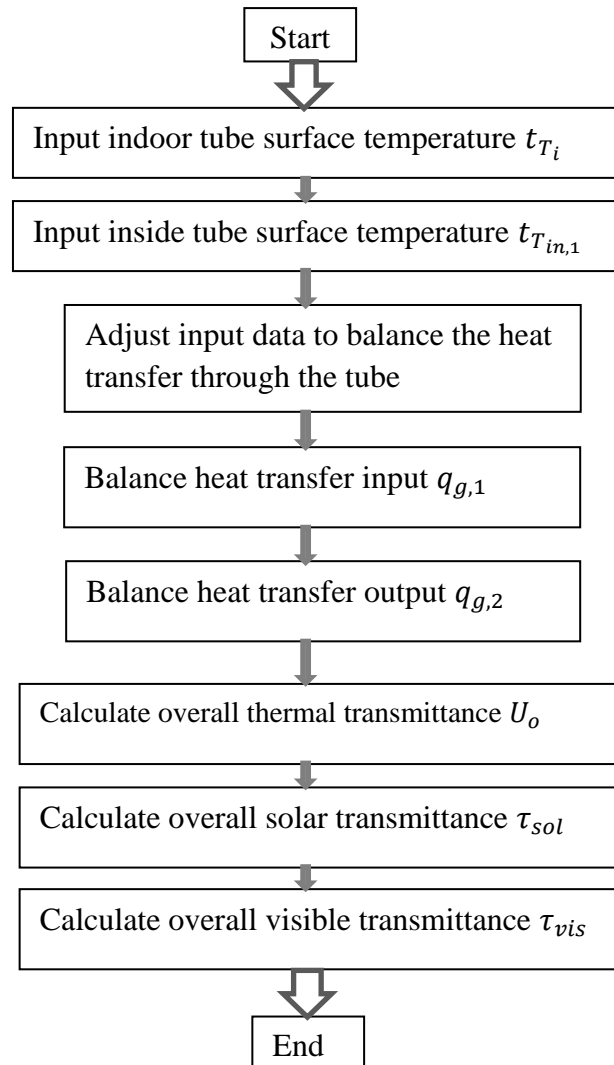


Figure 4. 9: Flow chart of calculation process

- A. Given a vacuum tube window unit structure, geometrical and thermodynamic parameters as well as standard boundary conditions in winter could be obtained as shown in Figures 4.1-4.3, 4.8 and Table 4.1-4.2;
- B. Given the certain types of glazing unit materials, including frame type, external glasses, for an instant thermal transmittance calculation;

C. Assuming an instant temperature t_{Ti} of indoor tube surface and then heat analysis is carried out as follows:

- a) Total heat transferred through the indoor tube surface could be analyzed by Equation 4-1. Total heat flow is all the same during each element of window unit which results in determination of the outside tube surface temperature, t_{To} based on equations 4-3 and 4-7;
- b) Assuming an instant temperature $t_{Tin,1}$ of inside tube surface and radiative coefficient of evacuated cavity 1, $e_{ec,1}$ is then determined using equations 4-1, 4-3, 4-8 and 4-9 with the result of heat transfer by emissivity E_{ec} :
 - 1) The temperature $t_{Tin,2}$ of another inside tube surface could be then analysed by equations 4-1, 4-3, 4-7 and 4-8;
 - 2) The temperatures of outside tube surface $t_{To,1}$ is calculated according to the total heat flow constant whilst the emissivity factor is then analysed by equations 4-1, 4-3, 4-8 and 4-9;
 - 3) The total thermal resistance R_g and transmittance U_g of glazing will come out by equation 4-3, 4-4 and 4-5.
 - 4) Total heat flow q_g could be calculated by total thermal transmittance by equation 4-1.
- c) If $(q_{g,2} - E_{ec})/ q_g > 0.5\%$ (error allowance), then decrease $t_{Tin,1}$ by 0.01°C and return to step b) for re-calculation;
- d) If $(q_{g,2} - E_{ec})/ q_g < 0.5\%$ (error allowance), then increase $t_{Tin,1}$ by 0.01°C and return to step b) for re-calculation;
- e) If $-0.5\% \leq (q_{g,2} - E_{ec})/ q_g \leq 0.5\%$, then first energy balance within the unit is achieved;

D. If $(q_{g,2} - q_{g,1})/ q_{g,2} > 0.5\%$ (error allowance), then decrease $t_{Ti,1}$ by 0.01°C and

- return to step b) for re-calculation;
- E. If $(q_{g,2} - q_{g,1}) / q_{g,2} < 0.5\%$ (error allowance), then increase $t_{Ti,1}$ by 0.01°C and return to step b) for re-calculation;
- F. If $-0.5\% \leq (q_{g,2} - q_{g,1}) / q_{g,2} \leq 0.5\%$, then second energy balance within the unit is achieved;
- G. Calculate overall thermal transmittance U_o by using equations 4-2 to 4-5.
- H. Calculate overall solar and visible transmittance using Equations 4-10 and 4-11;
- I. Program stops.

Based on the thermal procedures above, the calculation could be carried on by inputting necessary parameters. Temperature changes through the tube are given by Figure 4.10. Table 4.3 shows the preparing parameters of vinyl frame single wall vacuum tube window unit under the standard boundary conditions in winter and table 4.4 displays the output results.

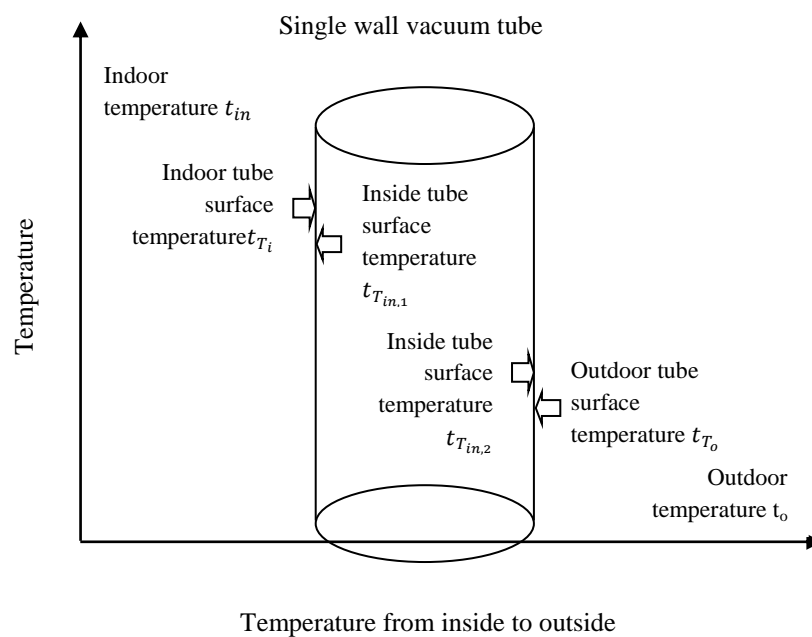


Figure 4. 10: Diagram of temperature changes through vacuum tube

Table 4. 3 Input parameters of vinyl frame single wall vacuum tube window unit for calculation

Winter standard boundary condition and specific parameters	Value	Unit
Indoor heat transfer coefficient h_{in}	3.6000	W/(m ² K)
Indoor thermal resistance R_{in}	0.2778	(m ² K)/W
Outdoor heat transfer coefficient h_{out}	8.5000	W/(m ² K)
Outdoor thermal resistance R_o	0.1176	(m ² ·K)/W
Heat transfer coefficient of static air space h_s & h_{tac}	7.4000	W/(m ² K)
Thermal resistance of static air space R_s & R_{tac}	0.1351	(m ² K)/W
Thermal conductivity of vacuum tube layer λ_T	800.0000	W/(m ² K)
Thermal resistance of vacuum tube layer R_T	0.0013	(m ² K)/W
Thermal transmittance of frame U_f	1.7000	W/(m ² K)
Thermal resistance of frame R_f	0.5882	(m ² K)/W
Thermal transmittance of silicone sealant U_{ss}	35.0000	W/(m ² K)
Thermal resistance of silicone sealant R_{ss}	0.0286	(m ² K)/W
Indoor temperature t_{in}	20.0000	°C
outdoor temperature t_o	5.0000	°C
Emissance of tube glass 1 ϵ_1	0.1000	
Emissance of tube glass 2 ϵ_2	0.1000	
Solar transmittance of tube glass $\tau_{Vsol,T}$	0.8700	
Visible transmittance of tube glass $\tau_{Vis,T}$	0.9200	
Prototype width a	1.0000	m
Prototype height b	1.0000	m
Prototype area A_g	1.0000	m ²
Frame to window area ratio	0.2000	
Frame area of prototype A_f	0.2000	m ²
Silicone sealant channel to window area ratio	0.0500	
Silicone sealant channel area of prototype A_{ss}	0.0500	m ²
Prototype net area A_{ng}	0.7500	m ²

Table 4. 4: Output of vinyl frame single wall vacuum tube window unit under standard winter condition (Indoor temperature at 20°C, outdoor temperature at 5°C)

Procedure temperatures	Value	Unit
Temperature of indoor tube t_{T_i}	18.9607	°C
Total heat transfer input glazing $q_{g,1}$	3.7416	W/m ²
Temperature of inside tube surface $t_{T_{in,1}}$	18.9560	°C

Radiative coefficient of evacuated cavity e_{ec}	0.2769	W/(m ² K)
Total heat transfer by radiation q_r	3.7416	W/m ²
Temperature of inside tube surface $t_{T_{in,2}}$	5.4449	°C
Temperature of outdoor surface tube t_{T_o}	5.4402	°C
Total thermal resistance R_g	4.0089	(m ² K)/W
Total thermal transmittance of glazing U_g	0.2494	W/(m ² K)
Total thermal resistance of silicone sealant R_{ss}	0.4240	(m ² K)/W
Total thermal transmittance of silicone sealant U_{ss}	2.3585	W/(m ² K)
Total thermal transmittance of vacuum tube window U_o	0.6450	W/(m ² K)
Total heat output from vacuum tube window q_o	3.7416	W/m ²
Total solar transmittance of vacuum tube window τ_{sol}	0.7569	
Total visible transmittance of vacuum tube window τ_{vis}	0.8464	

From above tables 4.3 and 4.4, it's shown that the thermal transmittance of glazing area could be achieved to 0.25 W/m²·K whilst the overall thermal transmittance reaches at 0.65 W/m²·K by coupling with vinyl frame. Also over 85% of the solar and visible beams would penetrate through the window with the transmittance values respectively at 0.76 and 0.85. So it could be obviously found the thermal potential of this vacuum tube window. However, it's essential to improve the thermal ability by exploring more relationships of different elements, such as outdoor wind speed, frame type and window size.

- Impact of outdoor wind speed

Based on the equation (4-6) and Figure 4.8, the relationship between outdoor wind speed and heat transfer coefficient could be worked out. Remaining unit configuration and internal conditions same, the variation of unit overall thermal transmittance against the outdoor wind speed of both windward and leeward was simulated using the above established program and the results were shown in Figure 4.11. Lower outdoor heat transfer coefficient leads to lower unit thermal penetration. However the

variation of overall U-values is not obvious even when outdoor wind speed changes from 0 to 20 m/s. The phenomena could be explained as follows: outdoor wind speed is as direct ratio to overall thermal transmittance, but its thermal resistance only accounts for small proportion of overall thermal resistance and then results in a limited final influence.

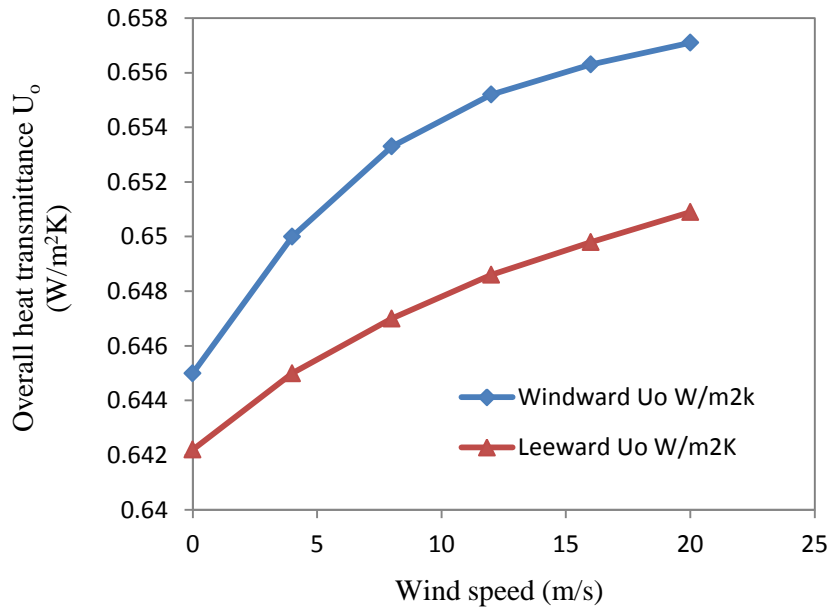


Figure 4. 11: Overall thermal transmittance of various wind speeds of outside air

- Impact of frame type

Remaining unit external, internal conditions and other configuration same, the variation of unit overall thermal transmittance against the different frames was simulated using the above established program and the results were shown in figure 4.12. Lower thermal transfer coefficient of frame leads to lower unit thermal penetration. Besides, the variation of overall U-values is remarkable, from 0.65 to 1.66 W/(m²·k), when thermal transfer coefficient of frame changes from 1.70 to 5.68 W/(m²·k). The phenomena could be explained as follows: thermal transfer coefficient of frame is as direct ratio to overall thermal transmittance, and its thermal resistance

accounts for great proportion of overall thermal resistance and then results in a prominent thermal affect.

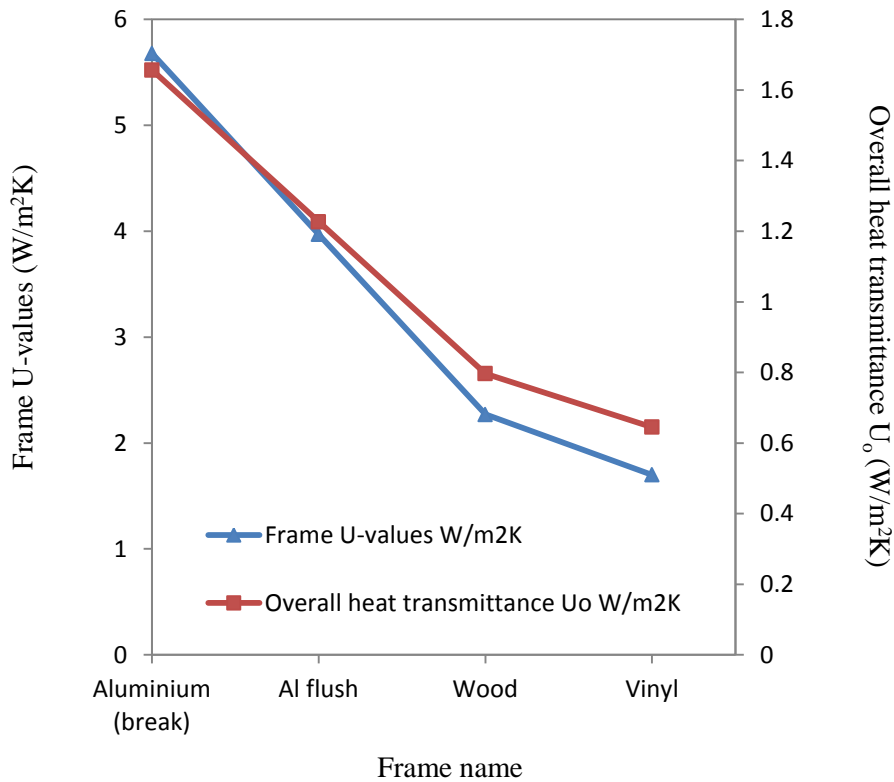


Figure 4. 12: Overall thermal transmittance of different frame types

- Impact of frame area to window area

Remaining unit external, internal conditions and other configuration same, the variation of unit overall thermal transmittance against the different ratios of frame area to window area was simulated using the above established program and the results were shown in Figure 4.13. Lower ratio of projected frame area to total window area leads to lower unit thermal penetration. Besides, the variation of overall U-values is notable, from 0.37 to 0.92 W/(m²·k), when the area ratio changes from 0.10 to 0.30 (window frame to window area percentage in general). The phenomena could be explained as follows: the ratio of projected frame area to total window area is

as direct ratio to overall thermal transmittance, and its thermal resistance accounts for large proportion of overall thermal resistance and then results in an obvious thermal influence.

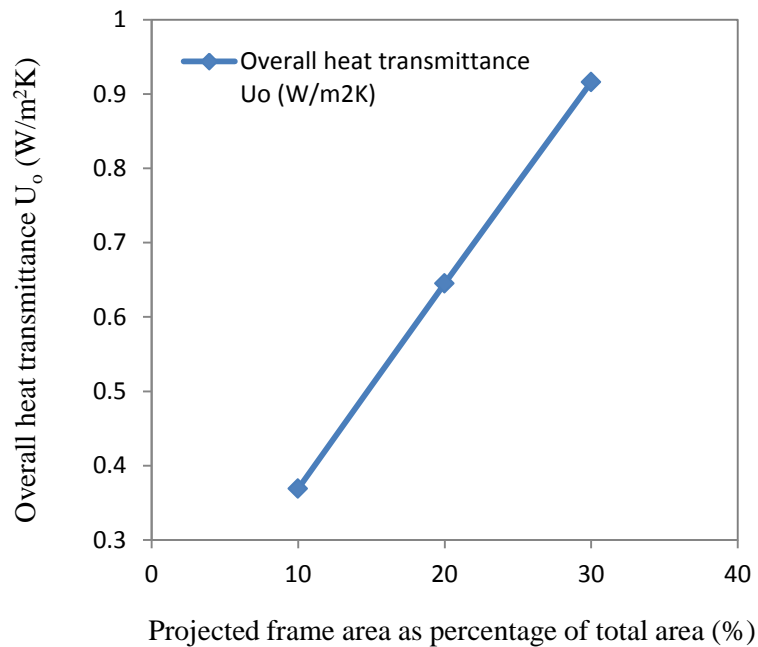


Figure 4. 13: Overall thermal transmittance of different frame area to total window area

Computer modelling simulation has demonstrated that the novel vacuum tube window unit has low thermal transmittance, thereby to reduce thermal dissipation from buildings. Computer model was developed to optimise the unit structure and constructed materials, simulate its performance and identify the favourite combination.

The major findings could be outlined as below:

- (1) The overall transmittance could be achieved low to around 0.65 W/m²K for single wall vacuum tube window unit by the combined configuration of low thermal conductive materials, such as the combination of vinyl frame.
- (2) Parameters of outdoor wind speed has limited influence to overall thermal transmittance while frame types and ratios of frame area to window area

impact the overall thermal penetration much more, especially frame types.

Those factors are all as the direct influence to the overall U-values.

- Computer simulation results of other parameters for Vinyl frames window prototype

By changing conditions of external and internal temperatures and external wind speed, vinyl framed single wall vacuum tube window unit's U-values were calculated as shown in Figure 4.14.

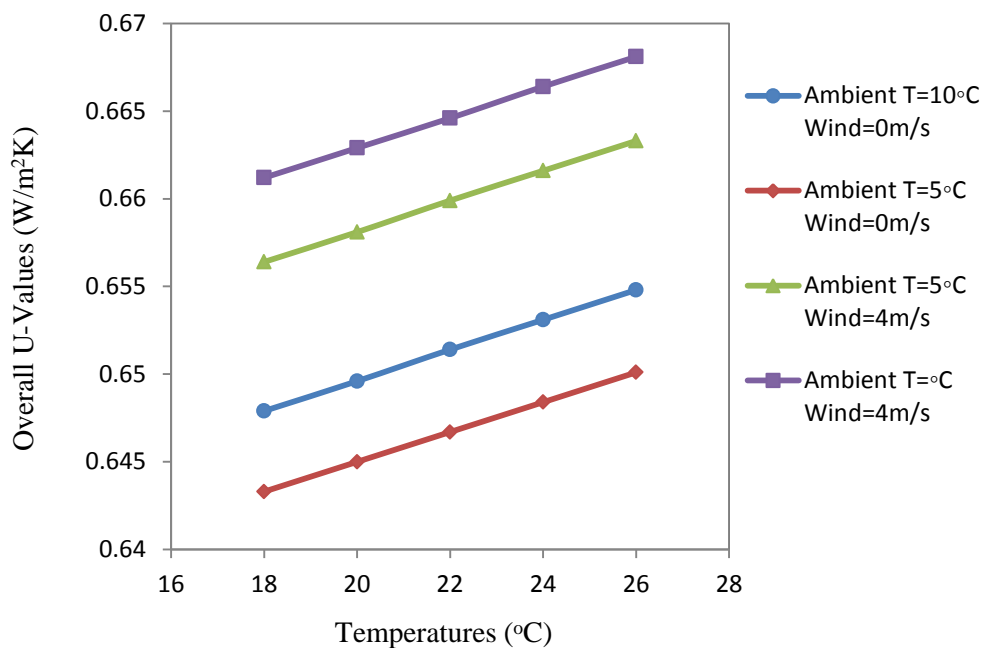


Figure 4. 14: Overall U-values of Single Wall Vacuum Tube Window in Various Conditions

The results show that in the same conditions of temperature and outdoor wind speed, window's U-values increase proportionally by temperature differences between indoor and outdoor. The similar results can be seen in the modelling of double wall vacuum tube window unit as Figure 4.15 shown.

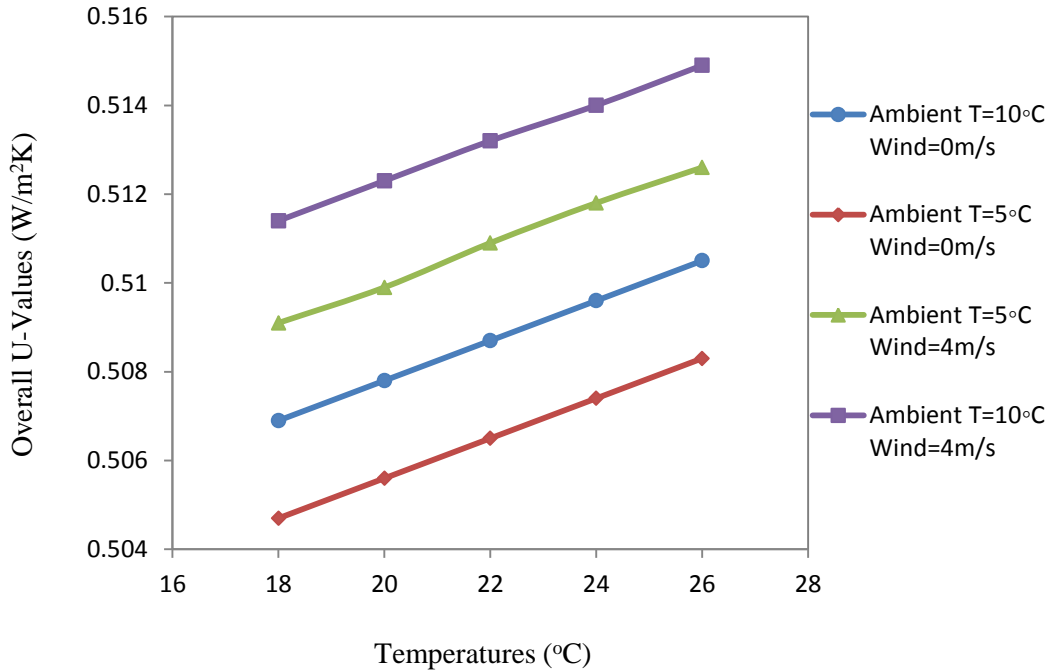


Figure 4. 15: Overall U-values of Double Wall Vacuum Tube Window in Various Conditions

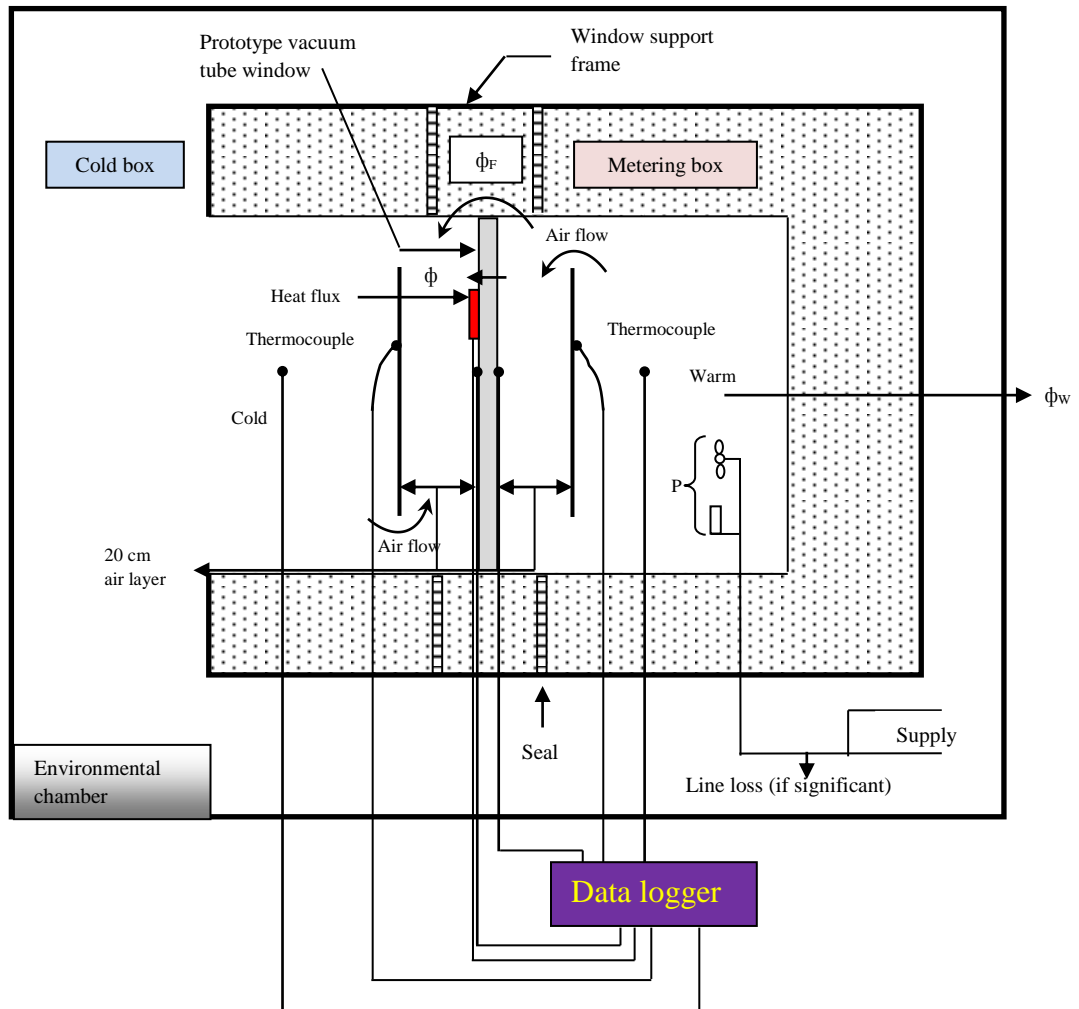
Computer modelling results show that single wall and double wall vacuum tube window units can achieve U-values low to $0.6433\text{W/m}^2\text{K}$ and $0.5047\text{W/m}^2\text{K}$, respectively. In order to validate vacuum tube window prototype thermal transmittances, laboratory tests for both window prototypes are described in the following contents.

4.3 Calibrated hot-box method for vacuum tube windows tests

Prototype vacuum tube windows are tested at Department of Architecture and Built Environment University of Nottingham. Windows U-value tests are based on British standard-methods for determining thermal insulating properties BS 874-Part 3: Tests for thermal transmittance and conductance, section 3.2 (1990) calibrated hot-box method. The method is used as an alternative to BS 864-3.1 guarded hot-box method. A slightly modified procedure enables tests to be made on smaller elements such as window systems. The method is suitable for construction elements with thermal

transmittances and conductances in the range $0.1\text{W/m}^2\text{K}$ to $15\text{W/m}^2\text{K}$ for testing within a temperature range of -50°C to 50°C (BS 874-3.2, 1990).

The basis for the test method is the measurement, at equilibrium, of the heat flux through the test element and corresponding temperature difference(s) across it. Apparatus is designed to be capable of measurement to an accuracy of $\pm 5\%$ on test elements of uniform thermal conductance (i.e. element with no thermal bridges between surfaces) in the conductance range $0.5\text{W/m}^2\text{K}$ to $5\text{W/m}^2\text{K}$. The apparatus is shown schematically in Figure 4.16 and consists of two principal items, a metering box and a cold box, between which the test element, assembled in a support frame, is placed.



NOTE: The energy flux through test element, ϕ is given by the following equation : $\phi = P - \phi_w - \phi_F$, where P is the power supplied to metering box (in W), ϕ_w is the heat flux to laboratory surrounds (in W), ϕ_F is the flanking loss (in W)

Figure 4. 16: Calibrated hot-box apparatus

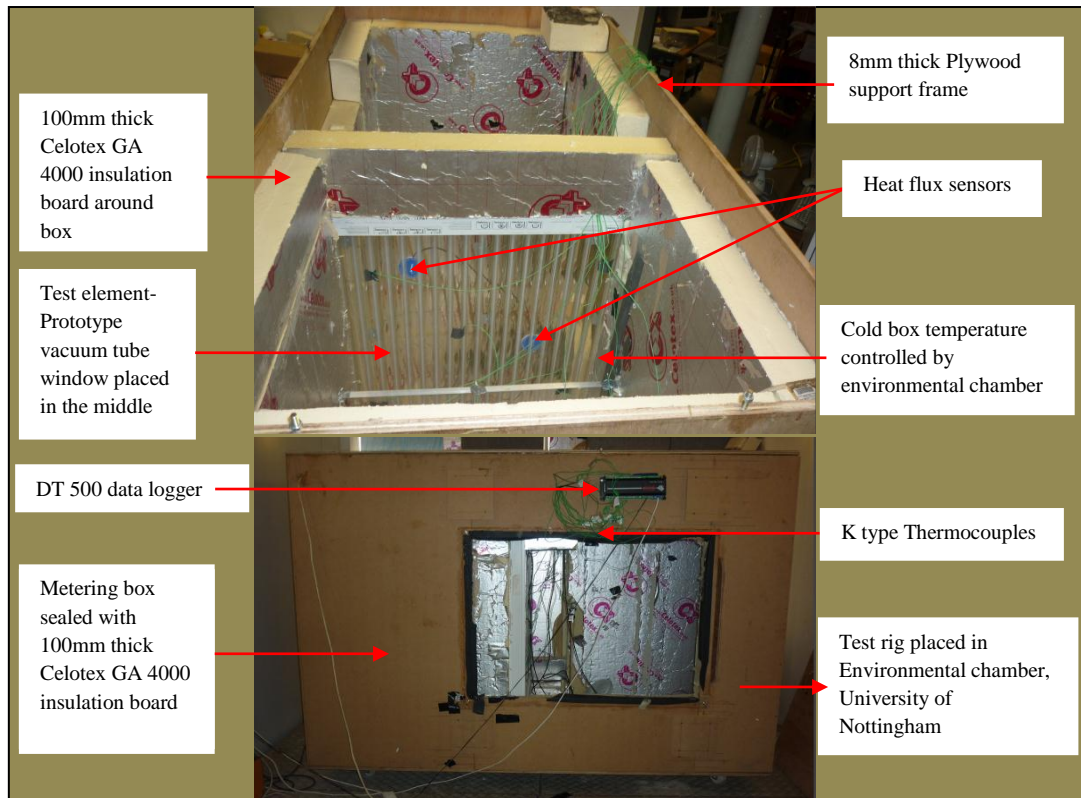


Figure 4. 17: Prototype vacuum tube window test rig

The apparatus is designed for automatic control of both metering and cold space temperature, so that the power input can be automatically adjusted for fluctuations in the temperature of the laboratory environment. Heat supplied to the metering box passed through the test element to the cold box, which is maintained at a constant low temperature. The heat flux through the test element is determined from the total power supplied to the metering box, correcting for losses or gains through the metering box walls and flanking loss to the cold box occurring around the perimeter of the specimen (see Figure 4.17). Insulation material around test element perimeter assists to reduce flanking losses. Normally the test element will be the same size as the open face of the metering box (see Figure 4.16), but in some instances, in particular for the testing of window units, it can be smaller. For this type of test, the test element is

surrounded by a panel of known thermal properties, enabling the heat flux through the test element to be deduced from the total heat input.

4.3.1 Test conditions and procedures

The following test conditions and procedures are applied in this measurement based on BS 874-Part 3 (1990):

- a) The environmental temperature on the cold side (T_{ac}) was set at 10°C and 5°C, on the hot side (T_{ah}) was from 20°C to 25°C and held constant to within 1% of the air to air temperature difference across the sample as specified in BS 874-3.1.
- b) Ten thermocouples were distributed over the metering box to measure the temperatures of the metering area, as well as indoor and outdoor window surfaces temperatures. The total surface resistance are determined from the mean surface temperatures and the environmental temperatures on either side.
- c) The power consumption of the heater was measured to an accuracy of $\pm 2.5\%$. The total uncertainty in the determination of the net power input into metering box due to the heater and fans, after correcting for heat exchange through the walls, flanking loss, and any power dissipation in the leads is not exceed $\pm 3\%$ (BS 874-3.2, 1990).
- d) Limitation of heat exchange through the metering box walls. As part of the procedure to ensure that the heat flux through the test element is accurately determined, the heat exchange through the side and back of the metering box were measured and corrected for. This correction does not exceed 20% of the total power supplied to the metering box.

- e) In order to produce uniform air velocities and temperature distribution, baffles of full width of the metering box were designed to fix paralleled to the window surface and had gaps at the top and bottom (Figure 4.16). The distance between window prototype and baffle was 200mm.
- f) Vertical temperature gradient in the air stream achieved less than 2K/m by altering suitable combination of airspeed and baffle position. Circulating fan was installed in the metering box to assist natural convection to achieve particular values of convection coefficient that cannot be obtained by using natural convection alone. Air speed was measured across the window prototype surface by anemometer.

4.3.2 Window prototype test

Followed the above test conditions and procedures, vacuum tube window prototypes were tested in the environmental chamber in the Department of Architecture and Built Environment University of Nottingham. HFP01-05 heat flux sensors (Figure 4.18 A) were used to measure conductive heat transfer (loss or gain) through window surface. The test window prototype manufactured by evacuated tube panels, its surface is different from conventional window glass panes. In this case, heat transfer through window surface are measured by using heat flux sensor by selecting ten different points, the mean value of test data is used for final calculation. Although HFP01-05 heat flux sensor is suitable for measuring flat surface, heat flux data collected from picked point on the tube window surface show less than 1% difference from each other, which are within the error allowance according to BS 874(1990). The sensor produces an output that is proportional to the heat flux in Watts/m^2 . Metering area was heated

by fan heater (Figure 4.18 B), temperatures were measured by thermocouples (Figure 4.18 C) and DT500 DataTaker collected data (Figure 4.18 D).

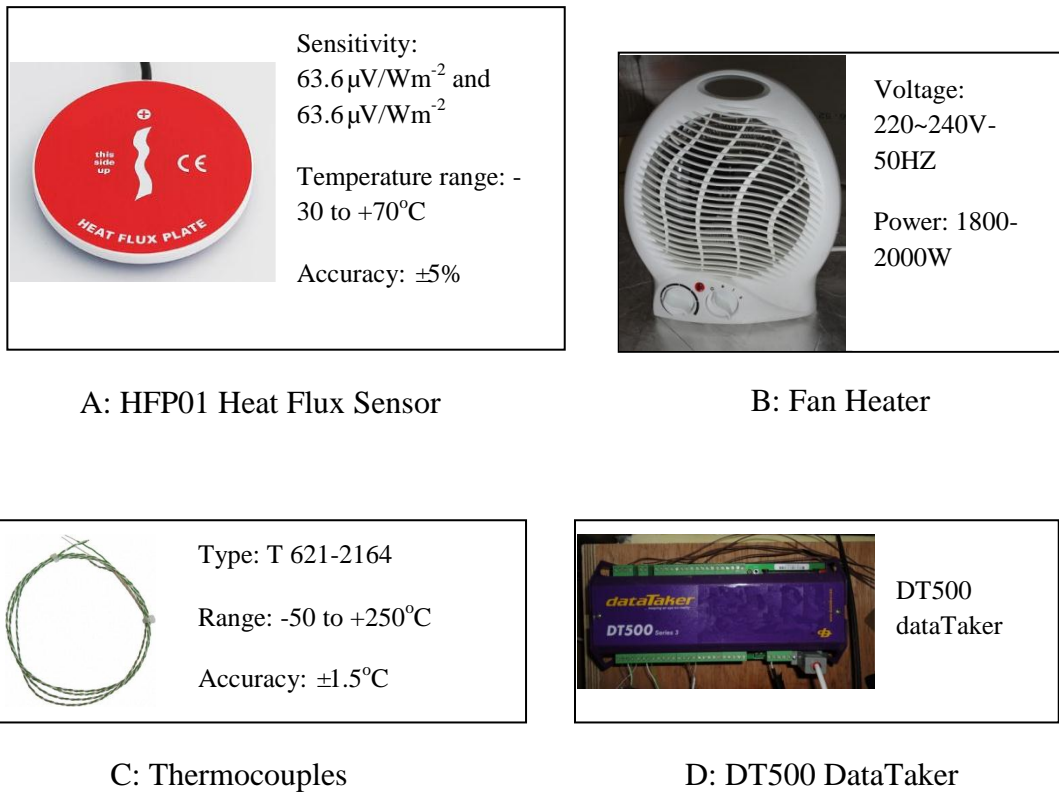


Figure 4. 18: Measurement equipment

In the tests, the temperatures in the metering box were kept constantly by using temperature controlled adaptor to control heat input. The results were taken when thermal equilibrium is achieved, i.e. when the temperatures on each side of the test element and the heat flux through it are essentially constant.

Heat exchange at the hot and cold surfaces of the test element involves both convective and radiative components. The former depends upon air temperature and air speed, while the latter depends upon the temperatures and emissivities of surfaces seen by the element surface. The effects of heat transfer to or from a surface by convection and radiation are conveniently combined in the concept of an environmental temperature and a surface heat transfer coefficient. Thermal

transmittance is defined between two environmental temperatures and therefore suitable temperature measurements are required to enable these to be determined.

4.3.3 Calculation and expression of results

Window thermal transmittance U-values ($\text{W}/\text{m}^2\text{K}$), are calculated as follows,

$$U = \frac{\phi}{A(T_{e1}-T_{e2})} \quad (4-12)$$

Where, ϕ is the heat flux through the metering area (in W), i.e. the rate of heat supplied to the metering box, including power supplied to any fans and corrected where necessary for:

- (a) heat flux through the metering box walls;
- (b) flanking loss around the perimeter of the test area;
- (c) any power loss in the leads to the heater or to the fans in the metering box

Where, A is the test area (in m^2), T_{e1} is the environmental temperature in the metering box (in $^{\circ}\text{C}$), T_{e2} is the environmental temperature in the cold box (in $^{\circ}\text{C}$).

The surface coefficients h_1 and h_2 (in $\text{W}/\text{m}^2\text{K}$) are given by the following equations:

- 1) surface coefficient (hot face)

$$h_1 = \frac{\phi}{A(T_{e1}-T_{s1})} \quad (4-13)$$

- 2) surface coefficient (cold face)

$$h_2 = \frac{\phi}{A(T_{s2}-T_{e2})} \quad (4-14)$$

Where, T_{s1} is the average surface temperature of the test element in the metering box (in °C), T_{s2} is the average surface temperature of the test element in the cold box (in °C)

For metering box and flanking loss correction, in the calibrated hot-box test, the measure power, P (in W) supplied to the metering box can be expressed by the following.

$$P = \phi + \phi_W + \phi_F \quad (4-15)$$

Where, ϕ is the energy flux (in W) through the test element, ϕ_W is the energy flux (in W) through the metering box wall (including any component through the support frame), ϕ_F is the flanking loss (in W).

ϕ and ϕ_F can be related by measuring surface temperature difference ΔT across the calibration element, and ϕ_w to the average surface temperature difference ΔT_w across the metering box walls. Equation (4-15) is given

$$P = \alpha \Delta T + \beta \Delta T_w + \gamma \Delta T \quad (4-16)$$

Where α is the heat exchange coefficient (in W/K) of the calibration element, derived from $\alpha = \Lambda A$, Λ being its conductance (in W/m²K) and A the test area (in m²); β is a heat exchange coefficient (in W/K) for heat flows to or from the laboratory surrounds (primarily through the metering box walls); γ is a flanking heat loss coefficient (in W/K).

- Single-wall vacuum tubes window U-value tests results

Base on equations in above section 4.3.3, single-wall vacuum tube window U-values results in various test conditions are calculated and shown in the following Figure 4.19.

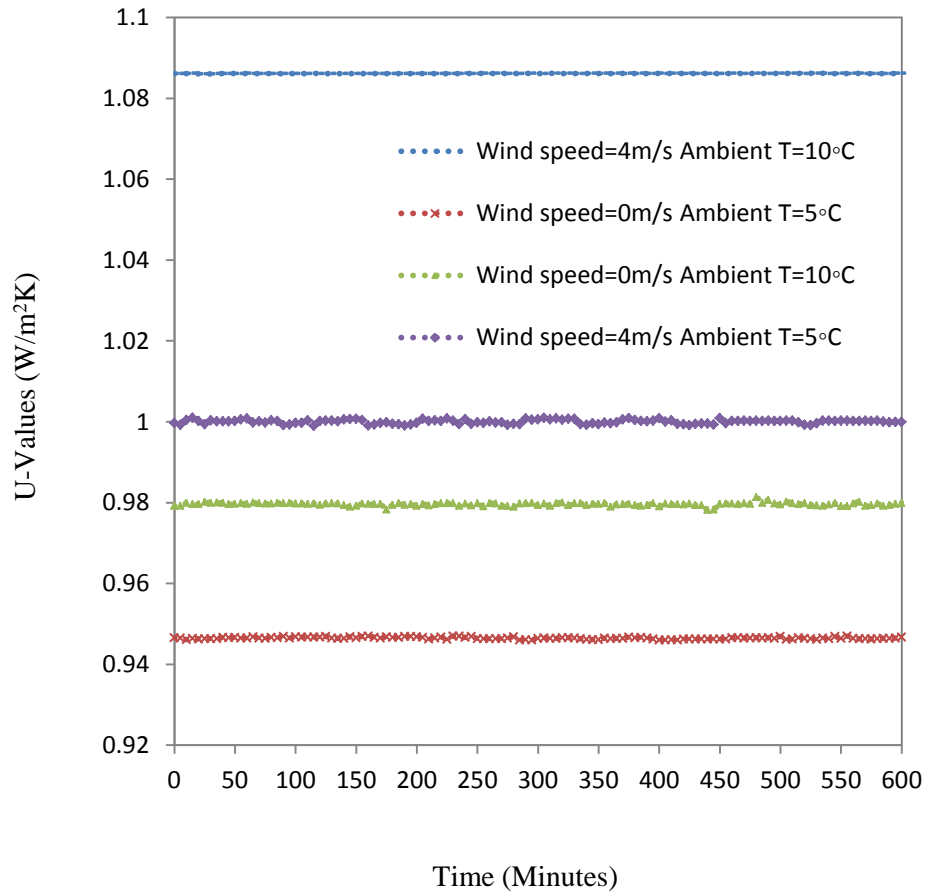


Figure 4. 19: Single-wall vacuum tube window U-values in specified test condition

When the apparatus has reached equilibrium, the temperatures, the power supplied were stable without continuously increasing or decreasing, the readings were taken and the test continued for 10 hours. Ambient temperature and wind speed have impact on u-values results. Figure 4.19 shows U-values in four different test conditions. When forced air flow is applied by fan, air velocity was measured as 4m/s, average U-value of the window become greater compared U-values results to when wind speed is 0m/s. The best U-value of 0.95W/m²K is achieved when outdoor wind

speed is 0m/s, outside temperature is 5°C. The total results of single-wall vacuum tube window under four different test conditions have shown the similarity to computer modelling results. The best U-value results are achieved when outdoor wind speed is 0m/s, overall U-values increase when indoor and outdoor temperature difference decrease. The same test procedures and conditions are applied to the double-wall vacuum tube window tests.

➤ Double-wall vacuum tubes window U-value tests results

Base on calculation method and equations described in section 4.3.3, double-wall vacuum tube window U-values results in various test conditions are calculated and shown in Figure 4.20.

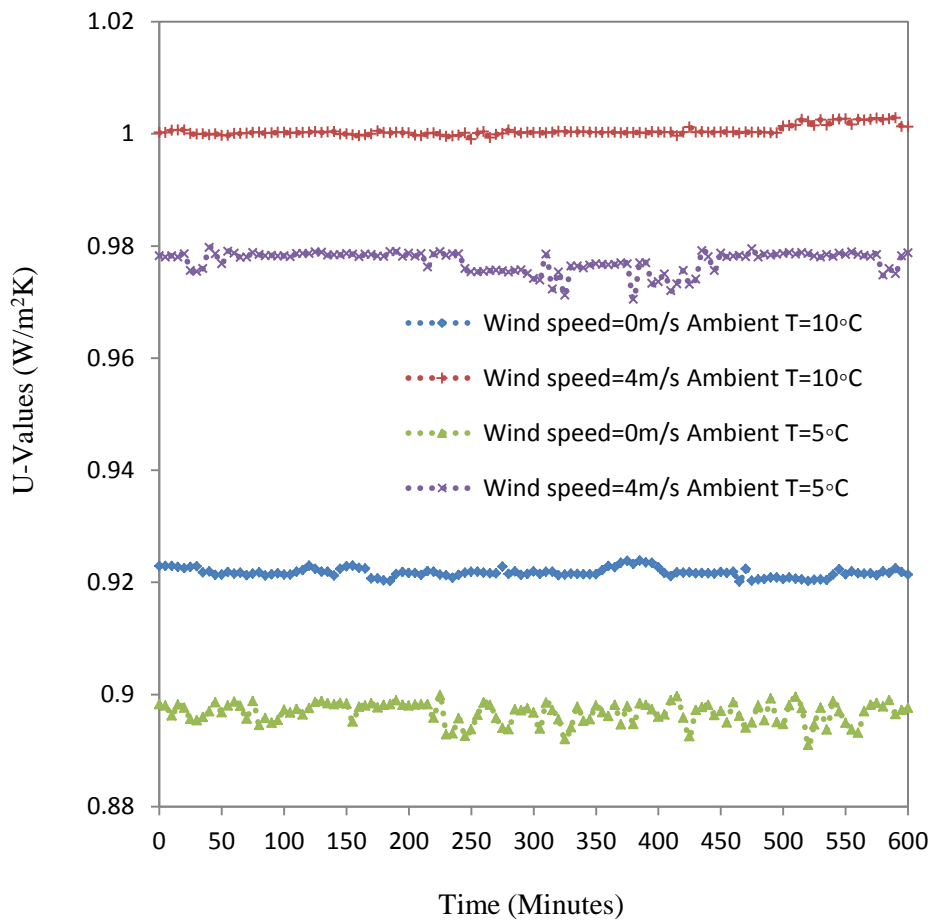


Figure 4. 20: U-values in specified test condition

The U-values test results are similar to single-wall vacuum tube window. Both ambient temperature and wind speed have impact on window's U-value. Figure 4.20 shows U-values in four different test conditions. When forced air flow is applied by fan, air velocity was measured as 4m/s, average U-value of the window become greater compared U-values results to when wind speed is 0m/s. The best U-value of $0.9\text{W}/\text{m}^2\text{K}$ is achieved when outdoor wind speed is 0m/s, outside temperature is 5°C . The total results of double-wall vacuum tube window under four different test conditions are also shown the similar trend to computer modelling results. The best U-value results are achieved when outdoor wind speed is 0m/s, overall U-values increase when indoor and outdoor temperature difference decrease.

4.4 Thermal image

4.4.1 Introduction of thermal imaging camera

Thermal imaging camera can convert the energy in the infrared wavelength into a visible light display and perform algorithms to interpret data to build an image. The camera uses multiple sources of data based on the areas surrounding the object to determine value rather than detecting the actual temperature. Thermal image shows an approximation of the temperature at which the object is operating (Web 4.1). Fluke TiS Thermal Imaging Scanner (Figure 4.21) is used to visualise double wall vacuum tube window thermal performance. Window prototype is south-east orientated installed in $2.25\text{m} \times 3\text{m}$ sized test room as Figure 4.22 shows. Room is constructed by 100mm Celotex insulation materials (U-value of $0.233\text{W}/\text{m}^2\text{K}$) and plywood. The average wall U-value of the test room is $0.21\text{W}/\text{m}^2$.

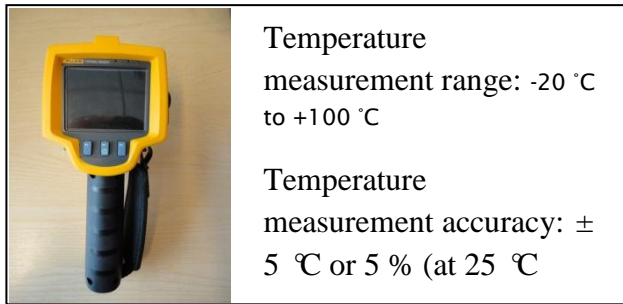


Figure 4. 21: Fluke TiS Thermal Imaging Scanner

4.4.2 Test procedure

Test room was heated by fan heater with a temperature controller to ensure stable indoor temperature at 35°C, shown in Figure 4.22. Laboratory temperature was 20°C monitored by thermocouple. Thermal images were taken when room temperature stabilized.

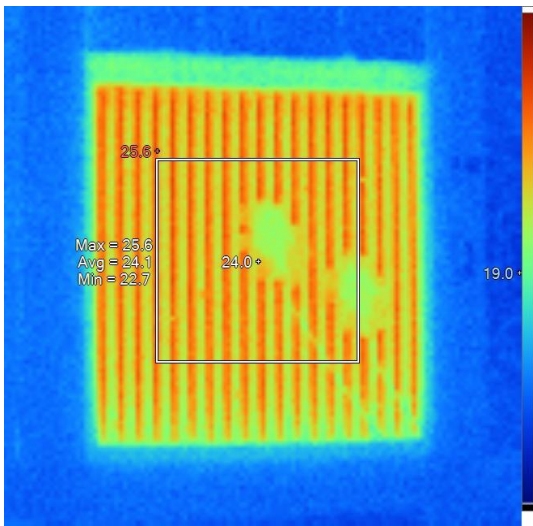


Figure 4. 22: Test room for double wall vacuum tube window prototype

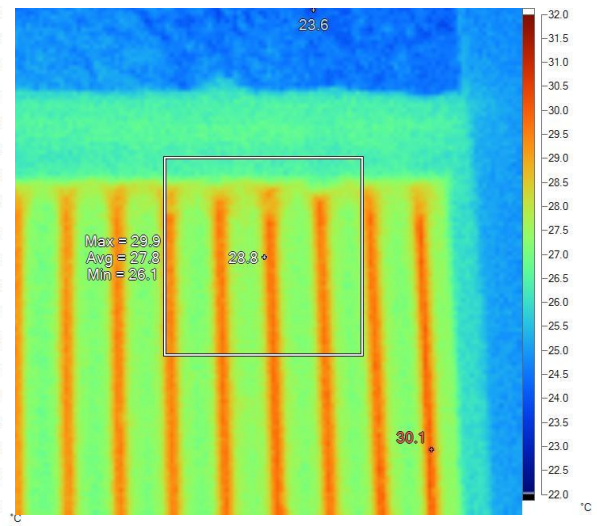
4.4.3 Thermal image result

The following Figure 4.23 shows vacuum tube window thermal performance in a real-size room simulation. Thermal images of (a), (b), (c), (d) show that significant heat losses through the window are mainly via vertical joints between vacuum tubes. From

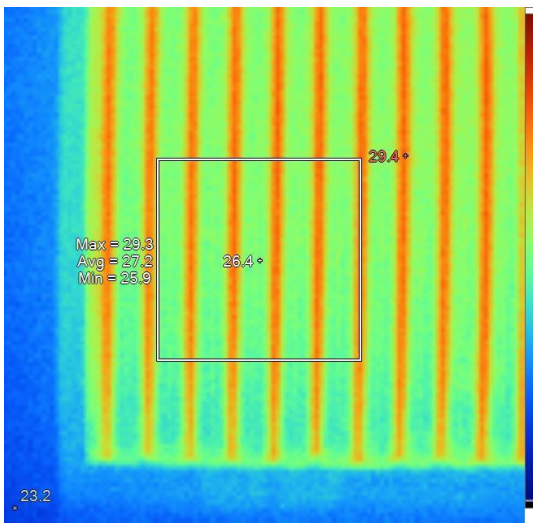
thermal images of (g), (h), (i), (j), it can be seen that the test room is well insulated with minimum heat loss.



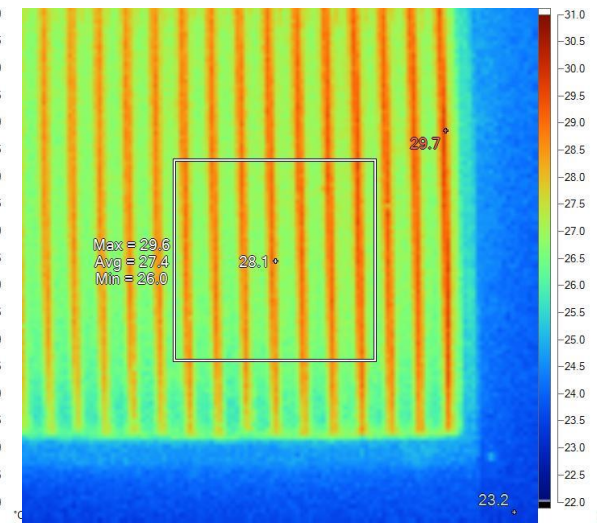
(a)



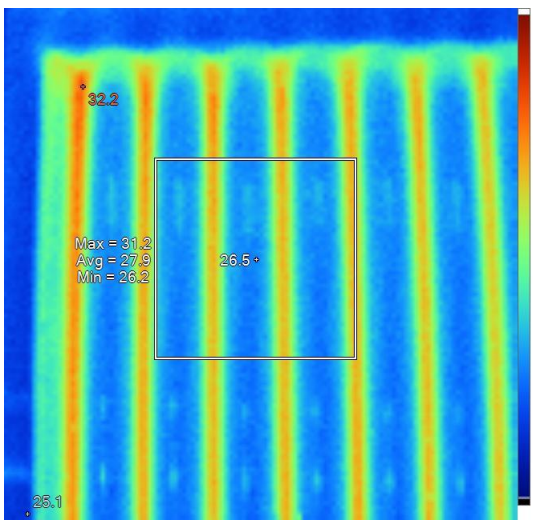
(b)



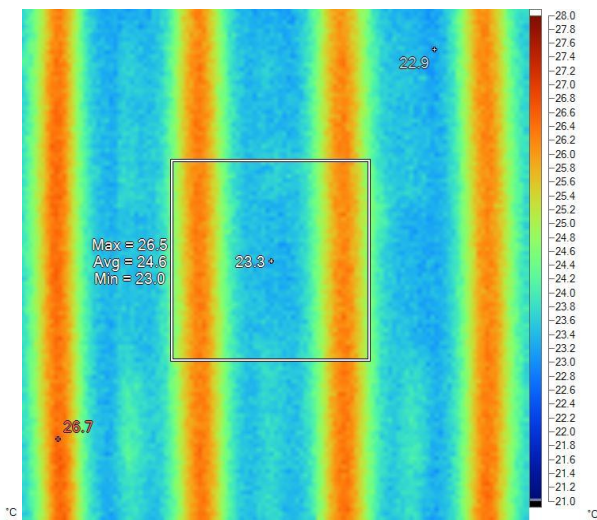
(c)



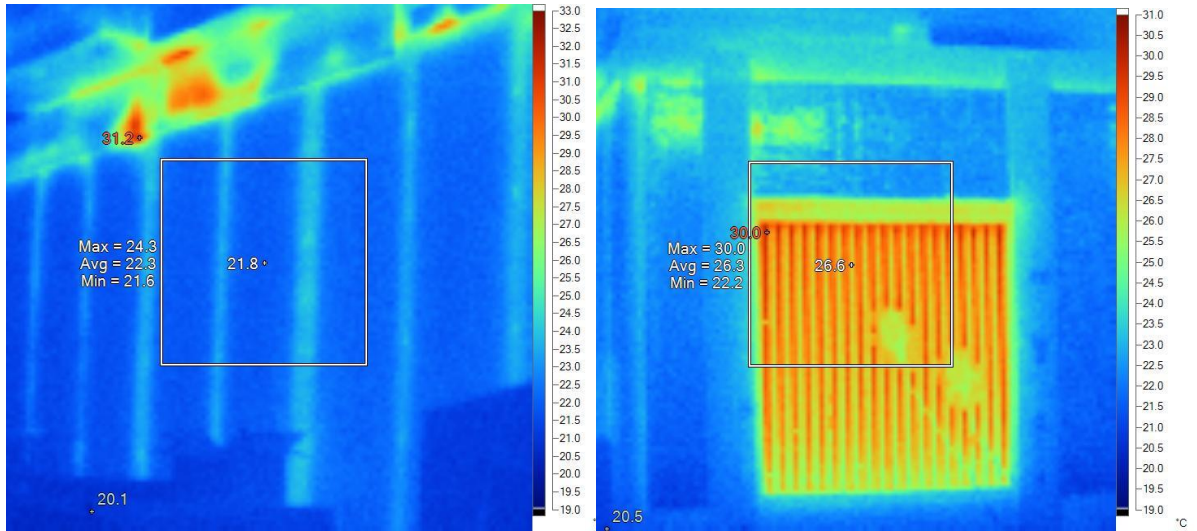
(d)



(e)

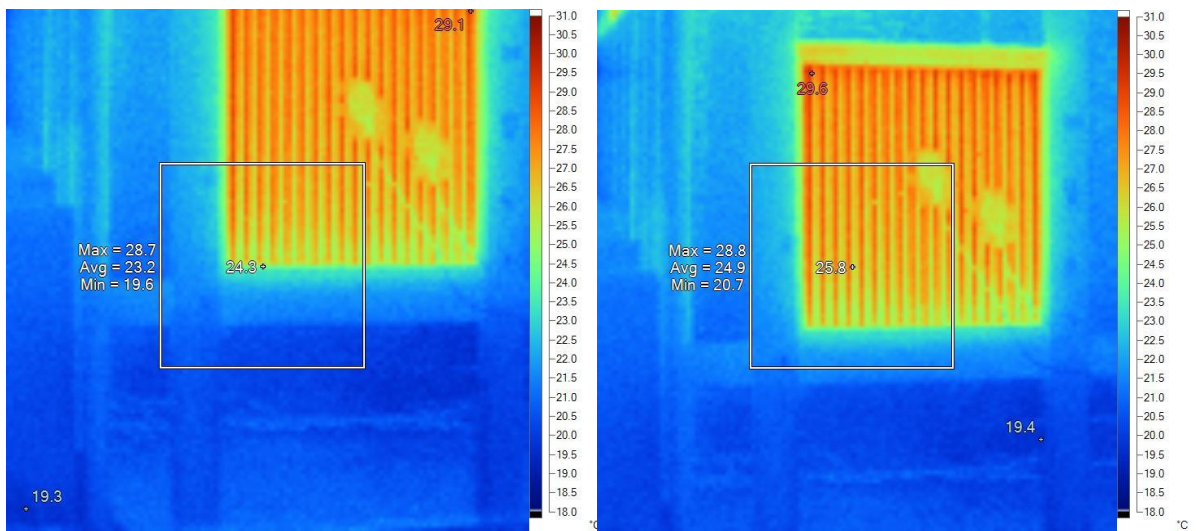


(f)



(g)

(h)



(i)

(j)

Figure 4. 23: Thermal imaging results

4.4.4 Result discussion

Above thermal image results show temperatures in different positions of the window, from the results it can be seen that vinyl frame has good thermal performance in terms of heat loss. However significant amount of heat dissipated via vertical joints between

tubes which may be caused by thermal bridging effect (heat flow through the path of least thermal resistance). To improve vacuum tube window better thermal performance in practical application, the sealant materials and manufacture technologies of tubes assembling are essential issue to address.

4.5 Economic and environmental analysis of the vacuum tube window system

4.5.1 Evaluation of the performance of the vacuum tube windows

The thermal transmittance of the vacuum tubes windows (U-value) was simulated and tested in previous sections. According to the results, under standard testing condition with the indoor temperature (T_{in}) of 20°C and the outdoor temperature (T_{out}) of 0°C, the U-value (U) of the vacuum tubes window is 1.08W/m²K, including the window frame. The U-value of double and triple glazing windows is 3.395 W/m²K and 2.585 respectively (ASHRAE, 2009). The heat loss rate through windows can be calculated as following:

$$q = U(T_{in} - T_{out}) \quad (4-17)$$

Therefore, for vacuum tubes windows, the heat loss rate is 21.6 W/m², which is less than 40% of heat loss rate of double glazing glass and around 50% of the heat loss rate of triple glazing.

4.5.2 Economic analysis

A preliminary economic analysis of the vacuum tubes windows was carried out in order to understand its commercial viability within the UK. The analyses were based on the computer modelling results.

The capital cost of the vacuum tubes windows was calculated by summing up the prices of the vacuum tubes, frames, and silicon for per square meter of the window, taking into account an appropriate rate of labour cost and sale profit. The prices of the vacuum tubes and frame were quoted from the manufacturers and the labour cost was estimated on the basis of mass production premise. The sale profile was considered to be 20% of the capital cost. Details of the calculation are presented in Table 4.5.

Table 4. 5: Capital cost calculation

Component	Unit Price (British Pound)	Quantity	Cost (£)
Vacuum tube	0.6	20	12
PVC Frame	51.48	1	51.48
Silicon	1	0.86m ²	0.86
White 1500mm Cill	5.2	1.1m	5.72
Labour cost	7.01	1	7.01
Sum of the individual cost			77.07
Profit (20%xSum)			14.01
Total			91.08

Owing to the high energy efficiency of the vacuum tubes windows, it has achieved significantly lower heat loss than the conventional double and triple glazing windows and consequently, it can greatly reduce the heating demand of the house and energy consumption.

The initial cost of the double glazing windows per square meter is currently around £78.82 and the initial cost of the triple glazing windows per square meter is currently around £80.77, which are both slightly lower than the initial cost of the vacuum pipes windows. This is due to the extensive sale volume and mature market established in association with the double and triple glazing windows. The increase in the capital investment will be rapidly repaid by significant saving from the energy bill for heating the house with the installation of the vacuum pipes windows.

Assuming the heating of the house is provided by a gas boiler with an efficiency of η , the gas consumption of the boiler can be calculated by:

$$Q = q \times (T_{in} - T_{out})/\eta \quad (4-18)$$

Assuming the gas price is £0.04/kWh, the energy savings created by vacuum tubes windows over double glazing windows can be calculated by:

$$S_{vt-dg} = 0.04 \times (Q_{dg} - Q_{vt}) \quad (4-19)$$

Similarly, the energy savings over triple glazing windows can be expressed as:

$$S_{vt-tg} = 0.04 \times (Q_{tg} - Q_{vt}) \quad (4-20)$$

Where Q , q , S are gas consumption (kW/m²), heat loss rate (W/m²), energy saving (£); subscription vt , dg , tg represent vacuum tube window, double glazing window and triple glazing window respectively.

For new buildings, the payback period of the vacuum tubes windows relative to conventional double and triple glazing windows can be calculated using the following equations:

$$PP_{vt-dg} = C_{vt} - C_{dg}/S_{vt-dg} \quad (4-21)$$

$$PP_{vt-tg} = C_{vt} - C_{tg}/S_{vt-tg} \quad (4-22)$$

Where PP , C are payback period (year) and the cost (£) of window.

For retrofit buildings, the calculation of the payback period should exclude the initial cost of the existing double or triple glazing windows, and therefore, the payback period will be relatively longer than the new buildings. The equations can be expressed as:

$$PP_{vt-dg} = C_{vt}/S_{vt-dg} \quad (4-23)$$

$$PP_{vt-tg} = C_{vt}/S_{vt-tg} \quad (4-24)$$

The U-value of the vacuum tubes windows is much lower than the U-value of the double and triple glazing windows. Assuming the energy efficiency of the gas boiler is 90%, the gas consumption to provide heating for house in order to compensate the heat loss through per square meter of windows. For per square meter double and triple glazing windows to be replaced by the vacuum tubes windows, the energy savings are £16.26 and £9.95 respectively.

The total areas of four typical types of houses in the UK are shown in Table 4.6 (Web 4.2).

Table 4. 6: Window areas of four typical types of houses in the UK

House Types	Window Area (m ²)
Detached House	23.7
Semi/Bungalow/Others	16.9
Terrace House	12.7
Flat	6.9

Assuming 20% of the total area of each house type can be replaced by vacuum tubes window, which are not clear view dominated, considered as the windows for conservatory, roof lights, and toilets, bathroom, the energy saving of each household can be calculated by multiply the energy saving per square meter of window replaced by the vacuum tubes windows. The annual energy savings of four typical types of houses are shown in Table 4.7. Data of both double and triple glazing windows replaced by vacuum tube windows are illustrated.

Table 4. 7: Annual energy savings of four typical types of houses in the UK

House Types	Annual Energy Savings (£)
-------------	---------------------------

	Double Glazing Replaced	Triple Glazing Replaced
Detached House	77.07	47.17
Semi/Bungalow/Others	54.95	33.64
Terrace House	41.30	25.28
Flat	22.44	13.73

The costs for new buildings were calculated while considering the compensations of the double glazing and triple glazing windows, as shown in Table 4.8. The payback periods for new buildings were calculated using equation (4-21) and (4-22), and the results are shown in Table 4.9.

Table 4. 8: Costs for new buildings

House Types	Costs (£)	
	Double Glazing Replaced	Triple Glazing Replaced
Detached House	58.11	48.86
Semi/Bungalow/Others	41.44	34.84
Terrace House	31.14	26.18
Flat	16.92	14.23

Table 4. 9: Payback period for new buildings

Payback Period	
Double Glazing Replaced	Triple Glazing Replaced
0.75	1.04

The costs for retrofit buildings without the compensation of double glazing and triple glazing windows were considerably higher than the costs for new buildings. As a consequence, the payback periods for retrofit buildings were considerably longer than that of the new buildings. Table 4.10 shows the costs for retrofit buildings. And Table 4.11 shows the payback periods as calculated from equation (4-23) and (4-24).

Table 4. 10: Costs for retrofit buildings

House Types	Costs(£)
Detached House	431.71
Semi/Bungalow/Others	307.84
Terrace House	231.34
Flat	125.69

Table 4. 11: Payback period for retrofit buildings

Payback Period (Years)	
Double Glazing Replaced	Triple Glazing Replaced
5.60	9.15

4.5.3 Environmental effect

Based on sections above, annual gas consumption of the vacuum tubes windows and the conventional double glazing and triple glazing windows can be worked out, in terms of kWh per annum. These figures could be also converted into carbon emission reduction by replacing double and triple glazing windows with vacuum tubes windows. The following equations can be used:

$$Em_{co2,vt-dg} = f_{c,c} (Q_{dg} - Q_{vt}) \quad (4-25)$$

$$Em_{co2,vt-tg} = f_{c,c} (Q_{tg} - Q_{vt}) \quad (4-26)$$

Where Em is emission (kg) and $f_{c,c}$ is carbon dioxide factor of gas (0.2 kgCO₂/kWh)

Assuming the carbon dioxide factor of 0.2 kgCO₂/kWh, the results derived from the calculation are presented in Table 4.12.

Table 4. 12: Environmental benefits of the vacuum tubes windows relative to the conventional double and triple glazing windows.

House Types	CO ₂ Reduction (kg)	
	Double Glazing Replaced	Triple Glazing Replaced
Detached House	385.35	235.85
Semi/Bungalow/Others	274.75	168.2
Terrace House	206.5	126.4
Flat	112.2	68.65

4.5.4 Life cycle analyses

Assuming an expected life cycle of 50 years, the total energy savings and CO₂ reductions can be calculated by multiplying the energy savings and CO₂ reductions per annum by life cycle time. The results are shown in Table 4.13. The net cost benefits for retrofit buildings can be calculated by subtracting the costs for retrofit buildings. The results are illustrated in Figure 4.24 for new buildings and Figure 4.25 for retrofit buildings respectively.

Table 4. 13: Life cycle analyses of vacuum tubes windows.

House Types	Double Glazing Replaced		Triple Glazing Replaced	
	Energy Savings (£)	CO ₂ Reduction (ton)	Energy Savings (£)	CO ₂ Reduction (ton)
Detached House	3853	19	2358	12
Semi/Bungalow	2748	14	1682	8
Terrace House	2065	10	1264	6
Flat	1122	6	687	3

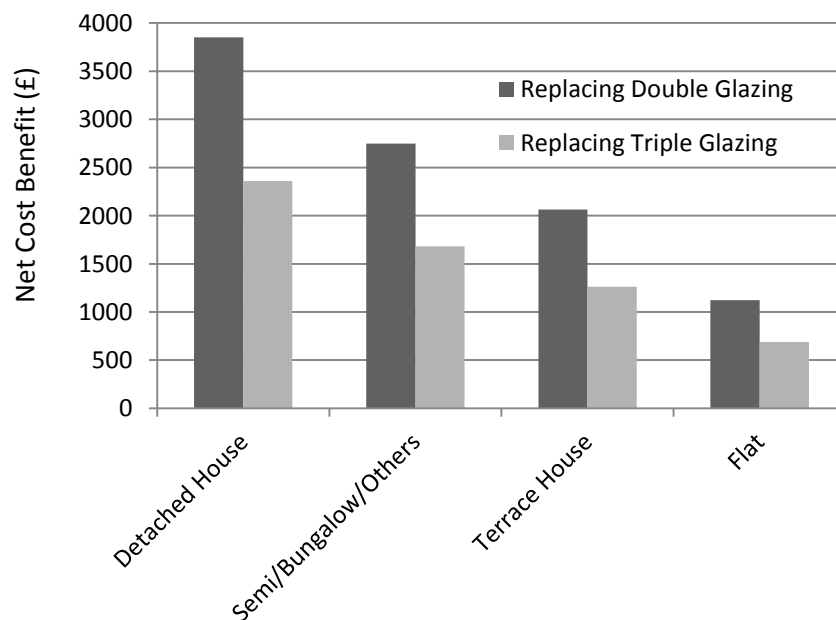


Figure 4. 24: Net cost benefits of replacing double and triple glazing windows with vacuum tube window for new-buildings with different house types.

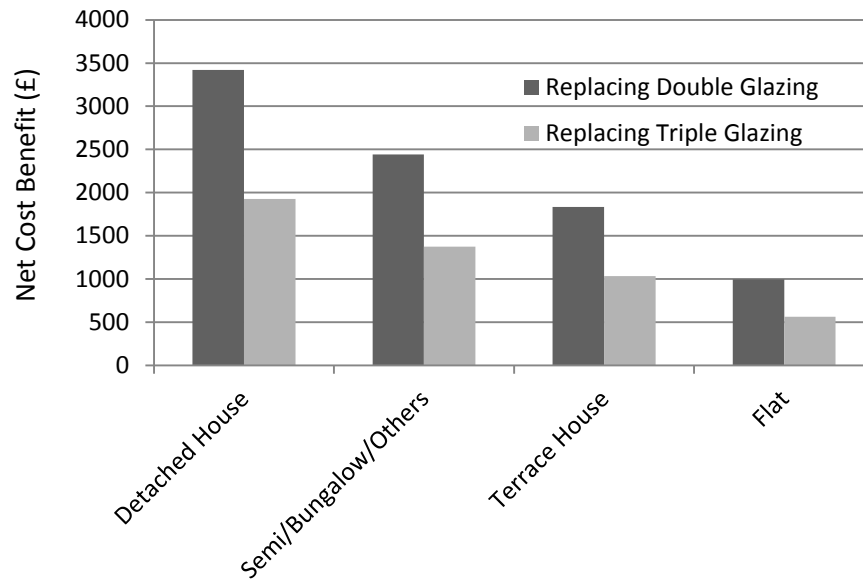


Figure 4. 25: Net cost benefits of replacing double and triple glazing windows with vacuum pipe window for retrofit buildings with different house types.

Due to its low thermal transmittance (U-value), vacuum tube window can reduce over 60% of heat loss compared to double glazing window system and nearly 50% compared to triple glazing window. The capital cost of vacuum tube window, on the other hand, is higher than both double glazing and triple glazing windows by a small margin, 15% and 10% respectively. Despite of the slightly higher capital cost of the vacuum tube window, for each square meter of double glazing window to be replaced by the vacuum pipe window, the annual energy saving is £16.26 and the CO₂ reduction is 81.29kg; and for each square meter of triple glazing window to be replaced by the vacuum tube window, the annual energy saving is £9.95 and CO₂ reduction is 49.76 kg. These values have been calculated based on the assumption that the heating of the house is provided by a gas boiler with 90% efficiency, the gas price is 4 pence/kWh, and the carbon dioxide factor is 0.2 kgCO₂/kWh. Consequently, the payback period for using vacuum tube in new buildings to replace double glazing is 0.75 year and 1.04 year to replace triple glazing. The payback periods for using vacuum tube in retrofit buildings, on the other hand, are longer. For replacing double

glazing, the payback period is 5.6 years, and for replacing triple glazing, the payback period is 9.15 years.

Vacuum tubes windows have huge potential in energy savings and CO₂ reduction in buildings. It has low U-value and significant lower heat loss rate than the conventional double glazing and triple glazing windows. Thereby the heating cost for the buildings will be greatly reduced. A replacement of 20% of the total double glazing window area by vacuum pipes windows can reduce the annual energy bill by £77, £55, £41, and £22, for detached houses, semi-detached houses, terrace houses and flats, respectively. For new buildings, the payback period is 0.75 year, but for retrofit buildings, the payback period is 5.6 years. For the same percentage of the total triple glazing window area to be replaced by vacuum tubes windows, the annual energy savings are relatively smaller due to the low heat loss of the triple glazing windows. A saving of £47 can be achieved for detached houses, £34 for semi-detached houses, £25 for terrace houses, and £14 for flats. Consequently, the payback periods are longer, 1.04 years for new buildings, and 9.15 years for retrofit buildings.

The annual carbon emission reduction is 385kg, 275kg, 296kg, and 112kg for detached houses, semi-detached houses, terrace houses and flats, respectively, if 20% of the total double glazing window area is replaced by the vacuum tubes window. If the replacement is for triple glazing windows, the carbon emission reduction is slightly less than that for double glazing windows. The figures for the four typical house types following the sequence are 236kg, 168kg, 126kg and 69kg.

The estimated life cycle of the vacuum tubes window is 50 years. Over this duration, for the 20% of replacement by vacuum tubes windows for double glazing windows, the net cost benefits can be range from £1100 to £3800, depending on the house types.

The carbon emission reduction can be ranged from 6 ton to 19 ton. For the 20% of replacement by vacuum tubes windows for triple glazing windows, the net cost benefits can be range from £670 to £2310, and the carbon emission reduction can be ranged from 3 ton to 12 ton, depending on the house types.

4.6 Summary

This chapter described prototype of a novel window system as well as mathematical analyses of the energy transfer process through a setup of computer programme. Computer model developed is to optimise the unit structure and constructed materials, simulate its performance and identify the favourite combination. The calculation results showed novel vacuum tube window unit is able to reduce thermal dissipation from buildings because of its low thermal transmittance. The overall heat transmittance could be achieved low to around $0.5 \text{ W/m}^2\cdot\text{k}$ by the combined configuration of double wall vacuum tube and vinyl frame. Parameters of outdoor wind speed has very limited influence to overall thermal transmittance while elements of frame types and ratios of frame area to window area impact the overall thermal penetration much more, especially frame types. Those factors are all as the direct ratio to the overall U-values. Even though laboratory test U-value results are slightly higher than computer modelling results, overall U-value achieved less than $1.0\text{W/m}^2\text{K}$ has shown the huge commercial potential of vacuum tubes window. Thermal images of vacuum tubes window installed in simulation room have indicated that the significant heat losses are through tubes' vertical joints. The improvement of manufacturing technic is essential to reduce U-value low to its theoretical results. Capital and operation cost of the vacuum tubes windows relative to the conventional double and triple glazing windows have been illustrated, as well as estimation of the payback

period of life cycle cost saving of the vacuum tubes windows. Carbon emission reduction potential of using vacuum tubes windows across the UK has also been analysed.

Chapter 5 Aerogel and Argon Window

5.1 Introduction

For advanced window technologies, high thermal resistance (low U-value) of windows has been considered as the important feature of current advanced glazing to meet low energy consumption requirement. High-tech glazing shall allow both for visual contact with the environment or for the passive use of the solar energy, e.g. daylighting purpose and realization of solar gain (Reim et al., 2001). Both applications are required to have high thermal resistance.

The thermal performance of the windows has significantly improved over the last few years. Low emissivity coatings and low conductivity gas filled windows have greatly increased the thermal resistance between the panes (Arasteh et al., 1985). However, the insulating potential for combinations of multiple low-E layers and gas filled gaps is limited by decreasing solar transmittances and increasing glazing thickness. Heat transfer across the gap between two glazing layers may be greatly reduced by evacuating the space or by filling it with a transparent insulating material such as aerogel (Hartmann, 1987).

Chapter 4 has studied thermal transmittance (U-value) of novel vacuum tubes window system, this chapter will investigate thermal performance of novel designed double glazed window system filled with Aerogel, argon gas or both, thereby to compare the U-value results of high performance windows.

5.2 Translucent insulating material - Aerogel

Silica aerogel has become a promising material applying for building envelopes as its high visual transmittance and low thermal conductivity (Fricke, 1985). Silica Aerogel

is as optically transparent and thermally insulating material, has a very low-density silica-based solid ($2\text{-}3\text{ mg/cm}^3$) composed of 99.8% air. It has high compressive strength and very low thermal conductivity ($0.01\text{ W/m}^2\text{K}$). Monolithic silica aerogel is a highly porous material with pore diameters in the range of 10-100nm (Brinker et al., 1990). The porosity is above 90%, which combined with the nanometer pore size makes the aerogel a highly insulating material with thermal conductivity lower than of still air (Fricke, 1986).

Aerogel glazing has a solar energy transmittance equal to plain double glazing and at the same time a heat loss coefficient equal to the best triple-layered gas-filled glazing units (Jensen, 2004). Silica aerogel can be produced to have high transmittance of solar energy and daylight making it a very viable material for energy efficient windows (Web 5.1). Monolithic silica aerogel is the only known material that has this excellent combination of high solar and light transmittance and low thermal conductivity-materials parameters that make it possible to achieve a net energy gain during the heating season for north-facing windows in a northern European climate such as the Danish climate (Jensen et al., 2004).

Comparing to other highly insulating glazing units, aerogel glazing has higher solar energy transmittance, which in cold climate has a large impact on the annual energy consumption for space heating (Jensen, 2004). Placing the aerogel between two layers of glass reduces the solar energy transmittance because of absorption and reflection in the glass panes. The iron content in the glass and glass thickness has influence on absorption. A common 4mm thick float glass absorbs 10% of the solar energy, while a 3mm thick glass absorbs 8% (Jensen, 2004).

In previous work, two main glazing type of daylighting applications for office buildings have been developed and investigated: (1) diffusely scattering systems, e.g. windows containing aerogel layers (Dengler and Wittewer, 1994) or fleeces between window panes (Geuder et al., 2000); (2) light redirecting systems with light redirecting elements (Beck et al., 1999) or prismatic layers, excluding direct sunlight via total internal reflection (Beck et al., 1999). Both systems reduce electricity consumption in office buildings as less artificial lighting is required as well as heating and cooling loads. Newly developed aerogel glazing aims to have above features and is described in the following contents.

5.3 Aerogel-argon window system description

Granular silica aerogel have been integrated into highly-insulating translucent glazing (Reim et al., 2002). A new design Aerogel-Argon window has been manufactured by Vale Window Company which can be satisfied with the requirement of insulation and lighting. Aerogel glazing offers the possibility to provide diffuse natural light. Following the current standards for testing and rating window thermal performance, the window thermal performance is represented by two characteristics, measured separately, the overall heat transfer coefficient U , and the Transmittance (Alvarez, 2000). The laboratory tests have been carried out to estimate its thermal performance of the new design aerogel-argon window.

The novel structures of aerogel window prototypes are produced by Vale Window Company. The prototypes have 4mm, 5mm, 6mm-thick double panes filled with granular silica aerogel only or aerogel and argon filled in half (Figure 5.3). The design combines Agerogel and argon can improve window's thermal performance and satisfy day lighting requirement. The pane-skin distance is adapted to avoid convection of

gas filling. Normally rare gas Argon and krypton have optimal spacing of about 16mm and 12mm, respectively. Convection will start when the spacing is greater as far as gases are concerned (Reim et al., 2002). The diffusely back-scattered light causes aerogel glazing whitish appearance. This novel window comprises two panes of glass, separated by a spacer bar and seals to create a hermetically-sealed environment. The cavity width between the two panes, aerogel and gas filling used and the type of spacer bar, are all key factors in the unit's final energy, solar and acoustic insulation properties. Double rim seal along the glazing perimeter are gas and moisture tight and have low thermal conductivities to reduce thermal bridge effects. The first sealed layer is Super Spacer[®] Standard insulation (Figure 5.1) from Edgetech Company, second layer is hot melt butyl edge sealant from Bostik Company.



Figure 5. 1: Manufacture Process for Super Spacer[®] Standard Insulation

There are several ways to minimize the thermal bridge effect: (1) select materials with a low thermal conductivity; (2) minimize the material thickness; (3) increase the heat flow path-length; or (4) a combination of all three (Jensen, 1992). As shown in Figure 5.1, the two single glaze windows are sealed and stick by the good performance warm edge insulation. It is a flexible, organic foam space product that provides excellent insulation for sealed glazing units. Desiccant-filled with re-applied side adhesive, the structural foam spacer significantly simplifies insulating glass production. The warm-edge can typical save of up to $0.2\text{W}/\text{m}^2\text{K}$ in overall window U-value improvement.

The lifespan are over 20 years. Good flexibility of the material makes the Aerogel possible to be easily filled into the space between of the two layers window (Web 5.2).

As shown in Figure 5.2, the two layer window filled with Aerogel and Argon gas was sealed again by melt butyl edge sealant. Bostik 5000 Hot Melt Butyl IG Sealant is a single part butyl rubber based sealant, specially developed for the edge sealing of factory produced insulating glass units (Web 5.3).



Figure 5. 2: Image of Hot Melt Butyl Edge Sealant



(a) 300mm×300mm Aerogel-Argon Window Prototype

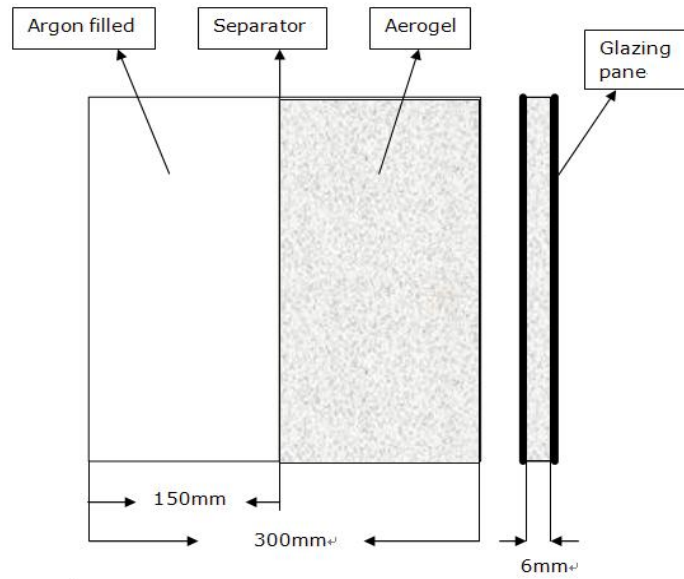


Figure 5. 3: Schematic Drawing and Prototype of 6mm Thickness 300mm×300mm Aerogel-Argon Window

As Figure 5.3 shows, 6mm thick Aerogel-argon window prototype, the space between two glass panes is separated into two parts in the middle by warm edge insulation. One part is filled with Aerogel and the other is filled with Argon gas. This design is easier to be manufactured and also can satisfy the requirements of both insulation and lighting.

There 5mm Aerogel window, 4mm Aerogel window and 20mm Argon gas filled double glazing window fitted with warm edge spacer are used to compare the test results. The technical characteristic of four window samples are summarised in Table 5.1.

Table 5. 1: Specifications of Window samples

Sample windows cavity filled with	Glazing Area (mm ²)	Inside glass pane thickness (mm)	Cavity distance (mm)	Outside glass pane thickness (mm)
Argon	300x300	4	20	4
Aerogel-Argon	300x300	4	6	4
Aerogel	300x300	4	5	4
Aerogel	300x300	4	4	4

5.4 Mathematical analyses of the energy transfer process

5.4.1 Energy flow chart and thermal transportation

To understand silica aerogel insulating performance in a window system, the study of window component heat transfer paths is shown in Figure 5.4. At ambient temperatures, for aerogel thickness of 0.5-5cm, radiation heat transfer through an unmodified aerogel window is less than 15% of the total heat flux. Thereby radiation heat transfer is negligible over much of this region (Hartmann et al., 1987). Aerogel's thermal performance can be improved by replacing the pore gas with one of lower conductivity or by evacuating the aerogel to pressure below 0.1 atm. This research was undertaken in order to optimize the design of aerogel windows' applications. Both radiation and conduction heat transfer are greatly reduced and convection is non-existent in aerogel. Energy flow through Aerogel-argon windows is via conductive and convective heat transfer caused by the temperature difference between outdoor and indoor air, shown as Figure 5.4.

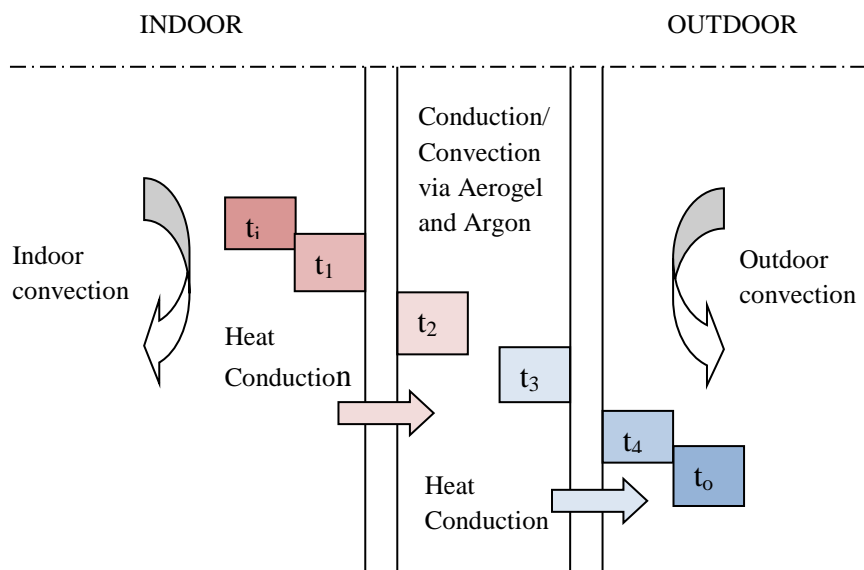


Figure 5. 4: Aerogel and Argon window construction details and heat Flow Process

The window consists of subdivisions like super spacer and frame. The overall thermal energy Q_{th} is simply calculated as:

$$Q_{th} = A_g q_g = A_g U_o (t_{max} - t_{min}) = A_{ng} q_{ng} + A_{ss} q_{ss} + A_f q_f \quad (5-1)$$

where q is heat transportation per square meter, W/m^2 ; A is the square meters, m^2 ; U_o is the overall heat transmittance; t is the temperature, $^{\circ}C$; the subscript ng , g , ss and f refer to the net glazing areas, glazing unit, super spacer and frame respectively.

Based on equation (5-1), the overall heat transmittance (U_o) is then estimated by using the area-weighted U-values for contribution (ASHRAE, 2009):

$$U_o = \frac{A_{ng} U_{ng} + A_{ss} U_{ss} + A_f U_f}{A_g} \quad (5-2)$$

In principle, the thermal transmittance is the reciprocal of the total thermal resistance (Holman, 1981):

$$R = 1/U_o \quad (5-3)$$

Thus the overall thermal resistance of the window unit could be given as following

Figure 5.5:

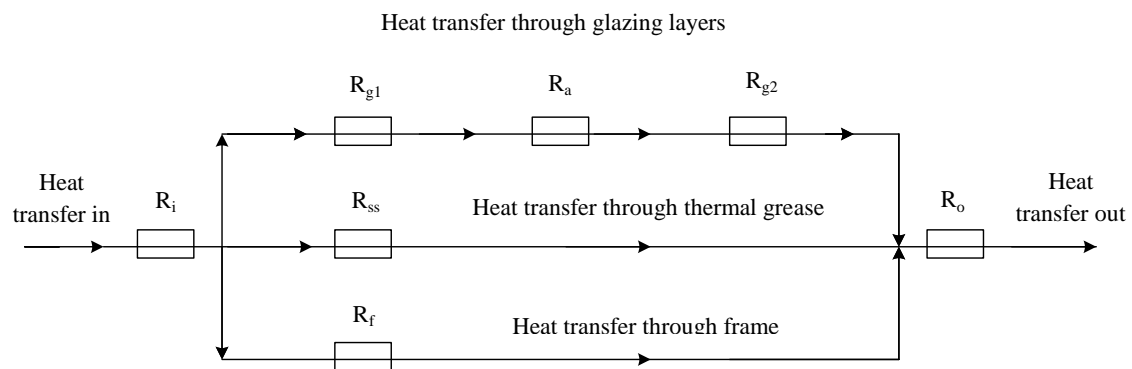


Figure 5. 5: Thermal network model of Argon & Argon window unit

Where the subscript i , g , a , ss , f and o refer to indoor, glazing layer, argon & argon, super spacer, frame and outdoor respectively.

5.4.2 Heat Transfer through vacuum tube glazing unit

For the thermal transmittance, heat transfer through glazing units can be derived from a double glazing unit. Figure 5.4 illustrates the heat transportation process in winter condition. The overall thermal transmittance of aerogel glazing unit is written by the following equation (5-4).

$$R_g = \frac{1}{h_o} + \sum_{i=1}^2 R_{g,i} + R_a + \frac{1}{h_{in}} \quad (5-4)$$

where h is the heat transfer coefficient, $W/m^2 \cdot K$ and subscription o , g , a and in respectively represent the outdoor environment, glazing layer, aerogel layer, and indoor thermal coefficient.

5.4.3 Calculation result

Base on the heat transfer analysis above, the calculation could be carried on by inputting necessary parameters. Table 5.2 shows the preparing parameters of a thickness of 6mm aerogel vinyl framed window under the standard boundary conditions in winter and Table 5.3 displayed the output results.

Table 5. 2: Input parameters of vinyl frame 6mm Aerogel window unit for calculation

Winter standard boundary condition and specific parameters	Value	Unit
Indoor heat transfer coefficient h_{in}	2.5	$W/(m^2 \cdot K)$
Indoor thermal resistance R_{in}	0.4000	$(m^2 \cdot K)/W$
Outdoor heat transfer coefficient h_o	8.5000	$W/(m^2 \cdot K)$
Outdoor thermal resistance R_o	0.1176	$(m^2 \cdot K)/W$
Heat conductance of glazing cover λ_g	332.8895	$W/(m^2 \cdot K)$
Thermal resistance of glazing cover R_g	0.0030	$(m^2 \cdot K)/W$
Thermal transmittance of frame U_f	1.7000	$W/(m^2 \cdot K)$
Thermal resistance of frame R_f	0.5882	$(m^2 \cdot K)/W$
Thermal transmittance of Super Spacer U_{ss}	0.1220	$W/(m^2 \cdot K)$
Thermal resistance of Super Spacer R_{ss}	8.1967	$(m^2 \cdot K)/W$
Indoor temperature t_{in}	18.0000	$^{\circ}C$

outdoor temperature t_o	10.0000	°C
Prototype width a	0.3000	m
Prototype height b	0.3000	m
Prototype area A_g	0.09	m ²
Frame to window area ratio	0.0500	
Frame area of prototype A_f	0.0045	m ²
Super Spacer channel to window area ratio	0.0500	
Super Spacer channel area of prototype A_{ss}	0.0045	m ²
Prototype net area A_{ng}	0.081	m ²
Thermal transmittance of Aerogel U_{aer}	0.017	W/(m ² ·K)
Thickness of Aerogel layer	0.006	m

Table 5. 3: Output of vinyl frame 6mm Aerogel window unit under standard winter condition (Indoor temperature at 18°C, outdoor temperature at 10°C)

Procedure temperatures	Value	Unit
Temperature of indoor glazing t_1	°C	17.5
Total heat transfer input glazing $q_{g,1}$	W/m ²	1.25
Temperature of inside glazing surface t_2	°C	17.5
Temperature of inside glazing surface t_3	°C	10.15
Temperature of outdoor surface tube t_4	°C	10.15
Total thermal resistance R_g	(m ² ·K)/W	0.88
Total thermal transmittance of glazing U_g	W/(m ² ·K)	1.15
Total thermal resistance of super spacer R_{ss}	(m ² ·K)/W	0.6396
Total thermal transmittance of super spacer U_{ss}	W/(m ² ·K)	1.5634
Total thermal transmittance of 6mm Aerogel window U_o	W/(m ² ·K)	1.18987
Total heat transfer output glazing $q_{g,2}$	W/m ²	1.25

U-values of various thicknesses, cavity filled with Aerogel, argon and Aerogel-argon windows are calculated by computer modelling program described above, the results are shown in Table 5.4 and Figure 5.6.

Table 5. 4: U-values of various thicknesses, cavity filled with Aerogel, Argon and Aerogel-argon windows

Window cavity filled with	Thickness (mm)	U-values (W/m ² K)
Aerogel	4	1.349
Aerogel	5	1.2637
Aerogel	6	1.1898

Aerogel	10	0.9726
Aerogel and Argon	6	1.5345
Argon	6	1.8791
Argon	20	1.873

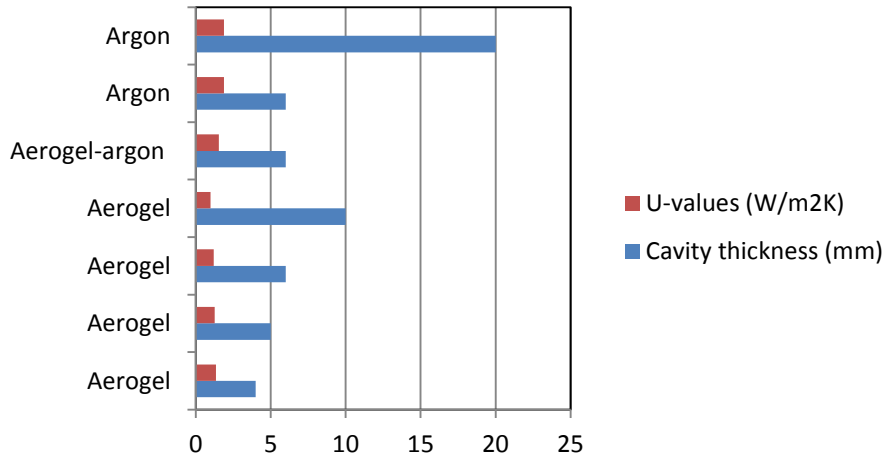


Figure 5. 6: U-values of various thicknesses, cavity filled with Aerogel, Argon and Aerogel-argon window

From above Tables 5.2 and 5.3, it's shown that overall thermal transmittance of 6mm Aerogel vinyl framed window could be achieved to $1.19\text{W/m}^2\text{K}$, which shows the thermal potential of aerogel window with less cavity thickness. Table 5.4 and Figure 5.6 demonstrate the relationship between window U-values and various thicknesses of window cavity filled with aerogel, argon or both. Chart trend shows U-Value can be reduced by enlarging the cavity thickness. For Aerogel insulating window, 10mm Aerogel window's U-value can reduce 28% compared to 4mm Aerogel window. For Argon filled window, cavity width has less impact on U-values results.

5.5 Laboratory test for Aerogel and Argon window prototype

5.5.1 Test method and procedure

The centre U-values of the window prototypes have been measured by using hot box method. Four of the optimized prototypes are used for test window measuring $300\text{mm}\times 300\text{mm}^2$ designed for hotbox measurements of the overall U-value. The test rig is shown in Figure 5.7, 6mm Aerogel-Argon window, 5mm, 4mm Aerogel window and 20mm argon double glazing window jointed together to construct a test box. The well insulated framing system is made to fix in place the four glazing. Temperature difference across inside and outside glazing surface were measured by K type thermocouples. Air temperature in the hot box and cold side (laboratory) were also measured. Heat flux sensors were used to measure the heat flux through window glazing. 40W lamp was used as constant power supplied to the hot box. Test data was collected by DT500 data logger.



Figure 5. 7: Aerogel Window Test Rig

5.5.2 Test results and analysis

The air temperature in the hot box was set up at 32°C . Laboratory temperature was 20°C measured by thermocouple. The test results for temperatures, heat flux through each window sample are summarized in Figure 5.9. Inside surface temperature of

aerogel glazing is closed to inside hot box air temperature. The measured overall U-value of the glazing is deduced from the measurements by subtracting the heat loss through the framing system. The average total U-value of 5mm aerogel glazing is $2.03 \pm 0.1 \text{ W/m}^2\text{K}$, comparing to its average centre U-value of $1.95 \text{ W/m}^2\text{K}$, which shows small thermal bridge effect of the developed rim seal solution.

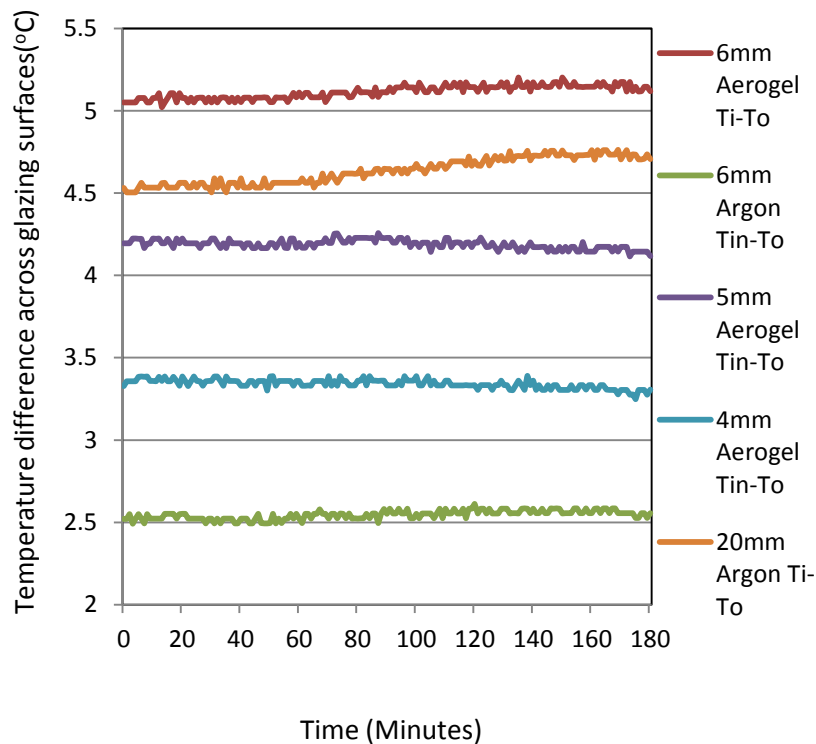


Figure 5. 8: Time against Inside and Outside Glazing Surface Temperature Differences of Window Samples

Figure 5.8 shows the temperature differences between inside and outside surface of window samples against time. Surfaces temperature differences measurement will demonstrate the capabilities of heat transfer resistance for each window sample, the higher values in surfaces temperature changes the lower heat transfer resistance for glazing sample, vice versa. It can be seen from the figure that inside and outside surface temperature difference of $2.6 \text{ }^\circ\text{C}$ for 6mm Argon window is lower than other

window samples. The temperature difference of 6mm Aerogel window with 5.1 °C is highest among all the window samples. The temperature difference of Aerogel-Argon window is calculated as 3.8 °C, which is better than 20mm double glass Argon window.

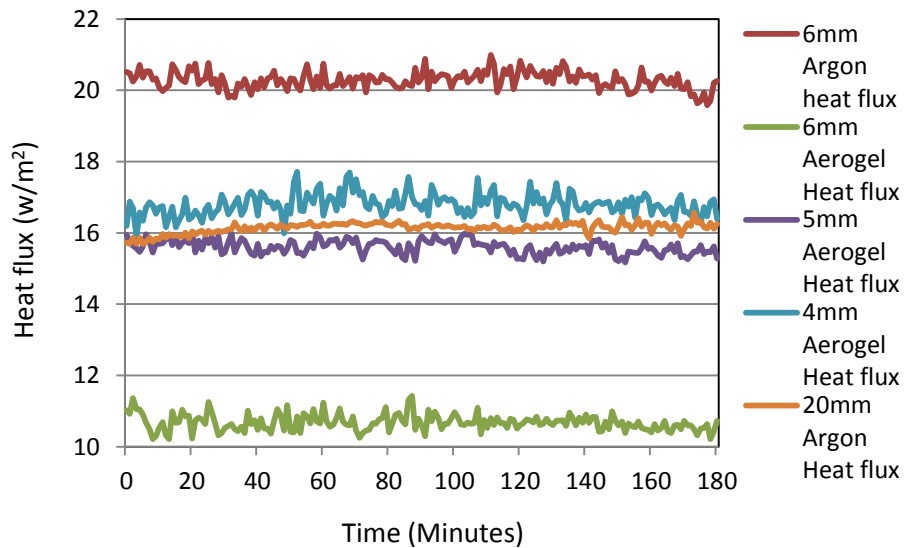


Figure 5. 9: Time against Heat Flux of Window Samples

Heat flux through four different prototype windows were measured by Heat flux sensor. The heat flux sensors used in this test have sensitivities of 63.6 $\mu\text{V}/\text{W}\cdot\text{m}^2$ and 63.9 $\mu\text{V}/\text{W}\cdot\text{m}^2$. Heat flux through glazing was calculated from dividing the voltage (measured by data logger) by sensors' sensitivity. The chart trend is similar with surface temperature difference measurements, the lower values in heat flux the less heat loss through the glazing sample. As shown in Figure 5.9, the heat flux of 20.28 W/m^2 for 6mm Argon window is higher than other windows. The heat flux of 10.68 W/m^2 for 6mm Aerogel window is the lowest among the window samples. The average heat flux was respectively 15.48 W/m^2 for 6mm Aerogel-Argon window, 15.61 W/m^2 for the 5mm Aerogel window, 16.79 W/m^2 for the 4mm Aerogel window and 16.14 W/m^2 for the 20mm Argon gas filled double glasses window fitted with

warm edge spacer. The results demonstrate Aerogel window has the best thermal performance compared to other samples.

5.5.3 U-value calculation

U-Value is a measurement of insulation in general, the lower the value the more efficient the window as less fabric heat is lost through the glass or frame. U-values are measured in $W/m^2 K$ which is the unit of watts per square meter per degree or in other words the amount of heat loss through one square meter of material for every degree difference in temperature between the inside and outside. U-values were calculated as a function of gap width for aerogel-filled and available window configurations under standard ASHRAE winter conditions.

$$Q = \frac{k \times A \times \Delta t}{d} \quad (5-5)$$

Where Q is heat transfer (Watts), K is thermal conductivity of the component ($W/m^{\circ}C$), A is area of the window (m^2), Δt is temperature difference between inside and outside ($^{\circ}C$), d is distance between the faces (m).

By calculating K thermal conductivity

$$R = \frac{d}{k} \quad (5-6)$$

Where R is thermal resistance of the component ($m K/W$)

$$U = \frac{1}{R} \quad (5-7)$$

Where U is thermal conductance ($W/ m K$)

(U value is a measure of the overall rate of heat transfer by all mechanisms under standard conditions through a particular section of the construction).

By using above heat transfer equation, U-Values have been calculated in the steady state condition when the temperature inside the box was at $32\pm 0.5^{\circ}\text{C}$. As shown in Figure 5.10 and Figure 5.11, The average U-values at the testing temperature were $1.97 \text{ W/m}^2\text{K}$ for the 6mm Aerogel-Argon window, $2.03 \text{ W/m}^2\text{K}$ for 5mm Aerogel window, $2.19 \text{ W/m}^2\text{K}$ for 4mm Aerogel window and $2.07 \text{ W/m}^2\text{K}$ for 20mm Argon gas filled double glazing window fitted with warm edge spacer. Compared to a standard double glazed window unit with 20mm air gap (U-value of $2.8 \text{ W/m}^2\text{K}$), the U-value of 6mm Aerogel-Argon window has improved by 45% in theory and 30% in reality, both outcome have shown the significant improvement of this novel window design's thermal performance.

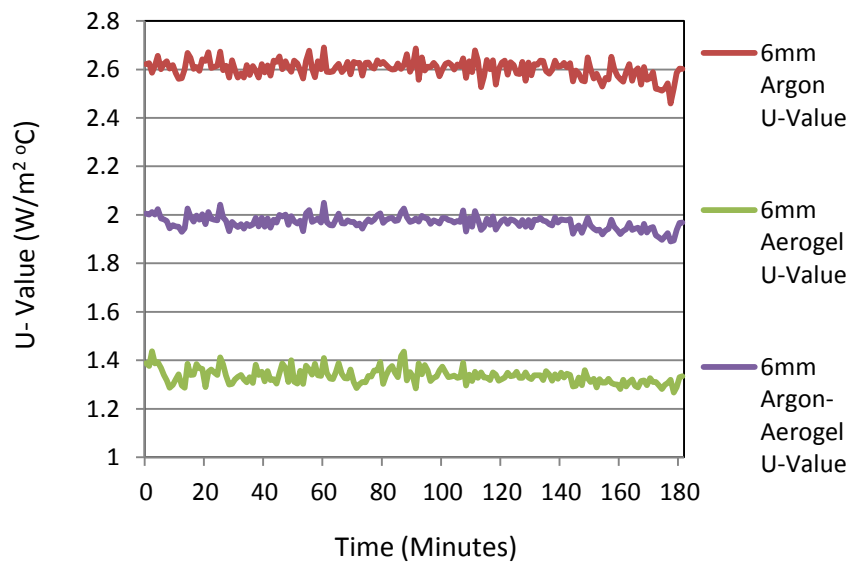


Figure 5. 10: U-Value of Aerogel Window sample

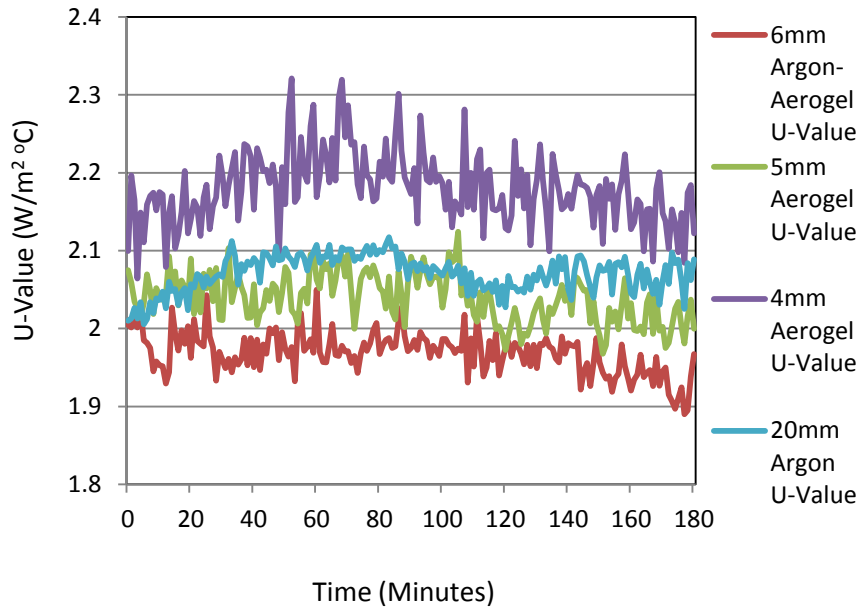


Figure 5. 11: U-Value of Window samples

U-value of Aerogel-Argon windows for different thickness can be calculated from heat transfer algorithm. A summarized results in is shown in Table5.5. Compared to standard double glazed window unit with 20mm air gap (U-value of 2.8 W/m²K), the U-value of 6mm, 10mm and 20mm Aerogel-Argon window can be improved by 30%, 35% and 45% respectively.

Table 5. 5: U-value of different thickness Aerogel, Argon and Aerogel-Argon windows

Window prototype with different materials	Window U-Value of (W/ m ² K) thickness 6mm	Window U-Value of (W/ m ² K) thickness 10mm	Window U-Value of (W/ m ² K) thickness 20mm
Aerogel	1.33	1.19	1.02
Argon	2.60	2.43	2.07
Aerogel & Argon	1.97	1.81	1.55

Windows U-values will decrease if extends gap width between window panes as Table 5.5 shows. Aerogel insulating window has the best thermal resistance compared to others. U-Value of $1.02\text{W}/\text{m}^2\text{K}$ for 20mm thick aerogel filled double glazed window can be achieved.

5.6 Thermal imaging results

Thermal imaging camera was used to record thermal performance for four different glazing samples as Figure 5.12-15 show. Window box was heated from inside by a heat supply lamp to maintain at a constant temperature $32\pm 0.5^\circ\text{C}$. Thermal images were taken when temperature equilibrium was reached, less than 1% fluctuations in the average air temperature on hot and cold sides of the metering area. Temperatures data (Figure 5.14) show that the highest temperature of 27.8°C appears on 6mm Argon filled glazing surface. 20mm argon filled double glazing has slightly better thermal resistance than 4mm and 5mm Aerogel windows with the surface temperature of 26.6°C .

The thermal images results correspond well with U-value test results, in which, 6mm Aerogel-argon window has the best thermal potential compared to other glazing samples. 20mm argon filled double glazing achieved better U-value results than 4mm Aerogel window glazing.

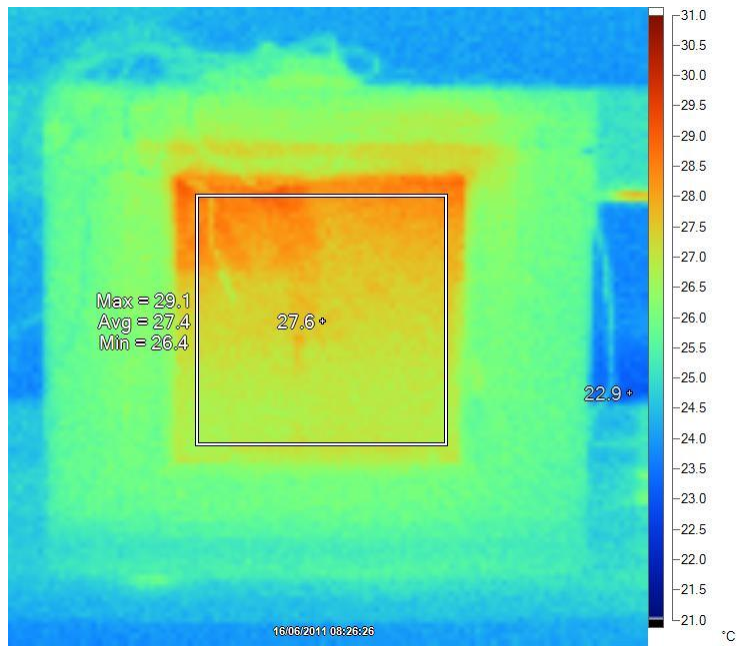


Figure 5. 12: 4mm Aerogel glazing

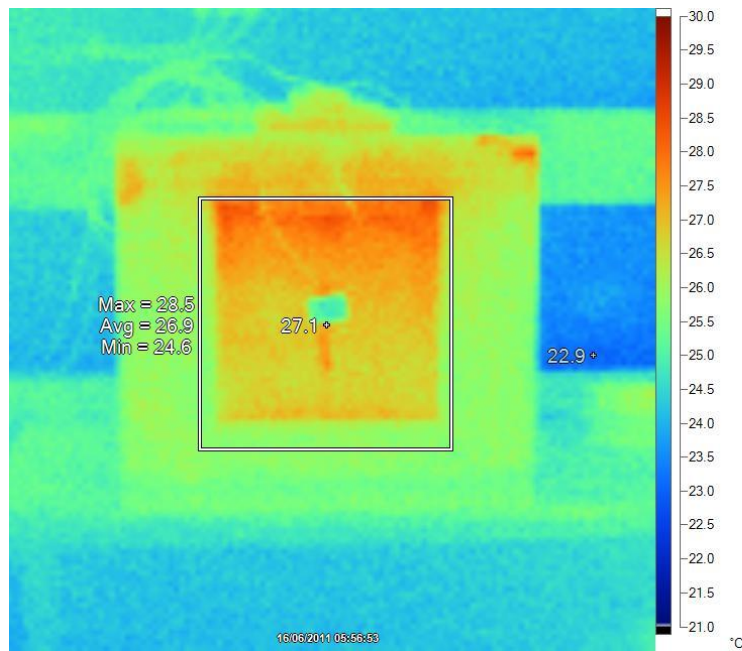


Figure 5. 13: 5mm Aerogel glazing

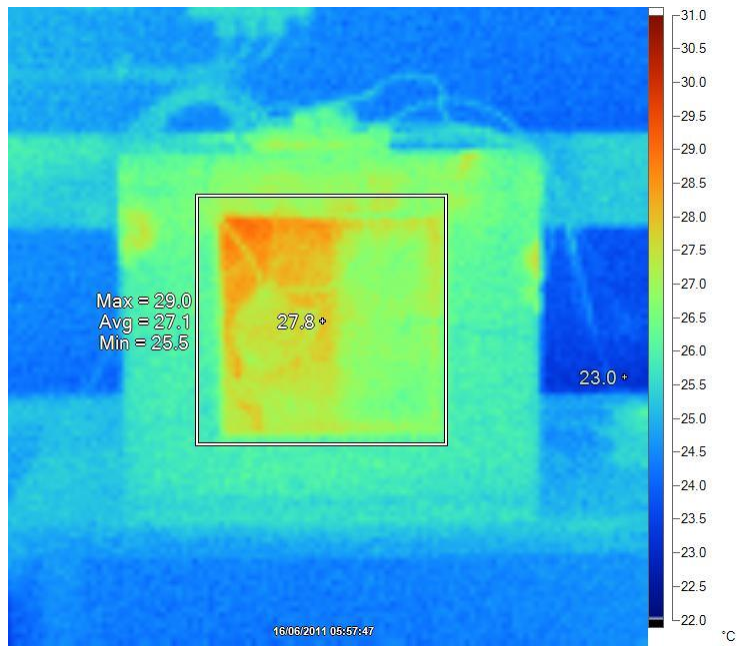


Figure 5. 14: 6mm Aerogel-argon glazing

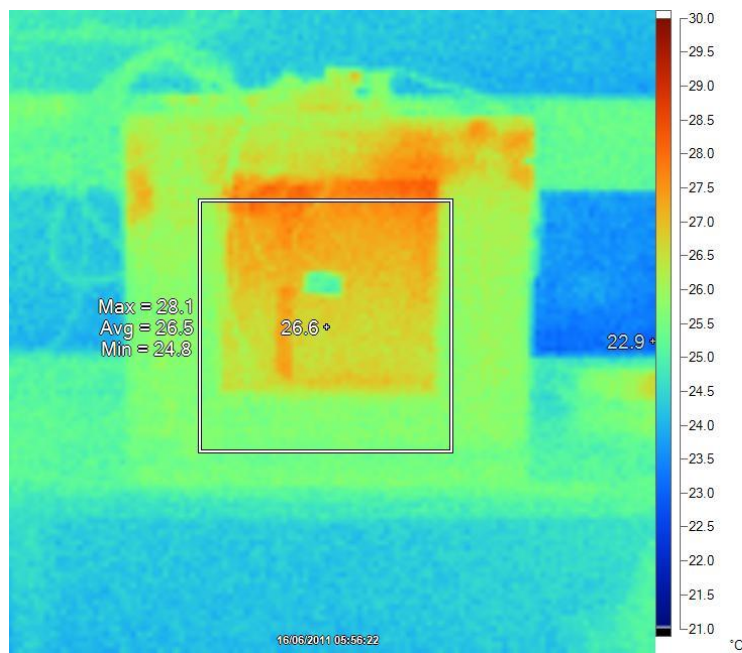


Figure 5. 15: 20mm Argon filled glazing

5.7 Summary

As a promising insulating material for daylighting function, the application of Aerogel has been applied to this novel window system design. U-values of four different window samples described in this chapter have been tested in the laboratory. Results show that using aerogel to fill the gap can significantly improve the thermal performance than standard double-glazed windows. For the new design Aerogel-Argon window, the U-value of 6 mm Aerogel-Argon window is $1.97 \text{ W/m}^2\text{K}$. Compared to a standard double glazed window unit with 20mm air gap (U-value of $2.8 \text{ W/m}^2\text{K}$), the U-value of 6mm Aerogel-Argon window has improved by 45% in theory and 30% in reality. Thermal image results visualise the heat loss level through different examples, thermal performances for sample windows have been analyzed by surface temperatures differences.

Chapter 6 Thermoelectric (TEC) Window System

6.1 Introduction

Chapter 4 has presented mathematical and experimental study of vacuum tube windows' thermal performance in terms of its significant improvement in U-values. In this chapter, evacuated tube panels window system is further developed to thermoelectric self-powered window heating system. Window system can become a heat pump by using thermoelectric (TEC) modules' Peltier effect. In future practice, PV system will be employed to transfer solar energy directly into electrical energy. This electrical energy is subsequently used to power TE heat-pump system. The TE and PV systems integrated into window and building surface are therefore to construct a self-powered window heating system. Depending on the direction of electrical current applied to the TE system, TEC window can operate in a heating or cooling mode. TEC window system has ability to actively control the flow of heat into the room during the daytime when solar radiation applies. As a result, window will become "Energy Suppliers" as well as "Energy Managers". Applications for this technology aim to reduce energy demands for both heating and cooling loads within the building.

In the following contents, thermoelectrics applications are reviewed. Proposed TEC window system is depicted and studied for its potential application. Coefficient of performance (*COP*) for TE system are presented when TE modules were operated under different voltage regimes and tested in various outdoor conditions. The thermal performance of TEC window system will be discussed by comparing measured data and computational models results of TE system.

6.2 Thermoelectrics (TE) application

The advantages of thermoelectric devices include: (1) Thermoelectric devices have no moving parts and noise free when it's in operation, need substantially less maintenance; (2) Life testing shows the capacity of thermoelectric devices to exceed 100,000 hours of steady state operation; (3) Thermoelectric devices contain no chlorofluorocarbons or other materials that may require periodic replenishment; (4) The direction of heat-pumping in a thermoelectric system is fully reversible. Changing the polarity of the DC power supply can cause heat to be pumped in the opposite direction - a cooler can then become a heater; (5) Precise temperature control to within $\pm 0.1^{\circ}\text{C}$ can be maintained using thermoelectric devices and appropriate support circuitry; (6) Thermoelectric devices can function in environments that are too severe, too sensitive, or too small for conventional refrigeration; (7) Thermoelectric devices are not position-dependent (Riffat and Ma, 2003).

Thermoelectric devices have very extensive applications in wide area due to their advantages, such as military, aerospace, instrument and industrial or commercial products in the past decade. The applications can be classified into three categories according to the working modes, which are coolers (or heaters), power generators or thermal energy sensors.

6.2.1 Thermoelectric devices as cooler

➤ Cooling electric devices

One of the applications of thermoelectric cooling device is cooling heat-producing device to keep the device in normal operation. Another application is to reduce the thermal noise of the electric components and the leakage current of the electronic devices, which can improve the accuracy of the electronic instruments (Riffat and Ma,

2003). Applications of thermoelectric devices for cooling electric devices require very small and low current thermoelectric devices. Thermoelectric coolers are also widely employed in microelectronics to stabilise the temperature of laser diodes, to cool infrared detectors and charge-coupled devices, and to reduce unwanted noise of integrated circuits (Riffat and Ma, 2003).

➤ Refrigerator and air conditioner

The early examples of using thermoelectric devices for refrigerators can be found in 1950s-1960s (Riffat and Ma, 2003). The low COP of thermoelectric devices has limited their development in the past decades. But in recent years the interests in the use of thermoelectric devices for domestic refrigerators have been revived. Many improved thermoelectric refrigerators have been reported by US patents (Riffat and Ma, 2003). Thermoelectric devices are also widely used in other niche applications where the cooling demands are not too great (such as portable cooler boxes) or cases in which the energy cost is not the main consideration (such as military applications). Thermoelectric equipment for specific application in military, aerospace, instrument, biology, medicine and industrial or commercial products have been reported in literature.

6.2.2 Thermoelectric devices for power generation

Thermoelectric converter for electric power generation is depicted in Figure 6.1. A thermoelectric module is sandwiched between a heat source and a heat sink. Heat from the source flows through the module and is rejected through the heat sink into the ambient. When a temperature difference is established across the module, electrical power will be generated.

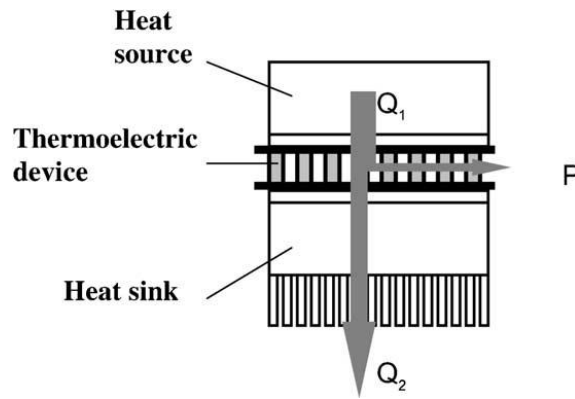


Figure 6. 1: Conventional arrangement for thermoelectric power generation (Riffat and Ma, 2003).

Where Q_1 is the heat supplied by the heat source, P is the electrical power generated, Q_2 is the heat dissipated to the heat sink, which is the thermal energy wasted.

➤ Low power generation

In the condition of none solar light available, small temperature differences can be used to operate a small thermoelectric generator. Therefore, small, inexpensive and efficient thermoelectric generators are gaining importance as a replacement for batteries in many systems (Glosch et al, 1999). Thin film thermoelectric generators for electric applications are currently commercially available (Web 6.1).

➤ High power generation

Thermoelectric devices using waste heat to produce electricity can reduce the cost-per-watt of the devices. Although thermoelectric generator has been improved significantly when used for waste heat recovery, the generator still dissipates a large amount of unconverted heat from its cold side due to its relatively low conversion efficiency. In order to overcome this drawback, a proposed concept of “symbolic” generation using the thermoelectric generator as a dual function device (heat exchanger/generator) has been designed. The basic arrangement of a thermoelectric

symbiotic cogeneration system is depicted in the Figure 6.2. The heat dissipated from the thermoelectric generator is used to preheat the fluid, i.e. Q_2 is not wasted. When heat flows through a thermoelectric generator, part of the heat absorbed is converted into electricity, while the rest, instead of being discharged to the ambient, is collected and used for preheating (Riffat and Ma, 2003).

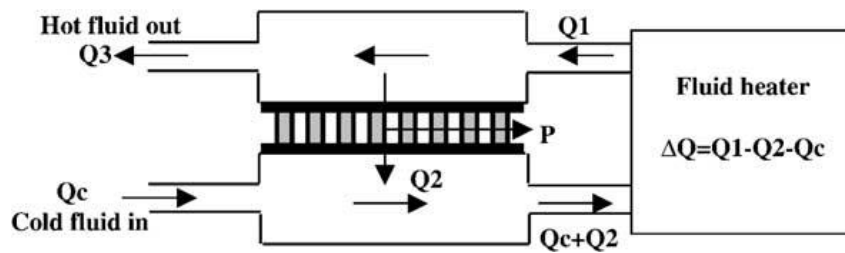


Figure 6. 2: An example of a thermoelectric generator as a fluid preheating/parasite generation device (Riffat and Ma, 2003).

Applications of solar thermoelectric generators are also attractive because solar energy is clean and inexhaustible. The use of solar thermoelectric generator usually combines a solar thermal collector in hot side with a thermoelectric generator. Electric energy will be generated once the temperature differences are established.

6.2.3 Thermoelectric devices as thermal energy sensors

Base on thermoelectric modules' Peltier effect and Seebeck effect, thermoelectric devices can be used as thermal energy sensors, such as Cryogenic heat flux sensor, Ultrasonic intensity sensor, infrared sensor, fluid sensor and thin film thermoelectric sensor (Riffat and Ma, 2003). The properties of novel sensors have improved compared to conventional thermal energy sensors.

6.3 Thermoelectric (TEC) window prototype description

Based on the previous study of thermoelectric application, a proposed thermoelectric (TEC) window system is depicted shown in Figure 6.3. In this system, PV panel integrating with building, converts solar energy directly into electrical energy to power TE heat-pump system. A prototype window of $1120\text{mm} \times 540\text{mm}$ was constructed by Vale Window Company Ltd. The window unit incorporated vacuum tubes with 28 mm external diameter. The TEC window system consists of a series of ten TE modules horizontally mounted on aluminium plate, aluminium heat sinks were attached on both sides of the TE modules. The heat sinks are adhered by using special high temperature thermal grease that has a great conductivity to minimize thermal contact resistance. Heat sinks can increase convective heat transfer areas either absorb or dissipate heat into the air. There are thermal insulation materials being placed in between each TE module units. The electric-drive air fans are installed at the end of each channel to enhance airflow through the tubes and channels, each channel section is sized $63\text{mm} \times 28\text{mm}$. The warm air flow into the room and cool air blow out in winter when heating is needed. During the bright sunny day the aluminium fins in each tube absorb more solar thermal and transport the excess heat into the room; during the cloudy day or night time, heat generation from TE modules will supplement heating needs within the buildings. Several tests have been carried out under various conditions. Since air flow rate and air temperatures in both input and output channels can be measured, coefficient of performance of system can be calculated as COP graphs show. Due to the theory of thermoelectric effect the system can be easily switched between heating and cooling mode to meet different season requirements. System thermal performance of heating and cooling effect will be validated by experimental tests.

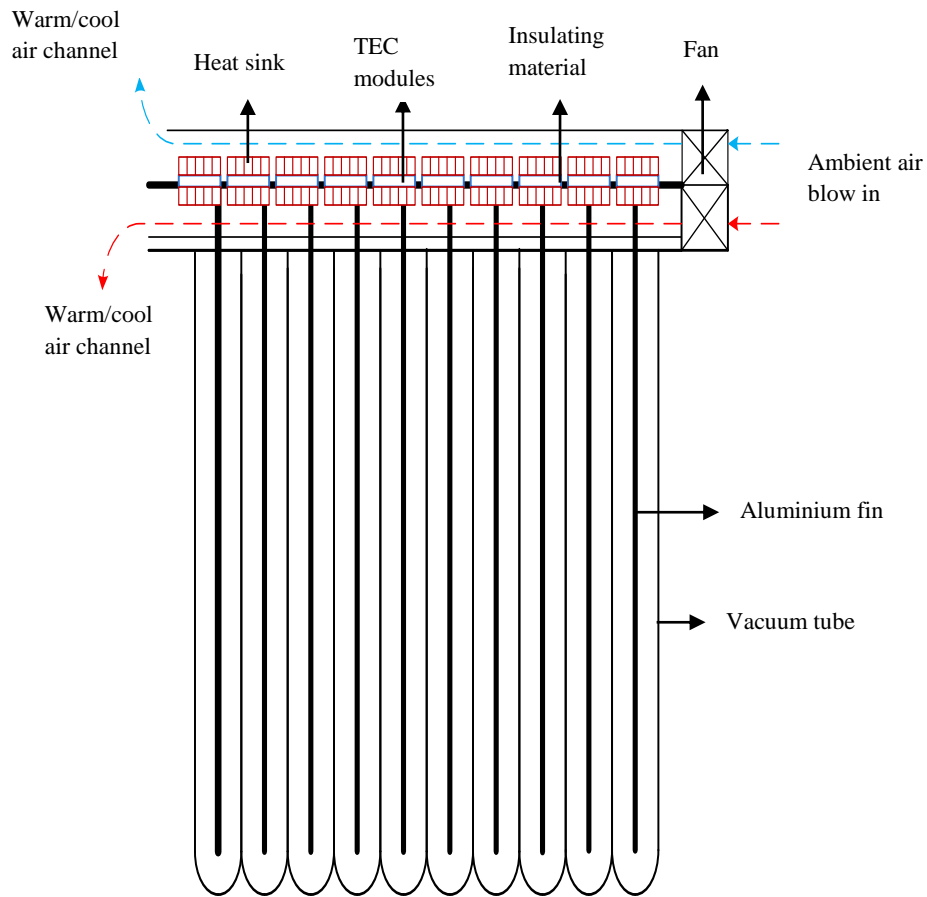


Figure 6. 3: The schematic of TEC window

6.4 Computational models for the thermoelectric window system

6.4.1 Theory of thermoelectric (TE) effect

The thermoelectric effect is the direct conversion of temperature differences to electric voltage and vice-versa. The conversion of electricity into heat is called thermoelectric cooling, whereas the conversion of heat into electricity is called thermoelectric generation. A thermoelectric device creates a voltage when there is a different temperature established on each side. Conversely, thermoelectric device can convert electrical energy into a temperature gradient when a voltage is applied to it. This phenomenon was first discovered by Peltier in 1834. Thermoelectric modules are solid state heat pumps devices used Peltier effect. The Peltier effect is controlled by

the Peltier coefficient, defined as the product of Seebeck coefficient of the semiconductor material and the absolute temperature. The Peltier coefficient relates to a cooling effect as current passes from the n-type material to the p-type material, and a heating effect when current passes from the p-type material to an n-type material.

In theory the amount of heat absorbed at the cold end and the heat dissipated at the hot end are dependent on the product of the Peltier coefficient and the current flowing through the semi-conductor material. In practise the net amount of heat absorbed at the cold end due to the Peltier effect is reduced by conducted heat and Joule heat. Heat will be conducted through the semi-conductor material from the hot to cold end when the temperature is different between the cold and hot ends. The net heat dissipated at the hot end is the sum of the net heat absorbed at the cold end plus the applied electric power. Peltier cooling effect increases when increasing current flow through the thermoelectric module (Riffat and Ma, 2003). The coefficient of performance (*COP*) used to define the cooling “efficiency” is defined as the net heat absorbed at the cold end divided by the applied electric power (Riffat and Ma, 2003).

6.4.2 Thermoelectric module performance of cooling mode

Thermoelectric heat pumping (Peltier effect) at the cold end of a thermal couple is given by:

$$Q = SIT_c \quad (6-1)$$

Where I is the current; T_c is the cold side temperature; S is Seebeck coefficient of the thermoelectric material. Equation (6-1) shows the relationship that heat is pumped when current flows through the couple. However the heat pumped may include other unwanted heat sources – Joule Heat and Conducted Heat. Current flow generates

resistive or Joule heating (Q_J) in the thermoelectric material. Fifty percent of Joule heat goes to the cold end and fifty percent goes to the hot end. The Joule heating is given by:

$$Q_J = I^2 R \quad (6-2)$$

Where R is the module's electrical resistance. During operation, heat is conducted from the hot end to the cold end through the thermoelectric material. The rate of heat conduction is given by:

$$Q_{cd} = K(T_h - T_c) \quad (6-3)$$

Where K is the module's thermal conductance; T_h is the hot side temperature Equation (6-3) shows that Q_{cd} increases with the temperature difference across the couple. Combining equations (6-1), (6-2) and (6-3) into an energy balance at the end of thermoelectric couple gives the following (Rowe, 2005; Simmons, 2000 and Nolas, 2001):

$$Q_c = SI(T_c + 273.15) - \frac{1}{2}I^2 R - K(T_h - T_c) \text{ (Watt)} \quad (6-4)$$

Where S is Seebeck coefficient of the thermoelectric material ($S = 2N\alpha$); R is the module's electrical resistance ($R = 2N\sigma/G$); and K is the module's thermal conductance ($K = 2Nk/G$). S , R and K are temperature dependent parameters. N refers to the total number of TE elements used in each module. G is geometric factors, area and length of TE element. α , σ , k are material properties for the specific type of TE element.

The current going through the TE module is given by (Web 6.2):

$$I = \frac{V - S(T_h - T_c)}{R} \text{ (Ampere)} \quad (6-5)$$

Where V is the input voltage.

The overall coefficient of performance of the TE module operating in a cooling mode is represented by (Rowe, 2005; Simmons, 2000 and Nolas, 2001):

$$COP_c = \frac{Q_c}{VI} \quad (6-6)$$

6.4.3 Thermoelectric module performance of heating mode

The heat Q_h produced on the hot side includes Q_c and power consumption P . The amount of heat transferred at the hot side of the TE module is expressed as (Web 6.2):

$$Q_h = Q_c + VI \text{ (Watt)} \quad (6-7)$$

Q_h and Q_c are further represented by (Web 6.2 and Simmons, 2000):

$$Q_h = SI(T_h + 273.15) + \frac{1}{2}I^2R - K(T_h - T_c) \text{ (Watt)} \quad (6-8)$$

Equations (6-1)-(6-8) are based on assumption that the Thomson effect is absent (Rowe, 1995 and Nolas, 2001).

The thermoelectric modules are operated in heating mode during the winter, transferring heat into the room. The coefficient of performance is given by:

$$COP_h = \frac{Q_h}{VI} \quad (6-9)$$

COP_h is always greater than 1 since Q_h is always larger than VI according to equation (6-7).

Base on equations (6-1)-(6-9) and the following test results, thermal heat flux and *COP* for TE module for various test regimes can be calculated. The results are summarized in Table 6.1 and 6.2.

A computer simulation programme has been done by Riffat et al. (2005), the results shown the relation between cooling capacity (Q_c) and optimum thermoelectric parameters (G , N , I , COP) for specific working temperature (T_h , T_c). The simulation results show: (a) The required number of thermocouples for optimum current and COP increases with the cooling capacity. This indicates that to obtain the optimum current and maximum COP , an increased cooling capacity requires an increased number of thermocouples (increased number of thermoelectric modules); (b) The optimum current and optimum COP are determined by thermoelectric material property coefficients, geometry factor and working temperature (T_h , T_c), they have no relationship with the cooling capacity. This indicates that for a specific working temperature, the optimum current and COP have definite values.

6.5 Laboratory test procedure

The performance of TEC window system was tested in the different testing regimes. Experimental work was carried out in the laboratory and outdoor environment. All testing modes are separately tested under 10V, 15V, 20V, 25V and 30V for indoor tests, each run time of 2h, indoor experimental set-up are shown in the Figure 6.4 and 6.5. Outdoor tests were carried out under 15V, 20V and 25V in the real climate. Figure 6.6 shows testing equipment and system set-up.

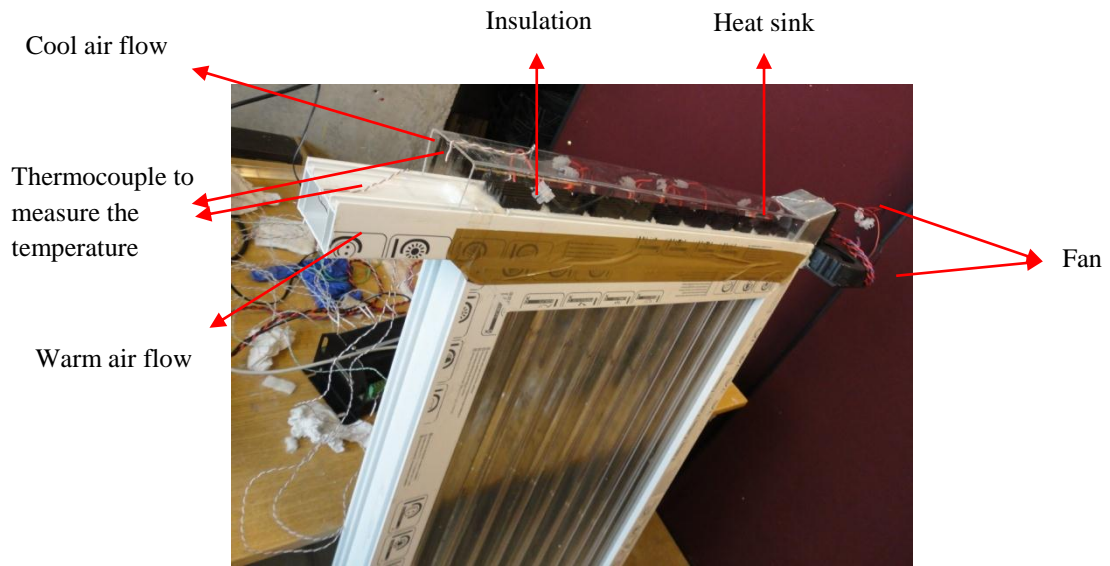


Figure 6. 4: TEC window prototype

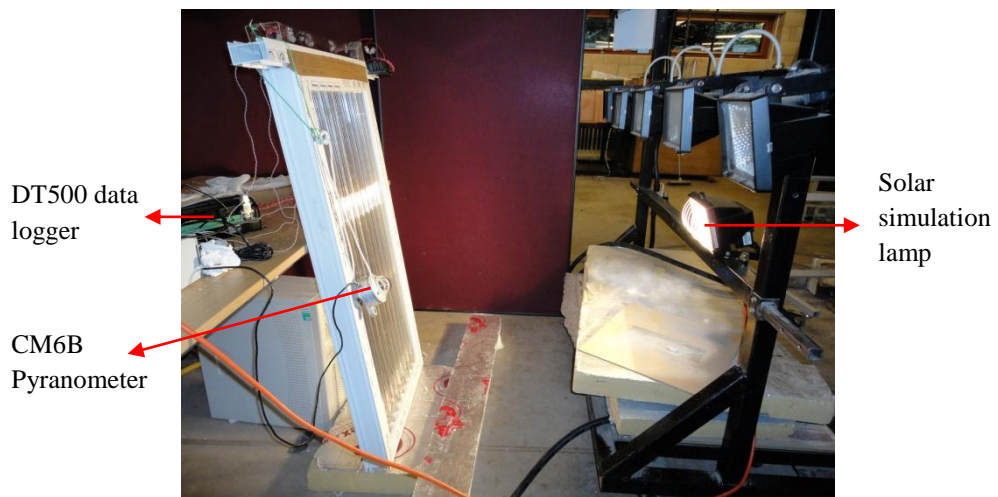


Figure 6. 5: TEC window lab test

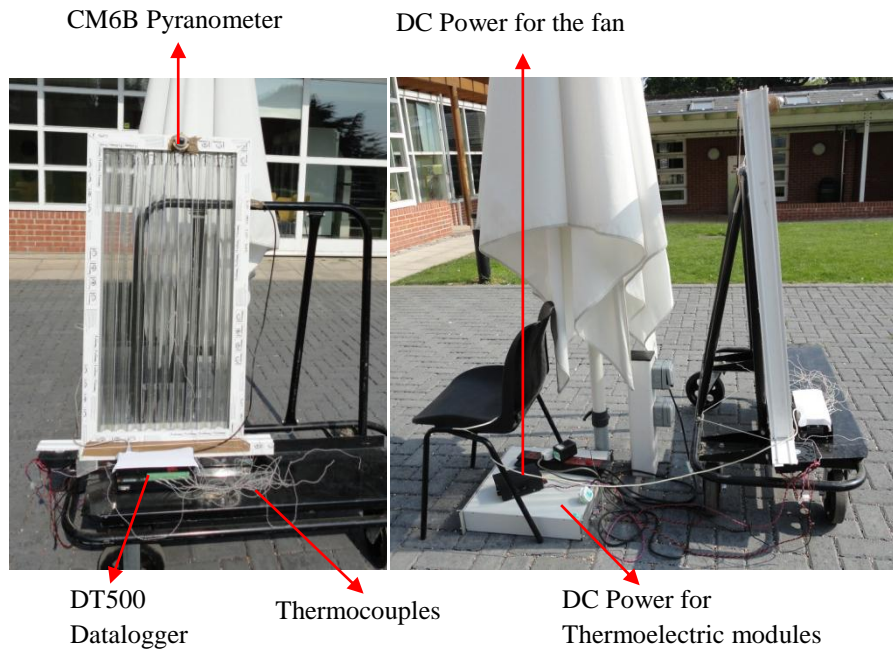


Figure 6. 6: TEC window outdoor test set-up

Experiments for TEC window laboratory tests have been carried out by using solar simulation light and DC power supply as shown in Figure 6.5. Outdoor measurements were run in the real climate thereby to obtain various solar radiation levels. DC power supply was used to power the TE modules. Temperatures of T_h and T_c were recorded by means of T-type thermocouples using DT800 data logger. The accuracy of temperature sensor used is $\pm 1.5^\circ\text{C}$. The input DC power supply (voltage and current) was recorded from LCD display of the DC power supply. The solar radiation was measured by using CM6B pyranometer, the sensitivity of CM6B pyranometer is $12.09 \times 10^{-6} \text{V/Wm}^{-2}$.

TEC window system was tested separately in a cooling and heating mode at 10V, 15V, 20V, 25V and 30V. The changes in current and temperatures were measured over a period of 2h. Each experiment was repeated five times. TEC window was tested outdoor in longer testing time of 7h-10h. The objective of these tests was to determine

if there is any significant different performance in longer time periods when changing solar radiation applies. The experiments were performed by adjusting voltage from 15V, 20V and 25V. The step-change tests are used to simulate the practical condition of changing PV output power under changing solar insolation values.

6.6 Results and discussion

6.6.1 Indoor test results

The system was tested in a cooling mode and heating mode at 10V, 15V, 20V, 25V and 30V. Fan was powered by voltage of 6V@1A. The changes in current and temperatures were measured over a period of 2 hours for each test. Each experiment was repeated four times. The solar radiation of simulation lamp was measured by using CM6B pyranometer as shown in Figure 6.5. Thermal heat flux in hot and cool channel can be calculated by using following equation:

$$Q_{c,h} = mC\Delta T \quad (6-10)$$

$$m = \rho v \quad (6-11)$$

Where C is Specific Heat Capacity (SHC) of the air, ρ is air density, v is air flow rate (m/s). Temperature differences and air flow rate can be measured by using thermocouple and anemometer, heat flux and COP for the system therefore can be calculated by using above equations and equations in section 6.4. The results are shown in the following Table 6.1 and 6.2. Figure 6.7 depicts the temperatures of laboratory ambient T_a , hot air generated T_h and discharged cold air T_c of TEC window system operating under different voltage regimes for heating mode. The lines indicate average temperatures for five testing cycles and points are the maximum and minimum variance in five cycles.

In the heating mode, the temperature changes rapidly in the first half an hour and remain more stable afterwards. Temperature in hot side increases when larger voltage are applied to TE modules, a maximum air temperature of 50.49°C at hot side can be reached under the regime of 30V applied to TE system.

Cold side temperatures of TEC window system operating under five different voltage regimes were compared (shown in Figure 6.7). At the case of 10V and 15V applied voltage to TE modules, discharged cold air is capable of maintaining lower temperatures at the cold side compared to laboratory ambient temperature. However T_c increases when higher voltage of 20V, 25V and 30V are applied. In this case, the TEC window system cannot cool efficiently; it will actually start to dissipate heat to the cold side, as the result the cold side temperature becomes higher than input laboratory ambient air temperature. From Figure 6.7, it can be seen that T_h increases when larger voltage are applied, however T_c shows less significant difference compared to temperatures in hot side. Hence a change in supply voltage has larger effect on T_h than T_c . Simultaneously current flows through TE system increase with increasing voltage.

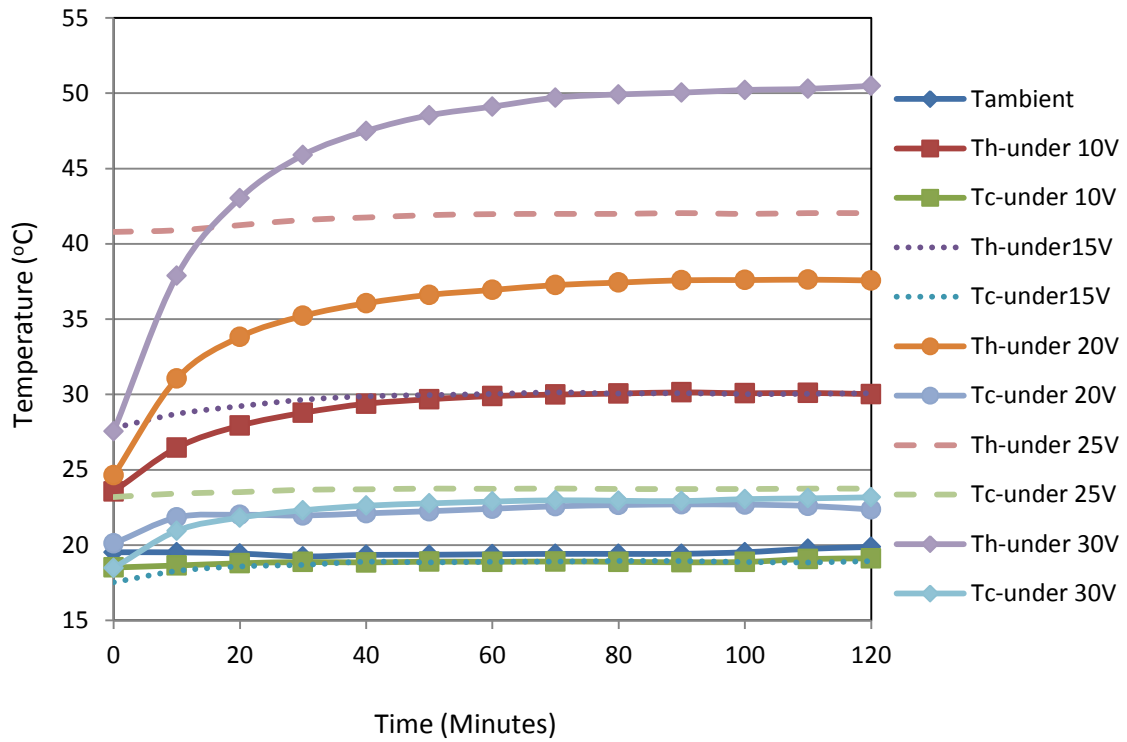


Figure 6. 7: Hot and cold side temperatures for TEC window system in heating mode

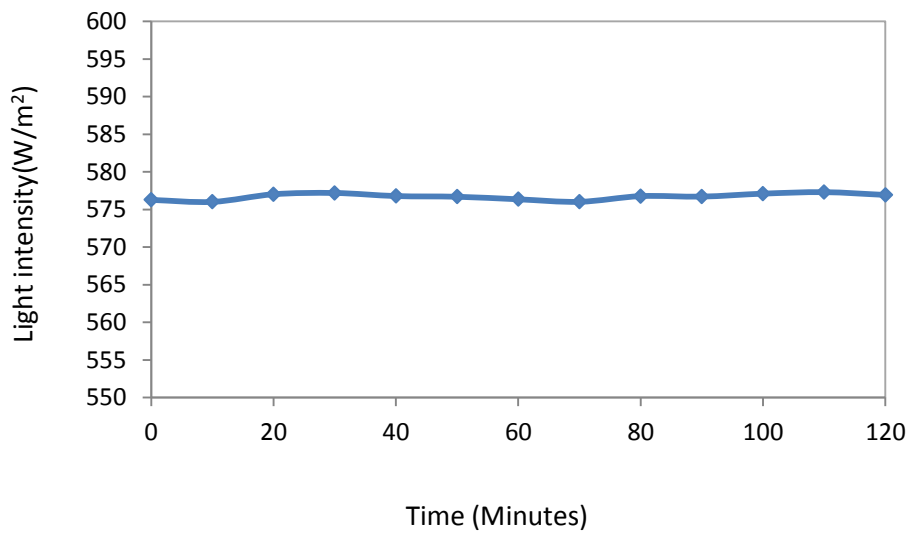


Figure 6. 8: Light intensity of solar simulation lamp

Base on equations (6-1)-(6-11) and the above testing results, thermal heat flux and TE modules heating mode *COP* in various test regimes are measured and calculated.

Test result of heat Q_h includes Q_c , power consumption P and heat from solar simulation light ($Q_h > Q_c + P$). The results are summarized in Table 6.1. The results shows that COP_h decreases when applied voltage increases from 10V to 30V.

Table 6. 1: Thermal heat flux and COP for TEC window system laboratory test results

Heating mode	Q_c (W)	Q_h (W)	VI (W)	COP_h
10V	0.5	15.7	6	2.62
15V	0.53	16.4	13.5	1.22
20V	2.59	26.2	22	1.19
25V	3.1	37.6	32.5	1.16
30V	3.6	56.9	51	1.12

6.6.2 Outdoor test results

The thermal performance of TEC window system was measured in the daytime April month by changing input voltage on TE modules. The outdoor tests are run for two weeks. Different test regimes and results are presented in the following.

- Outdoor test one: No applied voltage on TE modules

TEC window solar performance test was taken in a very warm and sunny weather condition at the campus of the University of Nottingham in April 2011. During the test, fan was powered by 6V@1A direct current to assist air flow through the vacuum tubes and TE modules were not powered. Therefore hot and cold side temperature changes are affected by solar radiation only in this test condition, results are shown in Figure 6.9. Comparing to ambient temperature, the maximum temperature rise can achieve 16.6°C, which occurs in the mid-day between 12-14pm when higher level of solar radiation exposure during the day. Figure 6.10 shows the measurement of solar light intensity measured by pyranometer.

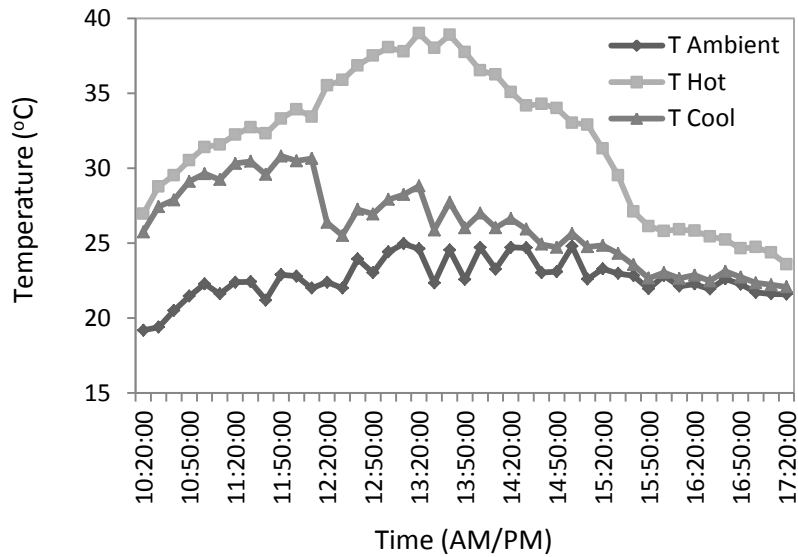


Figure 6. 9: Hot and cold side temperatures for TEC window system in heating mode (20/04/11)

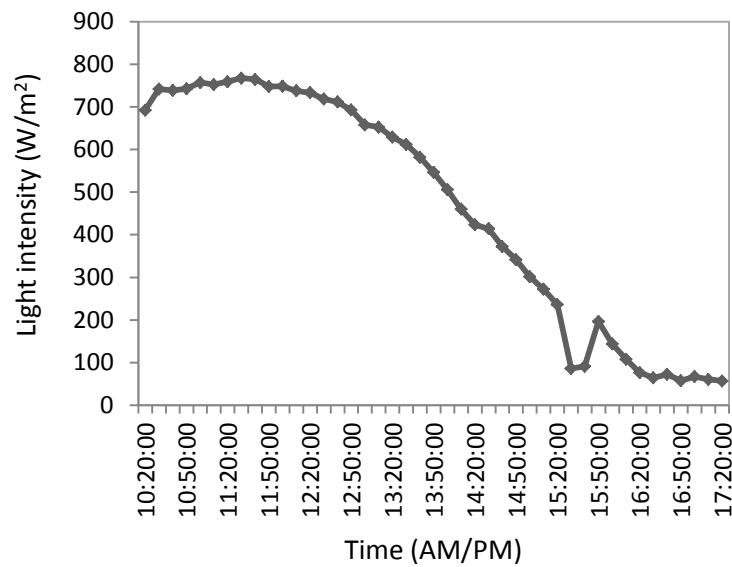


Figure 6. 10: Light intensity measured by pyranometer (20/04/11)

- Outdoor test two: Applied voltage of 15V on TE modules

In this test, fan and TE modules were powered by 6V@1A; 15V@0.9A direct current, respectively. As Figure 6.11 shows, solar heat gain has significant impact on temperature rise. Temperature started to drop after 13:00pm when solar radiation level

decreased. The solar radiation level was measured and recorded as shown in Figure 6.12.

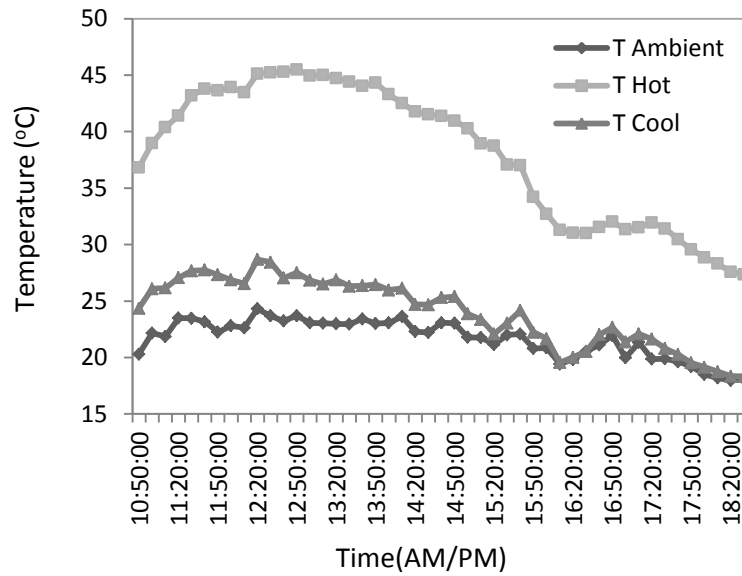


Figure 6. 11: Hot and cold side temperatures for TEC window system in heating mode (25/04/11)

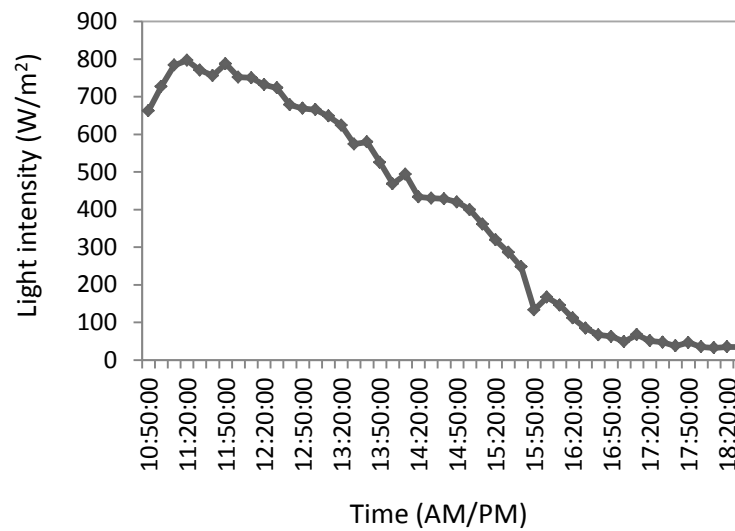


Figure 6. 12: Light intensity measured by pyranometer (25/04/11)

➤ Outdoor test three: Applied voltage of 20V on TE modules

In this test, fan and TEC was powered by 6V@1A; 20V@1.2A direct current, respectively. Figure 6.13 shows average 9.4°C, maximum 11.5°C of the temperature

rise obtained in the first 1.5 hours when TE modules were not powered. Temperature has significantly increased as soon as voltage was applied to TEC modules. The highest temperature in hot air channel has reached 44.1°C at around 15:00pm. Comparing to indoor test, the results indicate that temperature increased differently even though the same power input applied to the system, the increasing value of temperatures are affected by changing solar radiation.

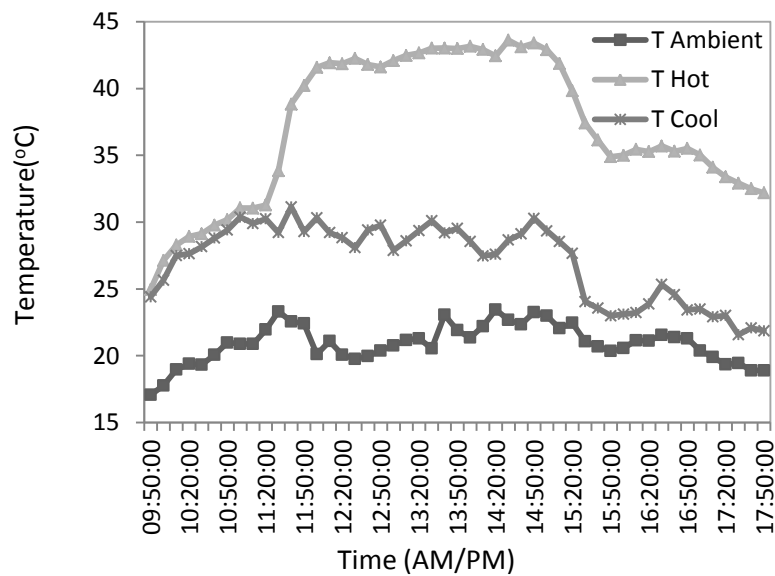


Figure 6. 13: Hot and cold side temperatures for TEC window system in heating mode (19/04/11)

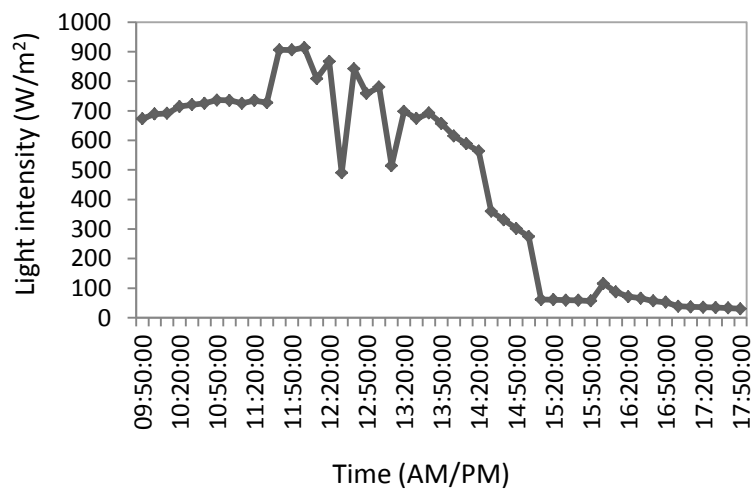


Figure 6. 14: Light intensity measured by pyranometer (19/04/11)

➤ Outdoor test four: Applied voltage of 25V on TE modules

In this test, TEC modules were applied to 25V@1.3A direct current. Figure 6.15 shows temperature input and output in both hot and cold side channels. The maximum temperature rise has reached 32.6°C from the period 12:00am to 14:00pm depending on solar radiation level. From the point of 16:00pm on the graph, temperature started to drop due to the absence of the solar radiation, average increased air temperature of 21.2°C were heated by TE modules.

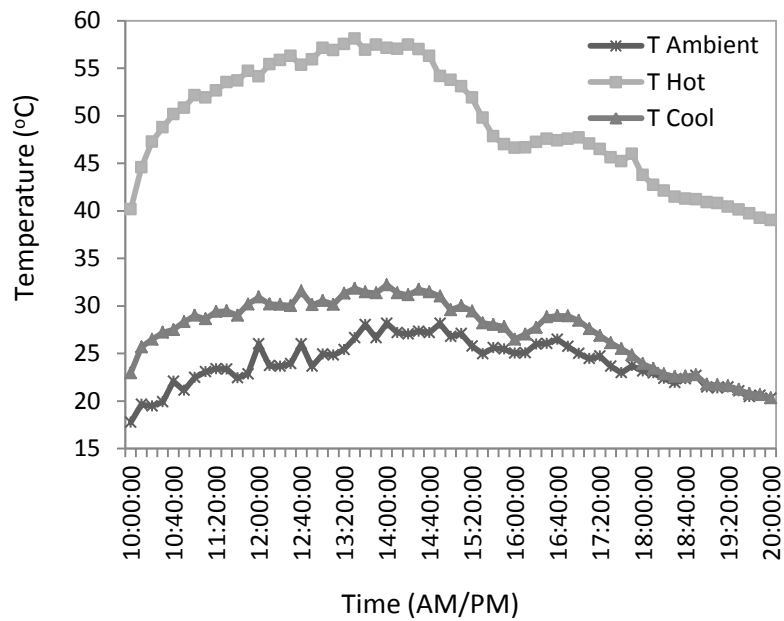


Figure 6. 15: Hot and cold side temperatures for TEC window system in heating mode (22/04/11)

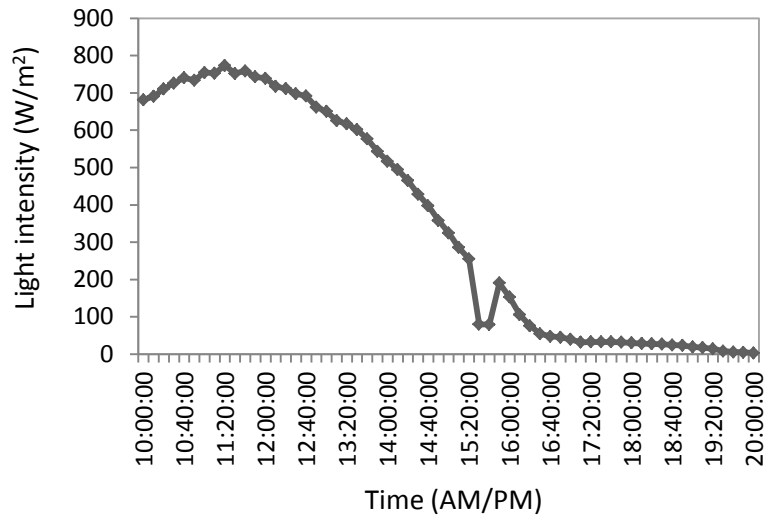


Figure 6. 16: Light intensity measured by pyranometer (22/04/11)

Outdoor tests of thermal heat flux and TE modules heating mode COP in various applied voltage regimes can be calculated by using equations in section 6.4 and the above testing results. Test result of heat Q_h includes Q_c , power consumption P and solar heat gain ($Q_h > Q_c + P$). The results are summarized in Table 6.2, listed figures are an average value through each test cycle. From Table 6.2, it can be seen that COP_h decreases when the applied voltage increases from 15V to 25V. Comparing to indoor test results, average thermal flux in both cold and hot side have increased because of increased solar heat gain by the system. Unlike indoor test simulated by solar simulation lamp, which can give relative constant light intensity, for outdoor test, the solar light intensity changes depending on the weather condition. Average solar intensity for the flowing outdoor tests are 400, 450 and 350W/m² respectively.

Table 6. 2: Thermal heat flux and COP for TEC window system outdoor tests

Heating mode	Q_c (W)	Q_h (W)	VI (W)	COP
15V	3.5	24.6	13.5	1.82
20V	7.8	26.7	22	1.21
25V	5.3	38.1	32.5	1.17

For the cooling test, TEC window system was operated in a cooling mode by converting applied electric voltage direction. Air fan and TEC was powered by 6V@1A and 20V@1.2A direct current, respectively. The results illustrate that temperature in cool channel T_c started to increase and become higher than ambient temperature T_a . The TEC system cannot cool efficiently because it will actually start to heat the flow-in air. A further investigation of TEC window system cooling effect will be carried out in future work.

6.7 Summary

An experimental investigation of TEC window system thermal performance has been carried out and tested in various voltage regimes and solar radiation conditions. Thermoelectric (TEC) window is a novel window design for heating purpose in winter climate. Heat production by using renewable energy contributes on heating demand thereby to save energy use. TE module is a solid-state active heat pump which transfers heat from one side to the other side. The use of TEC Peltier effect can create heat flux with consumption of electricity. Vacuum tubes together with aluminium separators are used as solar collector devices in this system. In a higher solar radiation condition, this window system can achieve significant heat gain according to the above test results. From test results, a change in supplied voltage has large impact on T_h thereby to heat flux, both values will increase when larger voltage applied to TEC modules.

For the indoor and outdoor heating mode test, the calculation results show that coefficient of performance (COP) of TEC window system decreases when applied voltage to TEC increases from 10V to 30V. From ventilation channel sized $63mm \times 28mm$, the system can generate 37.6W (indoor test using solar simulation lamp) and

38.1W (outdoor test) thermal energy and supply into the room when 25V electricity applied to the TEC modules.

In the present experiments, the TE system is powered by a DC power supply, this power supply will be replaced by a PV panel system in future application. The output power of the PV system should be approximate 40 to 50 W, or near 1.1 kWh, in order to allow the TE system to work sufficiently over a period of one day. The total output power of the PV system is approximately 0.8kWh/m^2 for each day. In order to satisfy the energy demand for the TE system, the total area for the PV panels should therefore be at least 1.4m^2 .

Chapter 7 Thermoelectric Generator (TEG) Window System

7.1 Introduction

It's generally known that solar panels are a great alternative energy source, but they only produce electricity during daylight hours. In addition their daily output is significantly reduced during winter months and cloudy days. Therefore using a TEG in conjunction with solar and wind, their combined output can contribute buildings energy use.

The use of thermoelectric generators has long histories since 19 centuries. The fields used TEG as power generation are, such as to power spacecraft, to power remote monitoring stations in oil and gas industry. Only in recent years this technology has become available to the general public especially when energy conservation became a crucial issue worldwide. A TEG has the advantage that it can operate from a low grade heat source such as waste heat energy. It is also attractive as a mean of converting solar energy into electricity. Almost any heat source can be used to generate electricity, such as solar heat, ocean heat, geothermal heat and even body heat.

Unlike solar panels, TEGs are not dependant on the sun to produce electric power. They can produce power day and night as long as there is a heat source available. Thermoelectric devices can be used either in the Peltier mode for refrigeration or in the Seebeck mode for electrical power generation. Chapter 6 has introduced and studied the performance of thermoelectric (TEC) window system. TEC window system using thermoelectric modules (TEMs) Peltier effect acts as a heat pump to heat input air and supply warm air into the room. The use of thermoelectric module's Seebeck effect, which heat is converted into electricity through a heat-to-electricity

conversion device, window system can become a power generation device. In order to investigate viability and further performance of the thermoelectric generator integrated with evacuated tubes window system, a proposed thermoelectric power generation system performance will be studied by integrating theoretic analysis and experimental tests in this chapter. The economic prospects of this application are also discussed.

7.2 Thermoelectric (TE) device

7.2.1 Introduction of thermoelectric materials

The basic requirements achieve a significant thermoelectric performance are the same for both generators and coolers (Thomson, 1851 and de Groot, 1952). The materials are used for thermoelectric cooler and generator are different due to the difference in temperature range of operation and intended application (Cadoff, 1959, Rowe, 1983 and Goldsmid, 1986). For the low temperature applications, the thermoelectric coolers usually utilize Bi_2Te_3 materials and are employed in the application below room temperature, generators are fabricated from high-temperature materials such as PbTe or SiGe alloys and are used in the temperature region 400 to 1200K. Generally it is inefficient for a generator to be used as a cooler and vice versa (Rowe, 1994).

7.2.2 Introduction of thermoelectric device

A typical thermoelectric device contains two ceramic substrates that serve as a foundation and electrical insulation for P-type and N-type Bismuth Telluride thermoelements. They are connected electrically in series and thermally in parallel between the ceramics. When heat flows through the cell, metals responded differently, the excess electrons in N-type components side cause negative load and default

electrons in P-type components cause positive load, thereby resulting in the formation of an electric flow. Conventional thermoelectric devices have various specifications for various applications; the dimensions vary from 3mm square by 4mm thick to 60mm square by 5mm thick, the maximum heat-pumping rate from 1W to 125W. The maximum temperature difference between the hot and cold side can reach 70°C. The devices contain from 3 to 127 thermocouples. There are multistage (cascade) series thermoelectric devices designed to meet requirements for large temperature differentials (up to 130°C). The lowest practically achievable temperature is about – 100°C (Riffat and Ma, 2003).

7.2.3 Thermoelectric power generation device

The TE power generation has the advantages of being maintenance free, silent in operation and involving no moving or complex parts. Thermoelectric generator (TEG) is a device that converts heat into electricity. It consists of two dissimilar materials, n-type and p-type semiconductors, connected electrically in series and thermally in parallel. Numbers of these thermoelectric elements are combined in series to form a thermoelectric generator module. Heat is supplied at hot side of the thermoelectric cell while the other end is maintained at a lower temperature by a heat sink. As a result of the temperature difference, Seebeck voltage is generated across the p-n junction that results in current flow through an external load resistance.

The working principles of TEG are based on its thermoelectric effect, which include Seebeck effect, conduction effect and Joule effect. The Seebeck effect is a phenomenon that the thermoelectric devices convert thermal energy from a temperature gradient into electric energy, discovered by German physicist Thomas Johann Seebeck in 1821. When a temperature differential is established between the

hot and cold ends of the semiconductor material, a voltage is generated, i.e., Seebeck voltage. The conversion of heat into electricity is called thermoelectric generation.

7.3 System description

A schematic diagram of the test section is shown in Figure 7.1. The test section consists of a thermoelectric generator made of eight TEMs ($30 \times 30\text{mm}$) connected electrically in series. Proposed system used high temperature thermoelectric modules as shown in Figure 7.2. This thermoelectric (Seebeck) Power generation modules has a large thermal expansion (and contraction) through the range of allowable temperatures -60°C to 325°C . One module has a power generation capacity of 5W. The design and construction of TEG power generation system is depicted in Figure 7.3.

The thermoelectric modules are sandwiched between heat source and water cooling plate. In the hot side, the modules harvest thermal energy from heat source (solar heat gain). Coated copper oil tank filled with heat transfer oil, stores thermal energy and maintains the thermal input (heat flux) to TEG module hot side when system is operated. Thermal insulation materials are placed between the modules. The clamping is created with stainless steel machine screws on either side of the TEMs with spring washer and fiber washer under each screw head for purpose of thermal isolation and to accommodate thermal expansion and contraction while maintaining a substantially constant force.

Thermoelectric modules are very thin that a thermal bridge will appear between the heat source and the heat sink, which could cause a decrease in both the electricity production and the system efficiency (Martinez et al., 2011). The most common way of improving the heat dissipation of a device is to attach a finned dissipater

(Rohsenow et al., 1998). In this system, temperature controlled water is used on cold side to dissipate the heat for cooling modules.

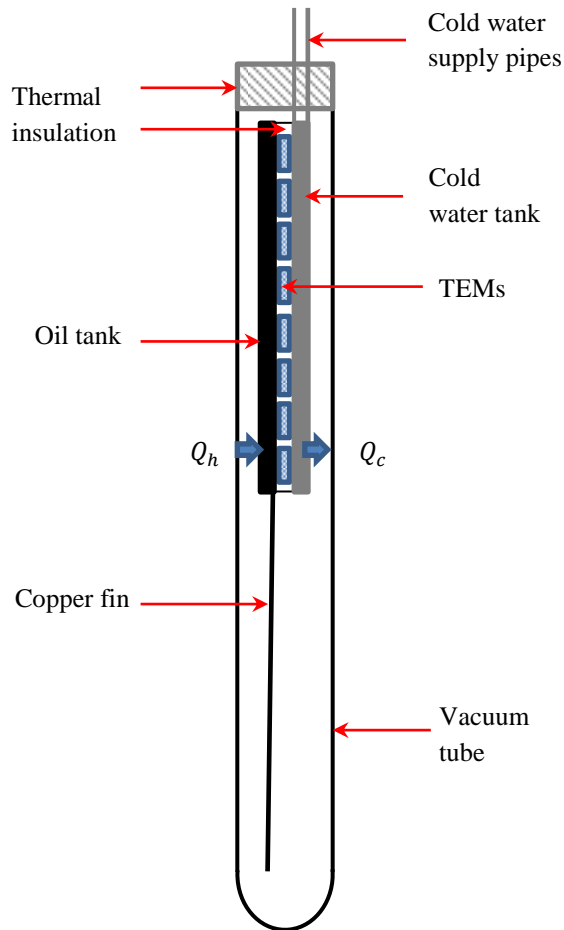


Figure 7. 1: Schematic diagram of the test section

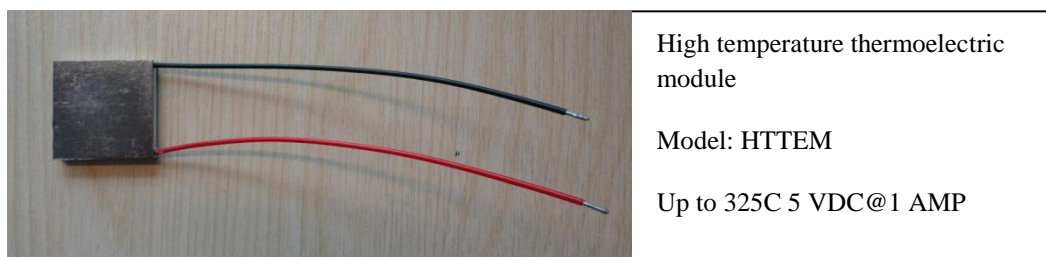


Figure 7. 2: High temperature thermoelectric module used for proposed thermoelectric power generator system

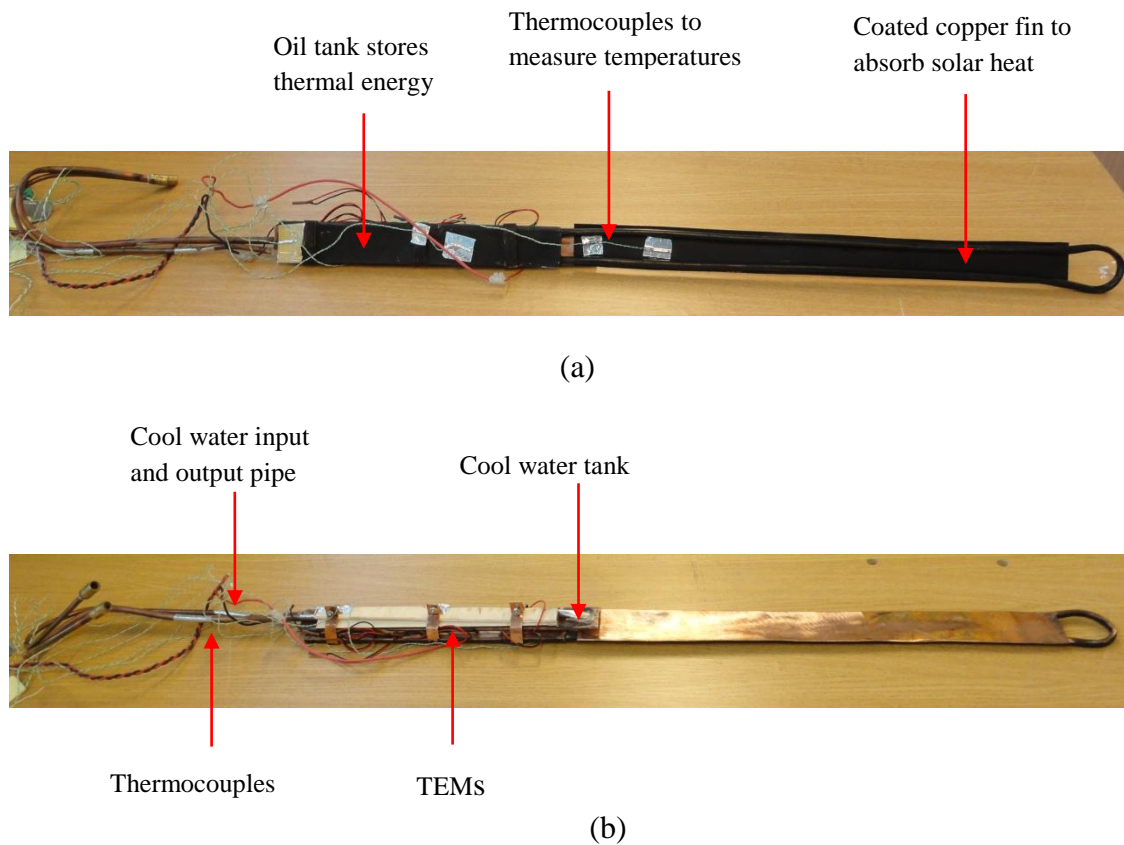


Figure 7. 3: Proposed TEG power generation system (a) hot side; (b) cool side

7.4 Computational analysis for the thermoelectric generator system and theoretic results

In order to predict the performance of the thermoelectric generator system, a lumped parameter model has been formulated. The theoretical model involves the electrical and thermal properties and gives the values of the main parameters, such as the temperature difference established by the heat flow.

7.4.1 Computational analysis for the thermoelectric generator system

Thermoelectric Seebeck effect is the conversion of temperature differences directly into electricity. This was because the metals responded differently to the temperature difference, creating a current loop and a magnetic field. The voltage created by this

effect is on the order of several microvolts per kelvin difference. Figure 7.4 (C.T. Hsu et al., 2011) illustrates one single TE couple for example, which is composed of P- and N- TE couple, electrical conductor (Cu) and ceramic plates. As heat source applies heat energy Q_h (W) to create a temperature difference ΔT (K) between both sides of the P-N ingot. The electric current I (A) is induced inside the TEG module in the circuit. For the conduction effect in this case, the amount of power is proportional to the thermal conductivity K (W K^{-1}) and temperature difference $\Delta T = T_h - T_c$ (K). As the electric current going through the TEM leg, Joule heat generated internally, which is proportional to the electrical resistance R (Ω) and square of the current. The same amount Joule heat is to heat both hot and cold side. The internal material properties are supposedly constant that independent of temperature and no heat losses. The rate of supply heat Q_h and removal heat Q_c , for the pair of thermoelements for steady operations, are composed of three terms due to heat conduction, Peltier and Joule effects. This heat flow can be estimated at the hot and cold junction respectively, the equations are given by (C.T. Hsu et al., 2011),

$$Q_h = (K_p + K_n)(T_h - T_c) + (\alpha_p - \alpha_n)IT_h - \frac{I^2R}{2} \quad (7-1)$$

$$Q_c = (K_p + K_n)(T_h - T_c) + (\alpha_p - \alpha_n)IT_h + \frac{I^2R}{2} \quad (7-2)$$

Where K_p and K_n are thermal conductivity of P- and N- type TE leg, T_h and T_c represent the hot and cold junction temperature, and α_p and α_n are the Seebeck coefficient of P- and N- type TE leg respectively.

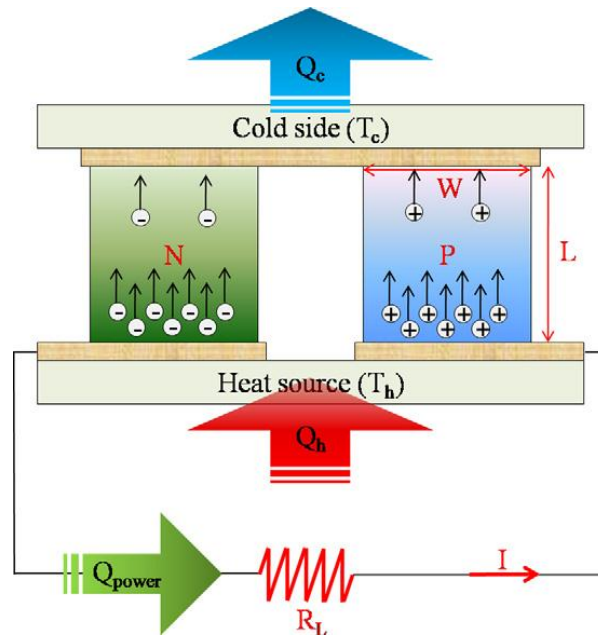


Figure 7. 4: Illustrates the formation of induced electrical current inside the TEG model (C.T. Hsu et al., 2011)

The heat input into the thermoelectric modules is given by,

$$Q_{TEM} = mNQ_h \quad (7-3)$$

Where m is the number of thermoelectric module, N refers the number of thermocouples per module.

Referring to Figure 7.4, the electrical power generated by TEG can form the voltage across the external load and current in the circuit. Base on the power balance equations, electrical power can be obtained and given by,

$$W = Q_h - Q_c = VI \quad (7-4)$$

According to equations (7-1) (7-2) (7-4), the following equations can be written as,

$$(\alpha_p - \alpha_n)I(T_h - T_c) - I^2R = VI \quad (7-5)$$

Both sides of equation (7-5) are divided by I , it can be expressed as,

$$V = (\alpha_p - \alpha_n)(T_h - T_c) - IR \quad (7-6)$$

In which, let $\alpha = (\alpha_p - \alpha_n)$ and $\Delta T = (T_h - T_c)$, therefore equation (7-6) can be simplified as,

$$V = \alpha\Delta T - IR = A\Delta T - BI \quad (7-7)$$

Equation (7-7) demonstrates that the output voltage as a function of the current for a given temperature difference, and characterizes the performance of a TEG module or system that composed of TEG modules. Furthermore, for the open circuit voltage, if $I = 0$ in equation (7-7), $A\Delta T$ has a maximum value in which A is defined as the “effective Seebeck coefficient”, expressing the behaviour of the TEG module operating in the actual provided conditions, which is given by,

$$A = \frac{V}{\Delta T} \quad (7-8)$$

Where V is the open circuit voltage, when $I = 0$. Value of B represents the matching load of a TEG module.

TEM power output depends on the temperature difference, the properties of the semiconductor materials and the external load resistance. The Seebeck coefficient squared divided by the product of electrical resistivity and thermal conductivity is called the figure of merit Z . Desirable properties for the thermoelectric material as a generator module are expressed by its figure of merit (Z) which is defined as:

$$Z = \frac{\alpha^2}{KR} \quad (7-9)$$

where, α is the Seebeck coefficient of the p-n junction, R is the electrical resistivity and K is the thermal conductivity of the thermoelectric element. Figure of merit Z depends on material properties and should be maximized to increase the module

efficiency. It can be expressed in non-dimensional form as ZT , in order to take the effect of the temperature on material properties. T is the average temperature of the thermoelectric module hot side and cold side.

Figure 7.5 illustrates the energy flow through the thermoelectric cell where P represents the useful electric power output by the TEC. Each thermoelectric element is assumed to be insulated both electrically and thermally from its surroundings, except at the junction to hot/cold reservoir contacts. The internal irreversibility for the TEC is caused by joule electrical resistive loss and heat conduction loss through semiconductors between the hot and cold junctions. The external irreversibility is caused by finite rate heat transfers at the source and the sink.

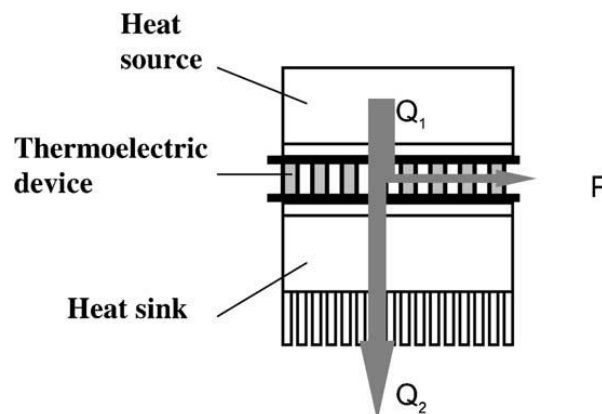


Figure 7. 5: Conventional arrangement for thermoelectric power generation (Riffat and Ma, 2003).

Where Q_1 is the heat supplied by the heat source, P is the electrical power generated. Q_2 is the heat dissipated to the heat sink, which is the thermal energy wasted.

An electromotive force is induced when heat flow through TEM and temperature gradient is established, which is given by equation (10):

$$E_{Seebeck} = N(T_h - T_c)(\alpha_p - \alpha_n) \quad (7-10)$$

where $E_{Seebeck}$ is electromotive force induced by Seebeck effect V, N is number of thermoelectric pairs in thermoelectric module, $(T_h - T_c)$ is temperature difference between the ends of a thermoelectric pair °C, α_p , α_n is Seebeck coefficient of conductor p and n respectively V/°C.

If the module is connected to an electrical load resistance, then an electric power is generated, which is given by equation (7-11):

$$P = E_{Seebeck}^2 R_{load} / (R_{load} + R_0)^2 \quad (7-11)$$

where P is electric power generated by the modules W, R_{load} is electrical load resistance connected to the thermoelectric modules Ω , R_0 is electrical resistance of a thermoelectric module Ω .

Equation (7-10) and (7-11) show that the electric power generated by a thermoelectric module depends on both the temperature difference between the ends of the module and the electric load resistance connected to it (Martinez et al., 2011). The higher electric power will be generated if the larger temperature difference is induced.

Most of the heat supplied by the heat source is conducted to the heat sink through the thermocouple branches that some is used to balance the Peltier effect associated with the flow of current and some is used to generate Joule heat, the current I is given by,

$$I = (\alpha_p - \alpha_n)(T_h - T_c) / (R_{load} + R_0) \quad (7-12)$$

When the load is inserted, the electric current circulating in the generator is given by,

$$I = mN(\alpha_p - \alpha_n)(T_h - T_c) / (R_{load} + R_0) \quad (7-13)$$

The thermodynamic efficiency of a single-couple thermoelectric generator without contact resistance is given by (Rowe, 1994):

$$\eta = P/q \quad (7-14)$$

The condition for the maximum power transfer can be achieved if the load resistance is matched to the resistance of the generator. However, if this condition is satisfied, the efficiency can never exceed 50% of the ideal thermodynamic value $(T_h - T_c)/T_h$.

In order to demonstrate the concept of this study, TE module employed in this experiment, its geometric features and transport properties are tabulated as references, which can help to compare with experimentally measured data. The associated geometric features and material properties at system operating temperature are provided by vender datasheets shown in Appendix A.

7.4.2 Theoretic data of 50Watt TEG power strip

Results of theoretic output data of 50Watt TEG Power Strip using high temperature thermoelectric modules are shown in Figure 7.6 to 7.8 simultaneously:

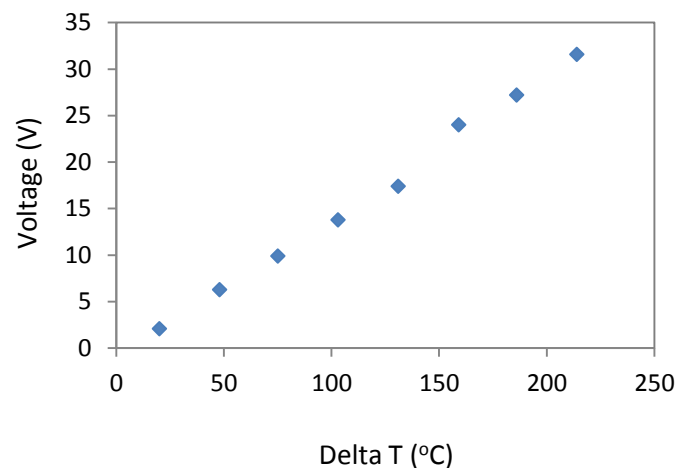


Figure 7. 6: Effect of ΔT on 50 Watt TEG power strip voltage generation (theoretic analysis)

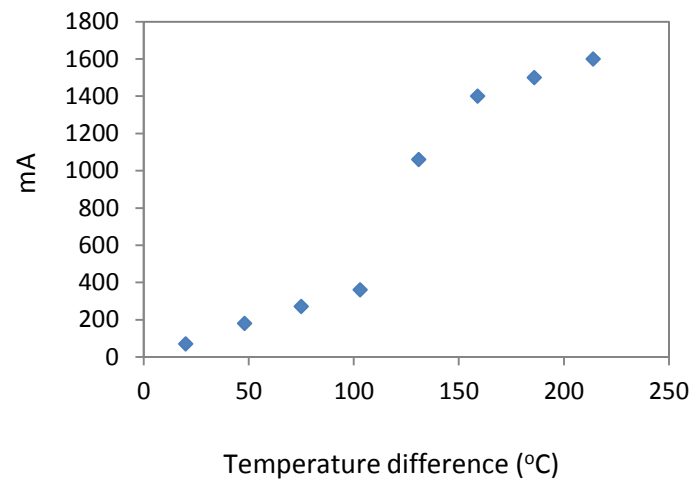


Figure 7. 7: Effect of ΔT on 50 Watt TEG power strip direct current generation (theoretic analysis)

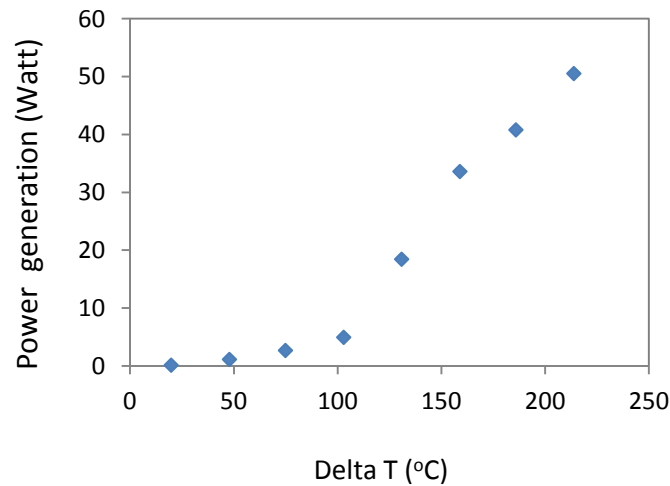


Figure 7. 8: Effect of ΔT on 50 Watt TEG power strip power generation (theoretic analysis)

Theoretic data shown in Figure 7.6, external load voltage increases with a boost of temperature difference (ΔT) in a linear trend. Minimum and maximum voltage output can obtain 2.1V and 31.6V when temperatures differences are 20°C and 214°C respectively. The increasing trend of electric current generation versus temperature differences are shown in Figure 7.7. Total power generation is determined by both

voltage and current as Figure 7.8 illustrates. A maximum power output of 50.5Watt can be achieved when temperatures differences of both sides of TEG modules reach to 214°C. Theoretic results of thermoelectric power generation device will be validated by the following experimental tests.

7.5 Instrumentation and test procedure

Measuring system, which equipped a sandwiched structure of solar heat/oil heating tank/copper plate/TEG modules/copper plate/liquid cooling system, was conducted for testing as shown in Figure 7.10. The copper plates were treated as heat spreaders to provide a uniform thermal field to both hot and cold sides of TEG modules. Thermocouples were inserted into these two copper plates to measure the temperature difference between the hot and cold sides of TEG modules. The coolant was supplied from temperature controlled water to maintain the cold side temperature (T_c). Various measuring and control devices, including thermocouples, pyranometer, a voltage/current analyzer and a data acquisition system were applied as shown in the following Figure 7.9. The readings were scanned and recorded every 20s. External load voltage could be obtained when applying an external load.



Thermocouples

Type: T 621-2164

Range: -50 to +250°C

Accuracy: $\pm 1.5^\circ\text{C}$



DT500 dataTaker



Pyranometer

Model: CM6B

Serial no: 036167

Sensitivity: $12.09 \times 10^{-6} \text{V/Wm}^{-2}$



Multimeter

Serial No: IS4358GKF

Cert No: 122174S



Hot plate

Type: 1900

Temperature range: 0-300°C

Figure 7. 9: Measurement equipments

The power output of the thermoelectric module is calculated from the load voltage and the electric current:

$$P_{TE} = IV \quad (7-15)$$

where V and I are the voltage and current at given load conditions, respectively. The power output may also be obtained from the load voltage and the electrical resistance:

$$P_{TE} = \frac{V^2}{R_{load}} \quad (7-16)$$

where R_{load} is the load electrical resistance.

7.6 Test results and discussion

7.6.1 Electricity power output for single TEG module

Electricity power output for single TEG module was tested outside the vacuum tube. Single TEG was placed on hot plate by adjusting high temperature levels, temperature controlled water plate was used to cool the other side of the module. A series of setup external load voltage (U) values changing with temperature difference have been measured, which are shown in Figure 7.11. Table 7.1 illustrates the measuring results of single thermoelectric module V versus power output (P) for different (ΔT), where V is external load voltage and ΔT refers temperature difference between both sides of the TEG module.

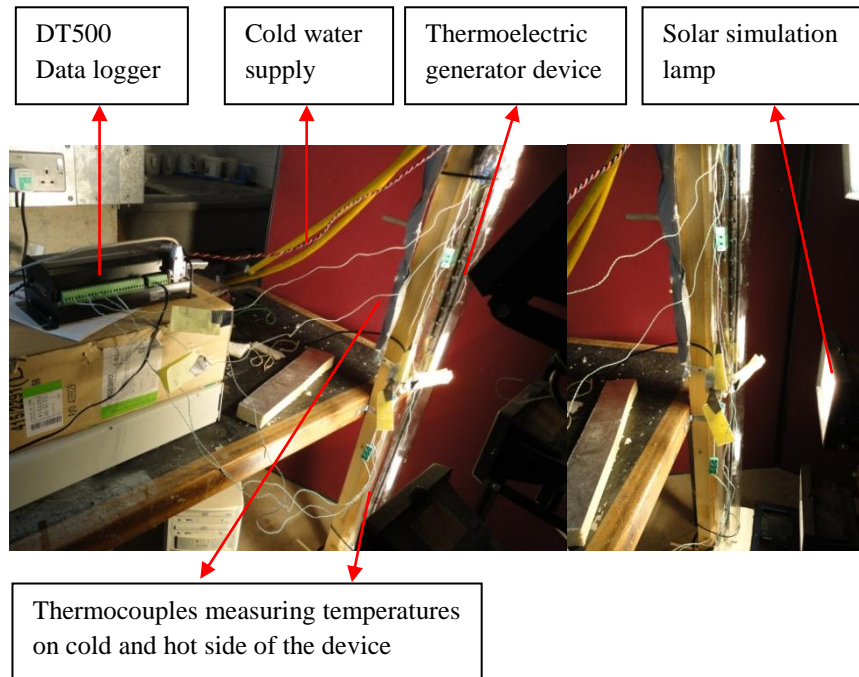


Figure 7. 10: Experimental test set-up

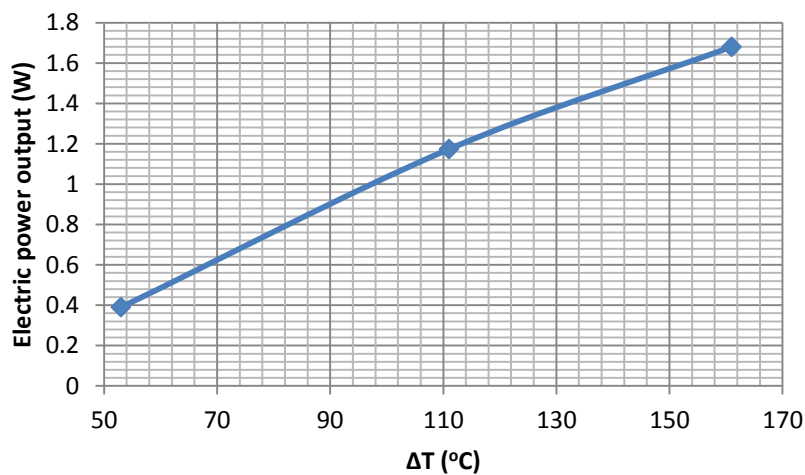


Figure 7. 11: Effect of ΔT on P characteristic for single TEG module

Shown in Figure 7.11, external load voltage increases proportionally when temperature difference increases between hot and cool sides of TEMs.

Table 7. 1: Effect of ΔT on power output characteristics for single thermoelectric module

ΔT (°C)	Load current (A)	Load voltage (V)	Power output (W)
53	0.3	1.3	0.39

111	0.51	2.3	1.17
161	0.6	2.8	1.68

Temperature difference refers to ΔT (multi-point average) between both sides of the TE modules, T_h and T_c refers to hot side and cold side temperatures of TEG modules. Table 7.1 summarized the power output characteristics of the single thermoelectric module. Figure 7.11 shows the power output versus the measured module hot and cold side temperature difference. The power output increases rapidly with the module hot side temperature increases. The cold side of the module maintained at 16-18°C during the experiments. The maximum temperature difference achieved on hot and cold side of the module in this work is 161°C, for single thermoelectric module can generate 1.68W. The experimental results obtained are in the agreement with the Seebeck thermoelectric theory.

7.6.2 Electric power output for thermoelectric generator device tests

➤ Solar simulation lamp test

The evaluation of the conversion efficiency is allowed at various temperature ranges. The designed generator system utilizes solar heat gain, is made using commercial TEG module made of bismuth-telluride based materials, which are sandwiched between coated copper oil tank and water cooling tank.

Thermoelectric generator device was tested in a double-wall clear vacuum tube, experimental test set-up is depicted in Figure 7.10. Hot side of the device was heated by solar simulation lamp. Light intensity shown in Figure 7.12, was measured by pyranometer and data was recorded by DT 500 Datalogger. Cold side of the device was cooled by temperature controlled flow-water, which has a constant temperature

around 16°C-18°C as Figure 7.13 shows. The average temperature difference (ΔT) of 30°C was remained constant between hot side and cold side of the device in this test condition. The electricity power output was given in Table 7.2.

Experiments were done to investigate the applicability of thermoelectric power generation. Figure 7.15 shows the power output versus the measured module cold side and hot side temperature differences. The power output increases rapidly when the module hot side temperature increases. The cold side temperature of module was maintained at 16-18°C during the experiments. The experimental results obtained are in agreement with the Seebeck thermoelectric theory.

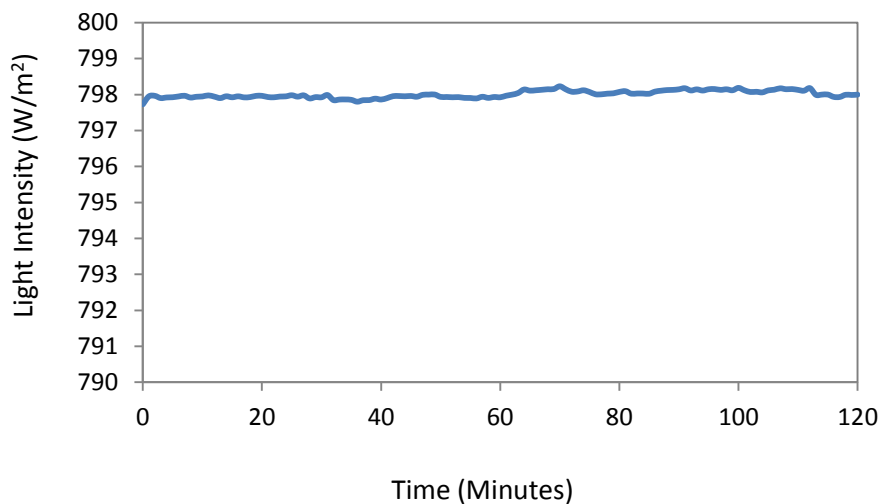


Figure 7. 12: Light intensity of solar simulation lamp

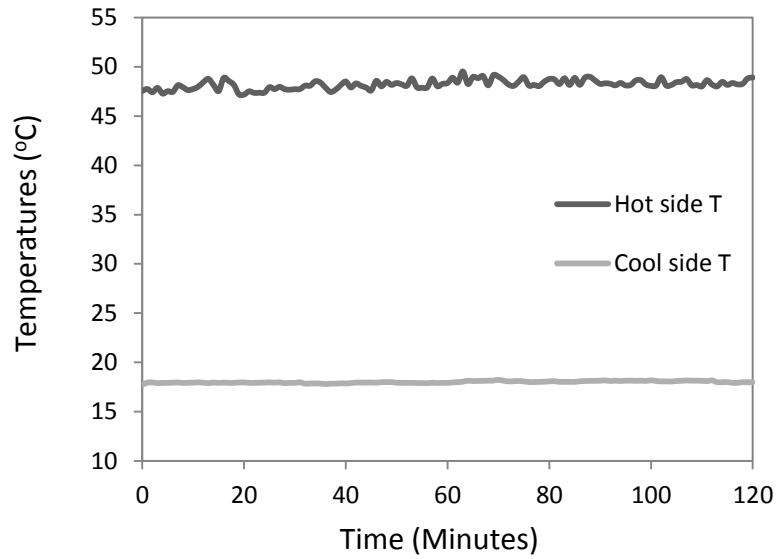


Figure 7. 13: TEG modules hot side and cool side temperature

➤ Hot plate test

System can achieve significant temperature difference (ΔT) of both sides of TEG modules by using hot plate as direct heat source. Figure7.14 illustrates the process and equipment used in the experiment. The test aims to demonstrate the system potential power output (V) by increasing temperature differences (ΔT) of both sides of TEG modules.

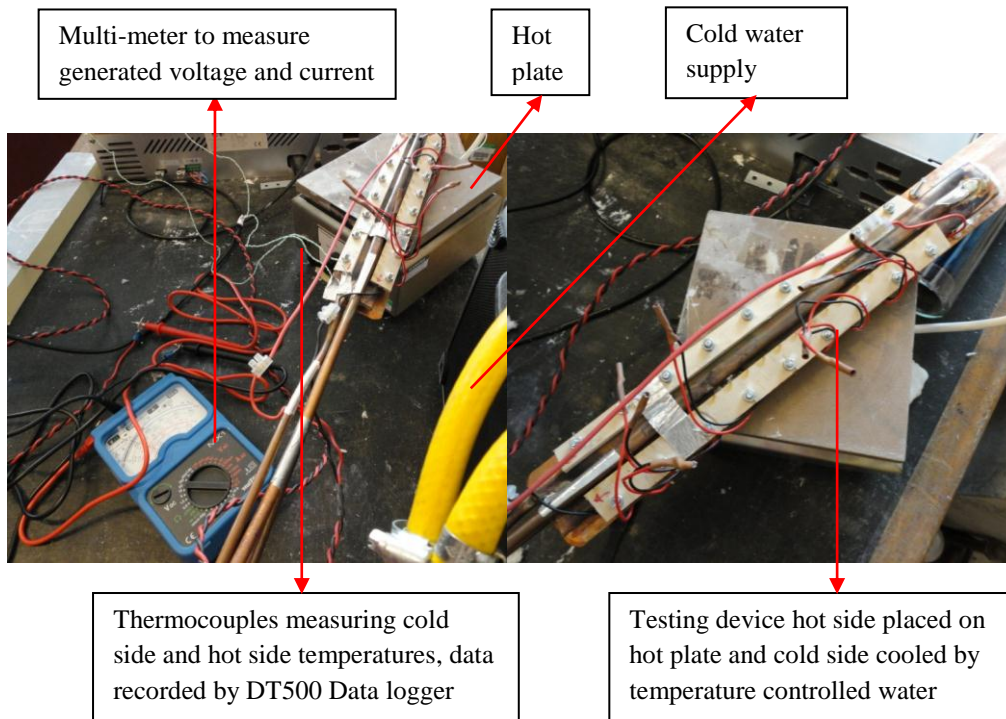


Figure 7. 14: System hot plate test setup

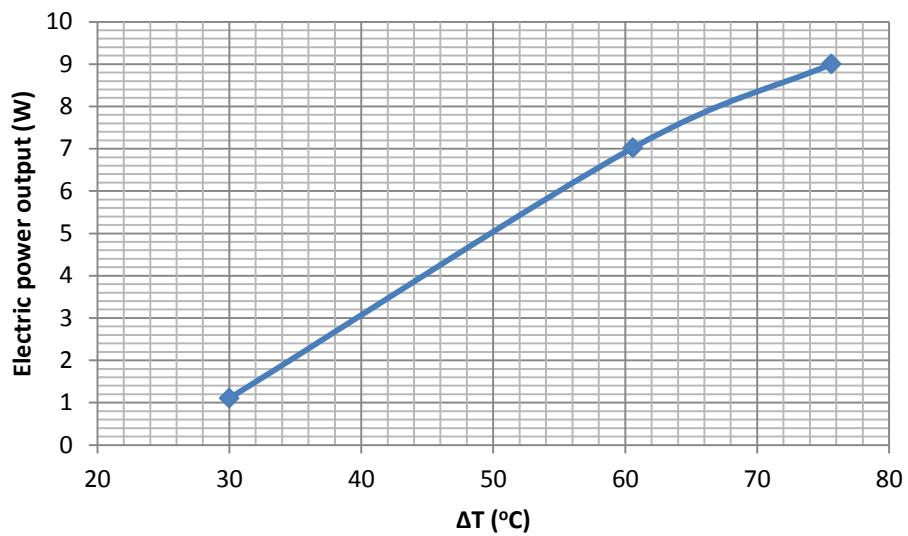


Figure 7. 15: Effect of ΔT on power output characteristic for thermoelectric generator device

The temperature changes on cold and hot side of modules were recorded by T-type thermocouple. The maximum temperature difference of system hot and cold side reached 75.6°C . System power output has significantly improved by increasing

temperature differences between cold and hot side of TE modules. Table 7.2 shows the maximum electricity generation has reached 15V@600mA.

Table 7. 2: Effect of ΔT on power output characteristics for system setup with eight TEG modules

ΔT ($^{\circ}\text{C}$)	Load current (A)	Load voltage (V)	Power output (W)
30	0.24	4.6	1.1
60.6	0.54	13	7.0
75.6	0.6	15	9.0

Table 7.2 summarized the power output characteristics of the thermoelectric power system. Under the conditions of the hot side and cold side temperature difference of 75.6°C , the maximum power achieved by the module tested in this work is 9.0W (for eight modules).

7.6.3 System experimental test results and discussion

System test results of voltage (V), current (I) and power output (P) versus temperature difference (ΔT) were summarized in following Figure 7.16-Figure 7.18.

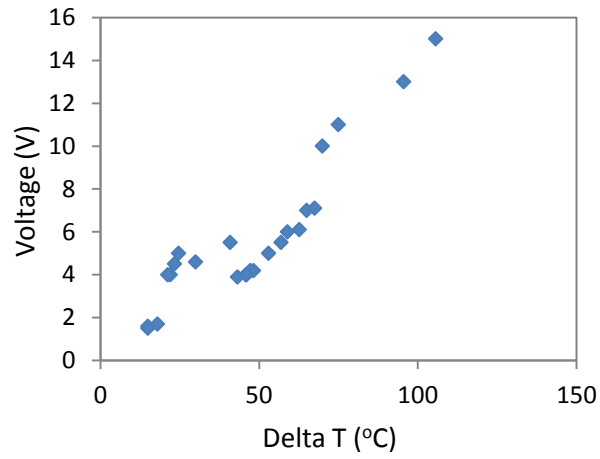


Figure 7. 16: Effect of ΔT on Voltages generation

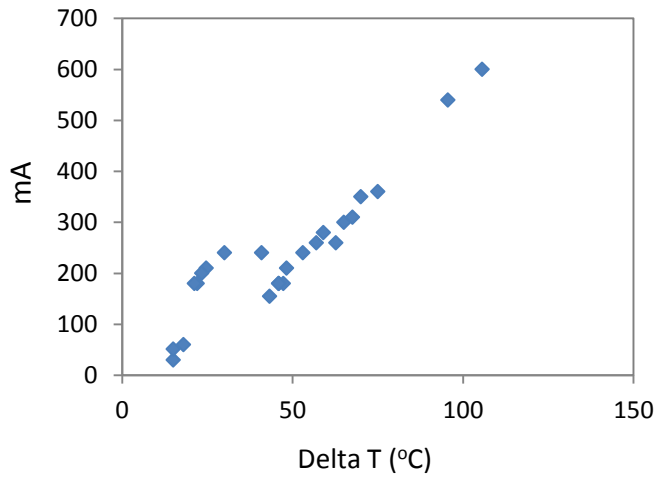


Figure 7. 17: Effect of ΔT on direct Current generation

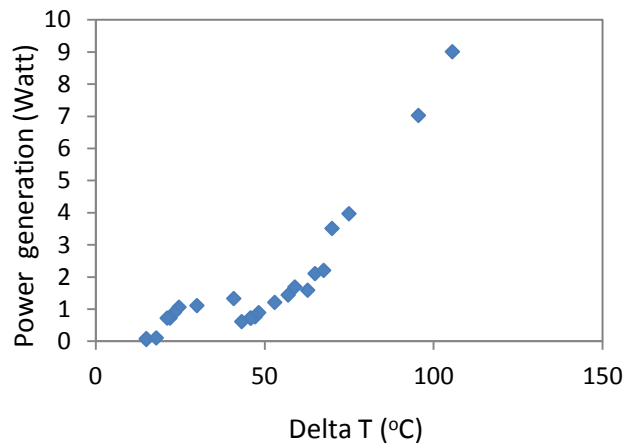


Figure 7. 18: Effect of ΔT on power generation

The power output of a thermoelectric generator depends on many factors such as the temperature difference between hot and cold junctions, the number of p and n junctions, the properties and dimensions of thermoelectric materials, and the external load resistance (Qiu, 2008). For a given temperature difference, the Seebeck coefficient of a p-n junction, α ($=dV/dT$), determines the output voltage (Qiu, 2008).

The theoretical energy conversion efficiency for a thermoelectric device is determined by the value of figure of merit (ZT) for a thermoelectric material. Geometric features and material properties of TEG module used in this system are provided by vendor datasheets listed in figures and the tables in Appendix A. Over a long period, the value of ZT has hovered at about one; thus the efficiency of thermoelectric power generation is at relatively low levels (Qiu, 2008).

In order to get a significant output voltage a very high Seebeck coefficient is needed (high $V/^\circ\text{C}$) as well as temperature differences. Heat sink on the cold side needs to be able to quickly get rid of heat from the hot side. It can be verified that the voltage is proportional to ΔT . Both solar simulation and hot plate test are done to identify the amount of power can be generated by increasing ΔT . However, the results from hot plate test can't be actually achieved once the device is placed into a vacuum tube and circulating cool water for modules' cold side, because the temperature within the tube will be cooled in whole.

According to above test results, system remain ΔT of $30^\circ\text{C}\sim 50^\circ\text{C}$ is generally achievable in practice, if the 25 TEMs are installed in one tube, the window unit will have 500 TEMs in total (prototype window sized $1\text{m} \times 1\text{m}$ contains 20 vacuum tubes). The electricity power output will approximately be $70\text{W}\sim 180\text{W}$.

7.7 Summary

Although the use of thermoelectric generator to generate electricity is not new, the application of thermoelectric device combined with vacuum tube window system is first reported in this research. This chapter depicted a proposed small scale power generation device integrated with vacuum tube window system. The system combines a solar thermal collector and temperature controlled water panel to establish temperature differences, therefore to generate electricity.

Experimental tests have illustrated the electricity generation results in different test conditions. The maximum electricity output for eight thermoelectric modules tested outside the vacuum tube is 9 W when the temperature difference reached to 75.6°C between hot and cold side of the modules. This generated power is enough to run a small ratio or a low power incandescent light bulb. With an achievable total generation capacity of 70~180W from prototype window unit sized $1m \times 1m$, it produces electricity to contribute the needs of the building.

The investigation have demonstrated the merit of further developing self-powered heating and possibility of a scale-up to a combined heating and power generation system with the modest net electric power output. The next step would be to integrate a purposefully designed thermoelectric module into a high-efficiency residential heating system designed to address integration of more electric power output.

Chapter 8 Conclusions and Future Works

8.1 Conclusions

This thesis starts with studies of low/zero energy buildings. Definitions of low/zero, net-zero, life cycle zero energy building are introduced, followed by the case studies of UK zero/low carbon houses. Technical methods of achieving zero/low carbon buildings were explained in each case. The construction details and materials used in each building were illustrated as well as U-factors of each building envelope components. Comparing to the U-values of other building envelope components, it has been found that windows are the weakest part in terms of heat loss and gain. Base on this finding, advanced glazing and window technologies are reviewed in order to carry out the development of novel window system. Four chapters focused on the studies on novel window systems, in which each novel window system was studied by both mathematical model and experimental tests. The results under various test conditions and modelling parameters have been discussed, which include window solar performance (contributing buildings' heating needs), power generation (amount of electricity generated by proposed device) and the improvement of thermal performances (U-factors). Laboratory tests have investigated the U-factor of novel vacuum tubes window systems; Aerogel and Argon window; TEC window system and window power generating system. Comparing to current window technologies, this research has proved: (1) lower U-value and cost window systems can be achieved by using evacuated tube panels; (2) TEC window system can achieve heating purpose by using solar energy , thereby to offset building energy usage in cold climate; (3) window can become a power generation device combined with thermoelectric generator device.

8.1.1 Performance of vacuum tube window system

Novel vacuum tube window systems are constructed with double wall and single wall vacuum tubes, the unique visual features of glass tube make the geometry of window architecturally attractive than conventional double or triple glazed windows. The U-value of novel vacuum tube window system has been studied. Computer modelling calculation results showed that the overall heat transmittance could be achieved low to around $0.5 \text{ W/m}^2\cdot\text{K}$ by the combined configuration of double wall vacuum tube and vinyl frame. Parameters of outdoor wind speed has very limited influence to overall thermal transmittance while elements of frame types and ratios of frame area to window area impact the overall thermal penetration much more, especially frame types. Experimental results show U-values of single and double vacuum tube windows are ranged from $0.95 \text{ W/m}^2\cdot\text{K}$ to $1.1 \text{ W/m}^2\cdot\text{K}$ and $0.89 \text{ W/m}^2\cdot\text{K}$ to $1 \text{ W/m}^2\cdot\text{K}$, respectively. Laboratory test U-value results are affected by outdoor wind speed, indoor and outdoor temperatures.

8.1.2 Performance of Aerogel window and Aerogel-Argon window system

Aerogel is a promising insulating material for day lighting function when it is applied on window system. Computer modeling simulates U-values of different window prototypes. The results show that 4mm, 5mm, 6mm silica aerogel filled, 6mm aerogel and argon filled window prototype are $1.35 \text{ W/m}^2\cdot\text{K}$, $1.26 \text{ W/m}^2\cdot\text{K}$, $1.19 \text{ W/m}^2\cdot\text{K}$ and $1.53 \text{ W/m}^2\cdot\text{K}$, respectively. Experimental results show that U-value of 6mm Aerogel-Argon filled window is $1.97 \text{ W/m}^2\cdot\text{K}$. The results demonstrate that aerogel filled double glazed window can significantly improve its thermal performance than conventional double-glazed windows because of its lower U-values. In comparison

with a conventional double glazed window unit of 20mm air gap (U-value of 2.8 W/m²K). The U-value of 6mm Aerogel-Argon window has improved by 45%.

8.1.3 Performance of Thermoelectric window system heating effect

Novel thermoelectric (TEC) window system is proposed to achieve heating purpose in winter. Both heating and cooling effect of the system are tested by switching electric current direction. For both indoor and outdoor heating mode tests, coefficient of performance (COP) of TEC window system decreases when applied voltage to TE modules increases. System can supply 37.6W (indoor test) and 38.1W (outdoor test) thermal energy into the room when 25V electricity applied to the TEC modules. Results illustrate that solar heat has impact on total power output when input voltage stays the same level.

8.1.4 Performance of Thermoelectric generator window system

Small scale power generation device using thermoelectric modules integrated with vacuum tube window system were introduced and tested. The achievable electricity output from 1m × 1m window unit is approximately 70~180W. In order to get a significant output voltage a very high Seebeck coefficient is needed (high V/ °C) as well as increasing temperature differences. The investigation have demonstrated the merit of further developing self-powered heating and possibility of a scale-up to a combined heating and power system with the modest net electric power output.

8.1.5 Economic analysis of the novel window system

The economic and environmental assessment of the proposed high performance vacuum tubes windows for buildings in the UK have been carried out. For feasibility aspect, several works including analyses of UK building stock, investigation of

viability of using vacuum tubes windows for new buildings and buildings for retrofits, and assessment of the energy efficiency of the windows, have been carried out. For economic and environmental analyses, the works involved included analyses of capital and operation cost of the vacuum tubes windows relative to the conventional double and triple glazing windows, as well as estimation of the payback period of life cycle cost saving of the vacuum tubes windows. Further, carbon emission reduction potential of using vacuum tubes windows across the UK has also been analysed.

8.2 Future works

A development of novel window system contains several issues. This research mainly focuses on window thermal transmission performance (u-values) study. Other issues also need to be addressed in future work, such as light transmission performance, self-clean window technology, safe and security glass, etc.

Self-clean window technology

Window glass should be cleaned regularly otherwise the surface will be discoloration and deterioration. The impact of gaseous and particulate pollution on glass surfaces has been investigated recently. Field experiments for vacuum tubes window will need to be carried out in order to analyse the self-cleaning mechanism of TiO₂-coated window float glass.

Real building demonstration in full scale buildings

Vacuum tube window thermal performance has been tested in a simulation chamber. Heat loss through the window has been recorded by thermal imaging camera. Monitor the window performance in the full scale house and buildings will need to be carried out in future research.

Safety and security glass

Building regulation states that window glass needs to be tested in accordance with BS 6206 either does not break, or breaks safely, and affords protection from cutting and piercing injuries in the event of accidental human impact and against specified level of attack. The materials used to manufacture vacuum tubes therefore need to meet the requirements of building regulations for glazing and large scaled windows. Safety and security test for vacuum tubes window will be further investigated to meet the requirement of building regulation.

Condensation test

In previous study, windows with U-value less than $1.3\text{W/m}^2\text{K}$ were found that external condensation usually occurs (Bülow-Hübe H., 2001 cited in G. Nair, K. Mahapatra and L. Gustavsson, 2011). However, for vacuum tube window systems, there was not condensation phenomenon occurred through the whole laboratory test. Therefore the conclusion of windows with U-value less than $1.3\text{W/m}^2\text{K}$ more likely to cause condensation problems need to be further studied and readdressed.

More geometry window design

Windows are the essential elements of the building façade. Vacuum tubes window can provide a distinguishing appearance from outside or inside of buildings, which can make buildings architecturally attractive. Buildings employing more geometric shape of windows will attract modern design interests.

Light transmission and day lighting

Windows thermal transmission performances have to be as low as possible in order to reduce energy consumption for heating and air conditioning; light transmission

characteristics have to be as high as possible for visual comfort and electric energy saving in lighting. The energy consumption in lighting will decrease if daylight entering through windows can be used appropriately. Optical characteristics issue, light transmission and day lighting factor studies for vacuum tubes window system are currently not covered in this research but will be future work to carry out.

Power generation

Electricity output of the proposed small scale power generation device has been tests in the laboratory. Experimental tests have illustrated the electricity generation results in different test conditions. The next step would be to integrate with a purposefully designed thermoelectric module into a high-efficiency residential heating system designed to address integration of more electric power output.

References

A

A. Fujishima, K. Hashimoto, T. Watanabe, TiO₂ Photocatalysis: Fundamentals and Applications, BKC, Inc., Tokyo, 1999.

A. Fujishima, X. Zhang, C. R. Chimie 9 (2006).

ASHRAE, ASHRAE Handbook: Fundamentals, SI ed., Chapter 31, American Society of Heating, Refrigerating and Air-conditioning Engineers Inc., Atlanta, USA, 2005.

ASHRAE Research, 2009 ASHRAE Handbook-Fundamentals (SI Edition), American Society of Heating, Refrigerating and Air-conditioning Engineers, Inc, 2009.

A.J. Marszal, P. Heiselberg, J.S. Bourrelle, E. Musall, K. Voss, I. Sartori, A. Napolitano, Zero Energy Building- A review of definitions and calculation methodologies, Energy and Buildings 43 (2011) 971-979

A.M. Omer, Energy environment and sustainable development. Renewable and Sustainable Energy Reviews 2008; 12:2265-300

A. Piccolo, A. Pennisi, F. Simone, Daylighting performance of an electrochromic window in a small scale test-cell, Solar Energy 83 (2009) 832-844

A. Piccolo, F. Simone, Effect of switchable glazing on discomfort glare from windows, Building and Environment 44 (2009) 1171-1180

B

Beck A., Köner W., Gross O. and Fricke J. (1999) Making better use of natural light with a light-redirecting double-glazing system. Solar Energy 66(3), 215-221.

Bülow-Hübe H. Energy-efficient window systems: effects on energy use and daylighting in buildings. Doctoral Dissertation. Lund Institute of Technology, Lund University, Sweden; 2001

B.P. Jelle, A. Hynd, A. Gustavsen, D. Arasteh, H. Goudey, R. Hart, Fenestration of today and tomorrow: A state-of-the-art review and future research opportunities, Solar Energy Materials & Solar Cells (2011)

BRITISH STANDARD, BS 874-3.2: 1990, Methods for Determining thermal insulating properties- Part 3: Tests for thermal transmittance and conductance- Section 3.2 Calibrated hot-box method

C

C.G. Granqvist, Materials Science for Solar Energy Conversion Systems, Pergamon Press, Oxford, 1991.

C.G. Granqvist, Oxide electrochromics: Why, how, and whither, Solar Energy Materials and Solar Cells 92 (2008) 203-208.

C.G. Granqvist, P.C. Lansaker, N.R. Mlyuka, G.A. Niklasson, E. Avendano, Progress in chromogenics: new results for electrochromic and thermochromic materials and devices, Solar Energy Materials and Solar Cells (2009).

Cadoff, I. B. and Miller, E., Thermoelectric Materials and Devices, Reinhold, New York, 1959.

Collins RE, Simko TM. Current status of the science and technology of VG. Solar Energy 1998; 62: 189-213

C.J. Brinker, G.W. Scherer, Sol-Gel Science: The Physics and Chemistry of the Sol-Gel Process, Academic, San Diego, 1990

C.M. Lampert, Heat mirror coatings for energy conserving windows, Solar Energy Materials and Solar Cells 6 (1981) 1-41

C.T. Hsu, G.Y. Huang, H.S. Chu, B. Yu, D.J. Yao, An effective Seebeck coefficient obtained by experimental results of a thermoelectric generator module, Applied Energy 88 (2011) 5173-5179

D

D. Arasteh, S. Selkowitz and J. Hartmann, "Detailed Thermal Performance Data on Conventional and Highly Insulating Window Systems", ASHRAE/DOE/BTECC Conference on Thermal Performance of the Exterior Envelopes of Buildings III, (1985)

D. Chahroudi, US Patent 3,953,110 Filed 1974.

D. Feuermann, A. Novoplansky, Reversible low solar heat gain windows for energy savings, *Solar Energy* Vol. 62, No. 3, pp. 169-175, 1998

D. J. Gardiner, S.M. Morris, H.J. Coles, High-efficiency multistable switchable glazing using smectic A liquid crystals, *Solar Energy Materials and Solar Cells* 93 (2009) 301-306

Dengler J. J. and Wittwer V. (1994) Glazings with granular aerogel. *SPIE* 2255, 718-727.

D. M. Rowe, (1994) *CRC Handbook of thermoelectrics*

E

Environmental design, CIBSE Guide A, 1999.

E. Hammarberg, A. Roos, *Thin Solid Films* 442 (2003) 222.

E.S. Lee, A. Tavit, Energy and visual comfort performance of electrochromic windows with overhangs, *Building and Environment* 42 (2007) 2439-2449

F

F. Chlela, A. Husaunndee, C. Inard, P. Riederer, A new methodology for the design of low energy buildings, *Energy and Buildings* 41 (2009) 982-990

Fricke, J., 1985. In: *Preface-first Int. Symp on Aerogels*. Springer, Würzburg.

F. Wolfgang, J. Schnieders, V. Dorer, A. Haas, Re-inventing air heating: convenient and comfortable within the frame of the Passive House concept, *Energy and Buildings* 37 (11) (2005) 1186-1203

F. Zoller (1924) Hollow pane of glass. German Patent No. 387655

G

G. Alvarez, M.J. Palacios, A test method to evaluate the thermal performance of window glazing, *Applied Thermal Engineering* 20, 803-812, 2000.

Goldsmid, H. J., *Electronic Refrigeration*, Pion Limited, London, 1986.

Geuder N., Fricke J., Körner W., Ehrmantraut M. and Beck A. (2000) Heat transfer coefficients of translucent glazing units for daylighting purposes. *High Temp. High Press.* 32, 39-45.

Gireesh Nair, Krushna Mahapatra, Leif Gustavsson, Implementation of energy-efficient windows in Swedish single-family house, *Applied Energy* 89 (2011) 329-338

G.V. Jorgenson et al., *Sol. Energy Mater.* 14 (1986) 205.

H

H. Bülow-Hübe, *Lighting Research and Technology* 27 (1) (1995) 37.

H. Glosch et al., A thermoelectric converter for energy supply, *Sensors and Actuators A: Physical* 74 (1999) 246–250

H.R. Wilson et al., *Proc. Window Innovations Conference*, June 1995, 489.

H.R. Wilson et al., *Proc. SPIE* 2255 (1994) 473.

H. Tommerup, J. Rose, S. Svendsen, Energy-efficient houses built according to the energy performance requirement introduced in Denmark in 2006, *Energy and Buildings* 39 (2007) 1123-1130

H. Watanabe, Intelligent window using a hydrogel layer for energy efficiency, *Solar Energy Materials and Solar Cells* 54 (1998) 203-211.

I

ISO 15099, Thermal performance of windows, doors and shading devices - Detailed calculations, American National Standards Institute, 2003 .

ITO, N., KIMURA, K. and OKA, J., A field experimental study on the convective heat transfer coefficient on exterior surface of a building, *ASHRAE Transactions*, 78, Part 1, 1972

J

J.A Clarke, M. Janak, P. Ruyssevelt, Assessing the overall performance of advanced glazing systems, *Solar Energy* 63 (1998) 231-241.

J.D. Garrison and R.E. Collins, Manufacture and cost of vacuum glazing, Solar Energy Vol. 55. No. 3, PP. 151-161, 1995

J. Fricke (Ed.), Aerogels, Proceedings of the First International Symposium on Aerogels, Springer, Berlin, 1986 ISBN 3-540-16256-9

J. Fricke (Ed.), Aerogels: Proc. 1st Intl. Symp. Aerogels, Sringer-Verlag, Berlin, 1986.

J. Han, L. Lu, H. Yang, Numerical evaluation of the mixed convective heat transfer in a double-pane window integrated with see-through a-Si PV cells with low-e coatings, Applied Energy 87 (2010) 3431-3437

J. Hartmann, M. Rubin, D. Arasteh, Thermal and Solar-Optical Properties of Silica Aerogel for Use in Insulated Windows, Presented at the 12th Annual Passive Solar Conference, Portland, OR, July 12-16, 1987.

J.M. Schultz, K.I. Jensen, F.H. Kristiansen, Super insulation aerogel glazing, Solar Energy Materials & Solar Cells 89 (2005) 275-285

J. P. Holman, Heat transfer (5th Edition), McGraw-Hill, New York, 1981.

J.S. Carlos, H. Corvacho, P.D. Silva, J.P. Castro-Gomes, Modelling and simulation of a ventilated double window, Applied Thermal Engineering 31 (2011) 93-102.

K

K.A.R. Ismail, C.T. Salinas, J.R. Henriquez, Comparison between PCM filled glass windows and absorbing gas filled windows, Energy and Buildings 40 (2008) 710-719

K. Duer and S.Svendsen, Monolithic silica aerogel in superinsulating glazings, Solar Energy Vol. 63, No. 4, pp. 259-267, 1998

K.E. Thmosen, J.M. Schultz, B. Poel, Measured performance of 12 demonstration projects. IEA Task 13 “ advanced solar low energy buildings”, Energy and Buildings 37 (2) (2005) 111-119

K. Hashimoto, H. Irie, A. Fujishima, Japan. J. Appl. Phys. 44 (2005) 8269_8285.

K. I. Jensen, J. M. Schultz, F. H. Kristiansen, Development of windows based on highly insulating aerogel glazings, *Journal of Non-Crystalline Solids* 350 (2004) 351-357.

K. I. Jensen, *J. Non-Cryst. Solids* 145 (1992) 237.

K. Qiu, A.C.S. Hayden, Development of a thermoelectric self-powered residential heating system, *Journal of Power Source* 180 (2008) 884-889

Kistler S.S. (1931) *Nature*, 127

L

L. Cassar, *MRS Bulletin* 29 (2004) 328_331.

Li HW, Lam NT, Chan WH, Mak HL. Energy and cost analysis of semi-transparent photovoltaic in office buildings. *Applied Energy* 2009; 86: 722-9

M

Martinez A, Astrain D, Rodriguez A, Experimental and analytical study on thermoelectric self-cooling of devices, *Energy* (2011) 1-11

M. Reim, A. Beck, W. Körner, R. Petricevic, M. Glora, M. Weth, T. Schliermann, J. Fricke, CH. Schmidt and F.J. Pötter, Highly insulating aerogel glazing for solar energy usage, *Solar Energy* Vol. 72, No. 1, pp. 21-29, 2002.

Nolas GS, Sharp J, Goldsmid HJ. *Thermoelectrics-basic principles and new materials developments*. Berlin, Heidelberg: Springer; 2001.

O

O. Chehab, The intelligent facade photovoltaic and architecture, *Renewable Energy* 5 (1994) 188-204.

P

P.D. Robinson, M. G. Hutchins, Advanced glazing technology for low energy buildings in the UK, *Renewable Energy*. Vol.5. Part 1. pp. 298-309, 1994.

P. Fath, H. Nussbaumer, R. Burkhardt, Industrial manufacturing of semitransparent crystalline silicon POWER solar cells, *Solar Energy Materials and Solar Cells* 74 (2002) 127-131.

P. Hernandez, P. Kenny, From net energy to zero energy buildings: Definition life cycle zero energy buildings (LC-ZEB), *Energy and Buildings* 42 (2010) 815-821

P. Torcellini, S. Pless, M. Deru, D. Crawley, Zero Energy Buildings: A Critical Look at the Definition, in: ACEEE Summery Stud, Pacific Grove, California, USA, 2006

P. W. Wong, Y. Shimod, M. Nonaka, M. Inoue, M. Mizuno, Semi-transparent PV: thermal performance, power generation, daylight modelling and energy saving potential in a residential application, *Renewable Energy* 33 (2008) 1024-1036.

R

R. Baetens, B.P. Jelle, A. Gustavsen, Properties, requirements and possibilities of smart windows for dynamic daylighting and solar energy control in buildings: a state-of-the-art review, *Solar Energy Materials and Solar Cells* 94 (2010) 87-105

Rowe, D. M. and Bhandari, C. M., *Modem Thermoelectrics*, Holt, Rinehart and Winston, 1983.

Rowe DM. *CRC handbook of thermoelectric*. Boca Raton, FL: CRC press; 1995

R. Wang, K. Hashimoto, A. Fujishima, M. Chikuni, E. Kojima, A. Kitamura, M. Shimohigoshi, T. Watanabe, *Adv. Mater.* 10 (1998) 135_138.

R.E. Collins, et, al, Vacuum Glazing—A New Component for Insulating Windows, *Building and Environment* 30(04) (1995): 459-492.

R.E. Collins and T.M. Simko, Current status of the science and technology of vacuum glazing, *Solar Energy* Vol. 62, No. 3, pp. 189-213, 1998

Rohsenow WM, Hartnett JP, Cho YI. *Handbook of heat transfer*. 3rd ed. New York NY: McGraw-Hill; 1998.

S

S.B. Riffat, Xiaoli Ma, Thermoelectrics: a review of present and potential applications, *Applied Thermal Engineering* 23 (2003) 913-915

S.B. Sadineni, S. Madala, R.F. Boehm, Passive building energy savings: A review of building envelope components, *Renewable and Sustainable Energy Reviews* 15 (2011) 3617-3631

Shahid H, Naylor D. Energy performance assessment of a window with a horizontal venetian blind. *Energy Build* 2005; 37: 836-43

S.J. Robinson and R.E. Collins (1989) Evacuated windows-theory and practice. In *ISES Solar World Congress*, International Solar Energy Society, Kobe, Japan

S. Kilkis, A New Metric for Net-zero Carbon Buildings, in: *Energy Sustainability Conference*, Long Beach , California, 2007

S.M. Babulanam et al., *Sol. Energ Mater.* 16 (1987) 347.

Simmons RE, Chu RC. Application of thermoelectric cooling to electric equipment: a review and analysis. 16th IEEE SEMI-THERM symposium; 2000. p. 1-8

S. Papaefthimiou, G. Leftheriotis, P. Yianoulis, T.J. Hyde, P.C. Eames, Y. Fang, P.-Y. Pennarun, P. Jannasch, Development of electrochromic evacuated advanced glazing, *Energy and Buildings* 38 (2006) 1455-1467

S.P. Corgnati, M. Perino, V. Serra, Experimental assessment of the performance of an active transparent facade during actual operating conditions, *Solar Energy* 81 (2007) 993-1013.

S. R. de Groot, *Thermodynamics of Irreversible Processes*, North Holland Publishing, Amsterdam, 1952.

T

T. Chow, C.Y. Li, Z. Lin, Innovative solar windows for cooling-demand climate, *Solar Energy Materials and Solar cells* 94 (2010) 212-220

T. E. Johnson, *The Low-E Glazing Design Guide*, Butterworth Architecture, 1991, ISBN 0-7506-9147-6.

T.E. Johnson, *Low-e Glazing Design Guide*, Butterworth-Heinemann, USA, 1991.

T. Rosencrabs, H. Bülow-Hübe, B. Karlsson, A. Roos, Solar Energy Materials and Solar Cells 89 (2005) 249-260.

T. R. Nielsen, K. Duer and S. Svendsen, Energy Performance of Glazing and Windows, Solar Energy Vol. 69 (Suppl.), Nos. 1-6, pp. 137-143, 2000.

T.T. Chow, C. Li, Z. Lin, The function of solar absorbing window as water-heating device, Building and Environment 46 (2011) 955-960

T.V. Esbensen, V.Korsgaard, Dimension of the solar Heating System in the Zero Energy House in Denmark, 1977 United States, PP. 195-199

Thomson, W., On a mechanical theory of thermoelectric currents, Proc. R. Soc. Edinburgh, 91-98, 1851

T. Watanabe, K. Hashimoto, A. Fujishima, 1st International Conference on TiO₂ Photocatalytic Purification and Treatment of Water and Air, 1992.

T.Y.Y. Fung, H. Yang, Study on thermal performance of semi-transparent building-integrated photovoltaic glazing, Energy and Buildings 40 (2008) 341-350.

W

W.Li, Sustainable design for low carbon architecture, Procedia Environmental Science 5 (2011) 173-177

WINDOW 4 Program Description, Window and Daylighting Group, Lawrence Berkeley Laboratory, Berkeley, California, USA, Mar. 1992.

Z

Z.J. Ma, S.W. Wang, Building energy research in Hong Kong: a review. Renewable and Sustainable Energy Reviews 2009; 13: 1870-83

Websites:

Web 1.1 <http://www.uvalue.co.uk/>

Web 2.1 http://www.planningportal.gov.uk/uploads/code_for_sust_homes.pdf

Web 2.2 http://en.wikipedia.org/wiki/Solar_chimney

Web 2.3

<http://www.bshf.org/published-information/publication.cfm?lang=00%26thePubID=81B12E18-15C5-F4C0-9904048F10A3C1E2>

Web 2.4 The Passive House Institute, <http://www.passivehouse.com>

Web 3.1 Serious Materials, Empire state building retrofit, retrieved 6 July 2010, www.seriouswindows.com/empire-state-building/home.html

Web 3.2 Serious Materials, SeriousGlass™ Technology, retrieved 6 July 2010, www.seriouswindows.com/empire-state-building/seriousglass-technology.html.

Web 3.3 NSG, Nippon Sheet Glass Spacia, The principle, retrieved 28 July 2010, www.nsg-spacia.co.jp/tech/index.html

Web 3.4 Trony Solar Holdings Company Limited. <http://www.trony.com>

Web 4.1 <http://en.wikipedia.org/wiki/Thermography>

Web 4.2 Energy Saving Trust Data Base. <http://www.energysavingtrust.org.uk/>

Web 5.1 Super insulating silica aerogel glazing, Results from EU Project HILIT+ (No. ENK6-CT-2002-00648), Technical University of Denmark, available online: <http://www.ecobuilding-club.net>

Web 5.2 Edgetech, Super Spacer@ Standard insulation, Retrieved from <http://www.edgetechig.com,USA>

Web 5.3 Bostik, Hot melt butyl edge sealant, Retrieved from <http://www.bostik.co.uk,UK>

Web 6.1 www.dts-generator.com

Web 6.2 <http://www.melcor.com/formula.html>

Appendix A: Thermoelectric Material Basic Data

Thermoelectric parameters as a function of temperature, P-type material

T, K	α , $\mu\text{V/K}$	ρ , $\text{Ohm}\cdot\text{cm}$	λ , $\text{W/cm}\cdot\text{K}$	Z, 1/K
182.6	147	4.27E-04	2.03E-02	2.49E-03
189.5	151	4.56E-04	1.96E-02	2.55E-03
201.1	161	5.05E-04	1.86E-02	2.76E-03
218.8	175	5.89E-04	1.77E-02	2.94E-03
235.3	185	6.69E-04	1.65E-02	3.10E-03
250.4	194	7.48E-04	1.58E-02	3.18E-03
264.3	201	8.27E-04	1.51E-02	3.24E-03
280.6	208	9.24E-04	1.44E-02	3.25E-03
293.9	214	1.01E-03	1.39E-02	3.26E-03
308.5	218	1.09E-03	1.35E-02	3.23E-03
320.8	223	1.18E-03	1.34E-02	3.15E-03
336.6	226	1.29E-03	1.32E-02	3.00E-03

T, K	α , $\mu\text{V/K}$	ρ , $\text{Ohm}\cdot\text{cm}$	λ , $\text{W/cm}\cdot\text{K}$	Z, 1/K
180	144	4.21E-04	2.00E-02	2.46E-03
190	153	4.62E-04	1.92E-02	2.64E-03
200	160	5.06E-04	1.85E-02	2.73E-03
210	168	5.51E-04	1.79E-02	2.86E-03
220	175	5.98E-04	1.72E-02	2.98E-03
230	181	6.47E-04	1.66E-02	3.05E-03
240	187	6.98E-04	1.61E-02	3.11E-03
250	193	7.51E-04	1.56E-02	3.18E-03
260	198	8.06E-04	1.51E-02	3.22E-03
270	203	8.63E-04	1.47E-02	3.25E-03
280	208	9.21E-04	1.43E-02	3.28E-03
290	212	9.82E-04	1.40E-02	3.27E-03
300	215	1.04E-03	1.37E-02	3.24E-03
310	218	1.11E-03	1.35E-02	3.17E-03
320	221	1.18E-03	1.33E-02	3.11E-03
330	223	1.24E-03	1.32E-02	3.04E-03
340	225	1.31E-03	1.31E-02	2.95E-03
350	227	1.39E-03	1.30E-02	2.85E-03

Thermoelectric parameters as a function of temperature, N-type material

T, K	α , $\mu\text{V/K}$	ρ , $\text{Ohm}\cdot\text{cm}$	λ , $\text{W/cm}\cdot\text{K}$	Z, 1/K
179.9	-157	5.42E-04	1.87E-02	2.43E-03
186.6	-162	5.65E-04	1.87E-02	2.48E-03
198.3	-170	6.07E-04	1.83E-02	2.60E-03
216.4	-179	6.75E-04	1.73E-02	2.74E-03
233.3	-185	7.39E-04	1.64E-02	2.82E-03
248.8	-192	7.98E-04	1.58E-02	2.92E-03
263.2	-199	8.53E-04	1.56E-02	2.98E-03
280.1	-205	9.23E-04	1.51E-02	3.02E-03
293.9	-208	9.81E-04	1.47E-02	3.00E-03
309.3	-213	1.05E-03	1.46E-02	2.96E-03
322.1	-216	1.10E-03	1.45E-02	2.93E-03
338.7	-218	1.17E-03	1.44E-02	2.82E-03

T, K	α , $\mu\text{V/K}$	ρ , $\text{Ohm}\cdot\text{cm}$	λ , $\text{W/cm}\cdot\text{K}$	Z, 1/K
180	-161	5.62E-04	1.93E-02	2.39E-03
190	-167	5.98E-04	1.87E-02	2.49E-03
200	-173	6.35E-04	1.81E-02	2.60E-03
210	-178	6.73E-04	1.75E-02	2.69E-03
220	-183	7.11E-04	1.70E-02	2.77E-03
230	-188	7.50E-04	1.66E-02	2.84E-03
240	-192	7.90E-04	1.62E-02	2.88E-03
250	-196	8.30E-04	1.58E-02	2.93E-03
260	-200	8.71E-04	1.55E-02	2.96E-03
270	-203	9.12E-04	1.52E-02	2.97E-03
280	-207	9.55E-04	1.49E-02	3.01E-03
290	-210	9.97E-04	1.47E-02	3.01E-03
300	-212	1.04E-03	1.46E-02	2.96E-03
310	-215	1.08E-03	1.44E-02	2.96E-03
320	-217	1.13E-03	1.44E-02	2.89E-03
330	-219	1.18E-03	1.43E-02	2.84E-03
340	-220	1.22E-03	1.43E-02	2.77E-03
350	-221	1.27E-03	1.43E-02	2.69E-03

Thermoelectric material basic data

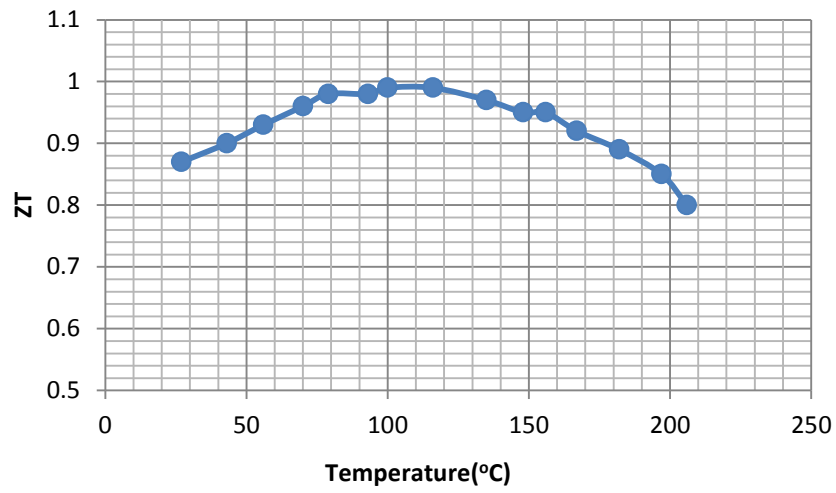


Figure A 1: ZT vs. temperature (measured on N-P couple)

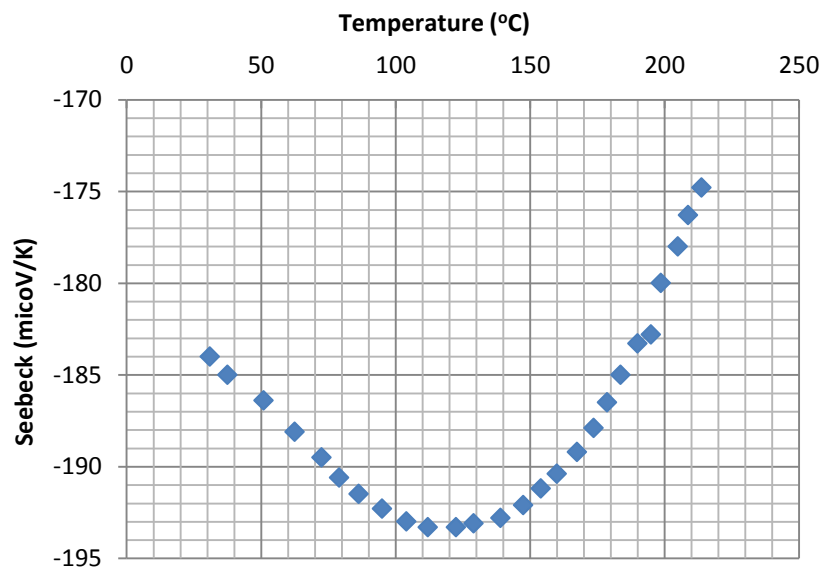


Figure A 2: Seebeck vs. temperature (N-type)

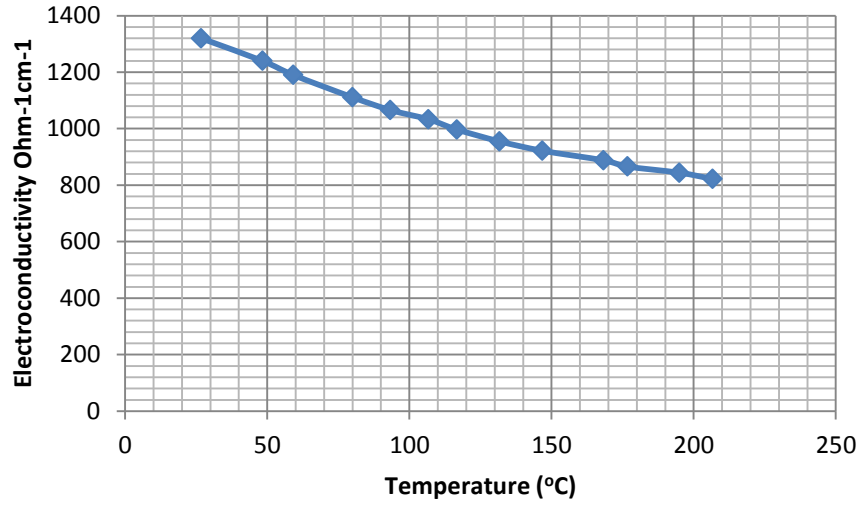


Figure A 3: Electric conductivity vs. temperature (N-type)

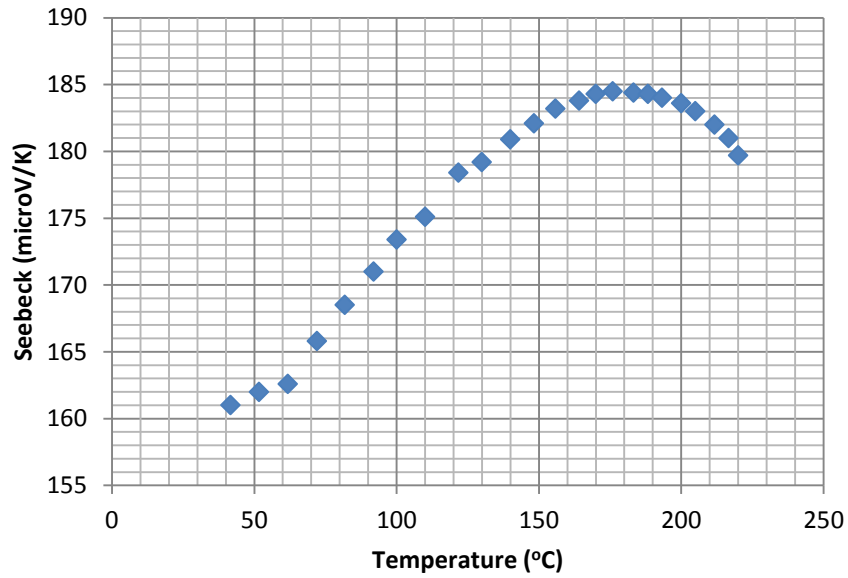


Figure A 4: Seebeck coefficient vs. temperature (P-type)

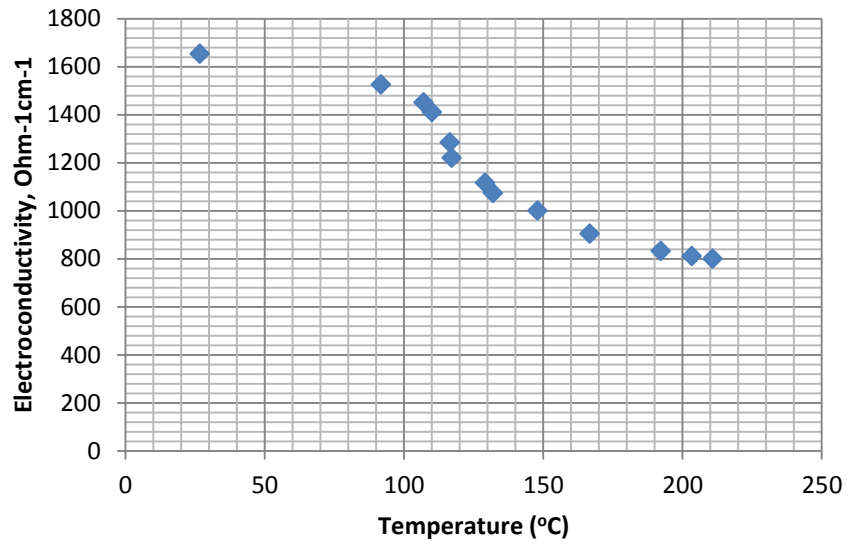


Figure A 5: Electric conductivity vs. temperature P-type

Appendix B: Publication

Conference Paper:

Creative energy home project-Zero carbon technologies in sustainable homes in UK

High performance glazing types and windows technologies review

A Novel Vacuum tubes Window System